2021

Peralkaline silicic extrusive rocks: magma genesis, evolution, plumbing systems, and eruption.

Ray Macdonald
University of Warsaw

John C. White
Eastern Kentucky University, john.white@eku.edu

Harvey E. Belkin
USGS

Recommended Citation

Comptes Rendus

Géoscience

Sciences de la Planète

Ray Macdonald, John C. White and Harvey E. Belkin

Peralkaline silicic extrusive rocks: magma genesis, evolution, plumbing systems and eruption

Perspectives on alkaline magmas / *Perspectives sur les magmas alcalins*

Peralkaline silicic extrusive rocks: magma genesis, evolution, plumbing systems and eruption

Ray Macdonald [a, b]**, John C. White** ® *, c **and Harvey E. Belkin** ® d

a Department of Geochemistry, Mineralogy and Petrology, University of Warsaw, 02-089 Warszawa, Poland

b Environment Centre, Lancaster University, Lancaster LA1 4YQ, UK

c Department of Physics, Geosciences & Astronomy, Eastern Kentucky University, Richmond, KY 40475, USA

d U.S. Geological Survey, 11142 Forest Edge Drive, Reston, VA 20190-4026, USA

E-mails: raymacdonald186@gmail.com (R. Macdonald), john.white@eku.edu
(J. C. White), harveybelkin@gmail.com (H. E. Belkin)

Abstract. Peralkaline silicic extrusive rocks are an important component of the volcanological record. Here we review several aspects of their formation and evolution, including the tectonic settings in which they occur, their main petrological and geochemical features, the magmatic lineages along which they evolve, and the parameters (T, P, fO_2, melt water contents) that control the lineages. Particular attention is paid to the composition of the extraordinary melts formed at the lowest temperatures. Various lines of evidence are presented to explain the silica gaps in some lineages. The partial melting of continental crust and the role of crustal contamination are considered to be of relatively minor importance in their genesis. High P–T experiments aimed at quantifying the lineages are assessed. Geophysical and petrological evidence for the depth and nature of the plumbing systems are presented. Differentiation mechanisms within reservoirs and the ubiquity of the formation of compositional zonation are discussed, as are the timescales involved. Volcanic hazards and the environmental impact of eruptions are described and a brief assessment of the ore potential of the extrusives is given.

Keywords. Peralkaline silicic rocks, Tectonic settings, Plumbing systems, Hazards, Ore potential.

Online first, 8th December 2021

1. Introduction

The focus of the review is on sequences of extrusive rocks that include peralkaline (Peralkaline Index, P.I. = mol. $(Na_2O + K_2O)/Al_2O_3 > 1$) and silica-oversaturated (quartz-normative) members, i.e., quartz trachytes and rhyolites. Peralkaline phonolites

are not included, hence the term silicic is preferred to felsic, which would include silica-undersaturated and silica-oversaturated rocks. Classification of the rocks of the various sequences is by the total alkalis–silica scheme [Le Bas et al., 1986]; the peralkaline types are further classified using the scheme of Macdonald [1974].

Peralkaline silicic extrusive rocks play important roles in many aspects of volcanology, petrology, geochemistry, economic geology and volcanic hazards.

* Corresponding author.

(1) They can form large volumes of eruptive material, resulting in significant additions to crustal growth. For example, Oligocene ignimbrites of the western plateau in Ethiopia had a dense-rock-equivalent volume of at least 60,000 km^3 [Ayalew et al., 2002]. Within the Main Ethiopian Rift, peralkaline rhyolites represent 90% of the volcanic products [Trua et al., 1999]. A phase of pantelleritic activity in central Kenya at 6.36–8.13 Ma originally covered an area of 40,000 km^2 [Claessens et al., 2016]. The Deccan flood basalts, India, have a preserved volume of 1.5×10^6 km^3. Peralkaline rhyolites associated with them have a volume between 500 and 1000 km^3 [Lightfoot et al., 1987] and could have had a volume of 50,000 km^3 [Javoy and Courtillot, 1989].

(2) In the past 20 years, there has been a remarkable surge in our understanding of magmatic systems. Volcanological and petrological studies of peralkaline extrusive rocks are revealing the complexity of the evolution of peralkaline silicic centres, all of which are to some degree unique, in, for example, the interplay of petrogenetic processes, the range of lithologies, the nature of the magma chambers and the detailed P–T–X conditions under which the magmas evolve. Such studies can also help to reveal magmatic phase associations and stability relationships in intrusive equivalents, which are complicated by secondary processes.

(3) Volcanic hazards. Many peralkaline volcanoes have the potential to erupt soon, with the consequent effects on life and property. For example, the Corbetti, Aluto, Bora and Haledebi volcanoes in the Ethiopian Rift have shown recent signs of unrest [Biggs et al., 2011, Hutchison et al., 2016a,b] and in the Kenya Rift the Longonot and Menengai caldera volcanoes [Biggs et al., 2009] and Olkaria volcanic complex [Clarke et al., 1990] could also erupt in the near future. The eruption of Changbaishan-Tianchi volcano, China/North Korea, in AD 946 (the "Millennium Eruption" or "Generalized Millennium Eruption"; Pan et al., 2020) was one of the two largest Holocene eruptions on Earth, the other being the great eruption of Tambora, Indonesia, in 1815 CE (Figure 1).

(4) There is an increasing awareness that peralkaline eruptions may, through, *inter alia*, sulphur emissions, have considerable environmental effects, to the extent of contributing to global cooling [Scaillet and Macdonald, 2006a]. There is a clear need to un-

Figure 1. The Changbaishan-Tianchi volcano, China/North Korea, the site in 946 CE of one of the two largest Holocene eruptions on Earth. The caldera is 5.5 km wide. Source: Global Volcano Program, Smithsonian Institution.

derstand the mechanisms of such emissions and to be able to predict their likely size.

(5) Peralkaline granites can be hosts for rare-metal deposits, such as Strange Lake, Canada [Salvi and Williams-Jones, 2006], the Ambohimirahavavy complex, Madagascar [Estrade et al., 2014], Khan Bogd, Mongolia [Kynicky et al., 2011], the Haldzan Buragtag massif, Mongolian Altai [Kovalenko et al., 2009] and the Siwana peralkaline granite, India [Mondal et al., 2021]. The extrusive equivalents carry important information on the rare-metal enrichment processes during the magmatic stages and provide a basis on which the effects of hydrothermal enrichment processes can be assessed. Furthermore, peralkaline extrusive rocks can show strong enrichment in critical rare metals and may also show large tonnages and grades. If their occurrences as superficial deposits makes them open to pit mining, they are worthy of increased exploration.

These issues require a full understanding of how peralkaline centres are initiated and how they evolve. This review focusses, therefore, on what we see as advances in our knowledge and on attempts to identify some of the gaps in that knowledge. Particular aspects addressed include the nature of the mantle sources of peralkaline silicic suites, the tectonic settings in which they occur, the nature and controls of their liquid lines of descent, the P–T–fO$_2$–melt water conditions under which they evolve, petrogenetic models of their origin, the nature and evolution of

peralkaline silicic magmatic systems, volcanic hazards associated with such systems, certain environmental effects of eruptive magmatism and their potential as hosts for ore deposits. The peralkaline types are further classified using the scheme of Macdonald [1974].

2. Tectonic settings

A major issue in the petrogenesis of peralkaline silicic rocks is whether they are associated with a particular tectonic setting or settings and therefore with specific types of crust and mantle. In fact, they can occur over a very wide range of settings, as follows.

2.1. *Continental extension zones*

The major occurrences of peralkaline silicic extrusive suites are in continental rift valleys. We noted above, for example, the huge volumes of Oligocene to Recent peralkaline silicic volcanics associated with the Ethiopian (Figure 2a) and Kenyan sections of the East African Rift System (EARS). The majority of occurrences are in extensional zones related to regional doming, perhaps a result of mantle plumes. Pantelleria, the type locality of pantellerite, is located in the NW–SE trending Strait of Sicily Rift Zone. The rift cuts the Pelagian Block, a promontory of the African plate. Felsic rocks of the Marie Byrd Land Province, Antarctica, include comendites, pantellerites, trachytes and phonolites and occur in an area of late Caenozoic doming similar to those in the EARS [LeMasurier et al., 2011, 2018] (Figure 2b).

Flood rhyolite lavas (~37.4 Ma) of the Davis Mountains volcanic field, Trans-Pecos Texas, are composed of mildly peralkaline quartz trachyte to rhyolite [Parker, 2019]. One such flood lava, the comenditic Bracks Rhyolite, had a minimum original extent of 1000 km^2 and a volume of 75 km^3 [Henry et al., 1990]. The field formed on Grenville basement north of the Ouachita fold belt, which formed in the late Palaeozoic as a result of closure of an ocean basin between North America and South America [Parker et al., 2017]. Magmatism may have been related to upwelling of asthenospheric mantle above the foundered Farallon slab. Closely associated with the flood lavas is the pantelleritic Gomez Tuff, which was erupted from, and ponded within, the Buckhorn caldera at 37.33 ± 0.07 Ma, possibly covering

an area as large as 14,000 km^2 [Parker and White, 2008] (Figure 2c). At ~220 km^3, it may be the largest known pantellerite eruption. Alkalic magmatism in the Davis Mountains may be attributed to asthenospheric upwelling over the foundering Farallon slab over a 10 Ma time span, during which silicic magmatism transitioned south-westward [Parker and Henderson, 2021]. Associated in time with the Davis Mountains volcanic field is the Pine Canyon caldera volcano in Big Bend National Park, Texas, which erupted, *inter alia*, peralkaline quartz trachyte and rhyolite. White et al. [2006] suggested that the volcano was formed in an early phase of post-collisional continental rifting resulting from lithospheric delamination and sinking of the detached lithosphere.

2.2. *Oceanic islands*

Peralkaline silicic rocks are known from many ocean islands, occurring in several different settings, as comprehensively reviewed by Jeffery and Gertisser [2018] for the Atlantic Ocean. The Canary Islands in the NE Atlantic may be related to relatively fixed plumes rising from the core–mantle boundary into the African plate from the late Jurassic to Recent [Hoernle et al., 1995]. van den Bogaard [2013] has nominated the islands as the oldest hotspot track in the Atlantic Ocean and the longest lived on Earth. On Gran Canaria, a Miocene basaltic shield is overlain by ~20 trachytic to peralkaline rhyolitic ignimbrites erupted from the large (~20 km across), multiply reactivated Tejeda caldera [Schmincke and Sumita, 2010, Troll and Schmincke, 2002]. Iceland lies on the Mid-Atlantic Ridge above the Icelandic plume; peralkaline silicic rocks are known from several centres, including Thorsmörk [Jørgensen, 1980], Torfajökull [McGarvie et al., 2006], Öræfajökull [Prestvik et al., 2001] and Ljósufjöll [Flude et al., 2008].

Comenditic trachytes and pantellerites are known from São Miguel and Terceira Islands, Azores [Mungall and Martin, 1995, Jeffery et al., 2016, Pimentel et al., 2016, 2021, D'Oriano et al., 2017]. The Azores are located near the triple junction between the Eurasian, African and North American plates and are related to shear motions between the plates [Miranda et al., 1998, Hildenbrand et al., 2014]. Bouvetøya, which has erupted comenditic rhyolites, is located near a triple junction on the South Atlantic Ridge, possibly above a mantle plume [Imsland et al.,
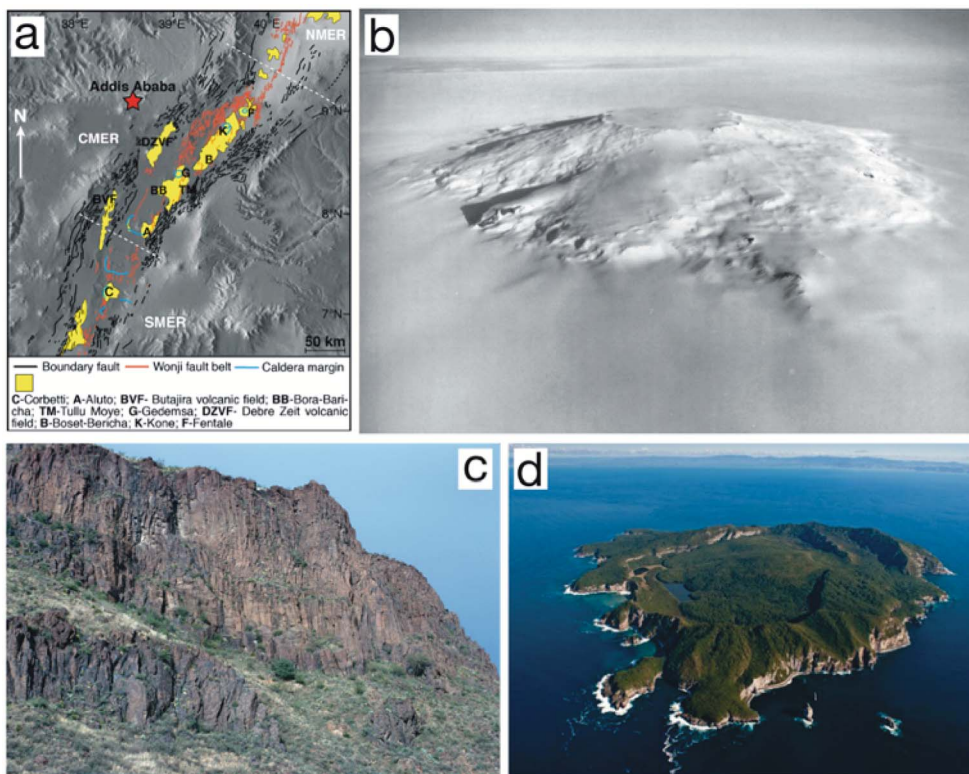
Figure 2. Examples of peralkaline extrusive rocks in various tectonic settings. (a) Volcanoes in part of the Main Ethiopian Rift (MER; N-Northern, C- Central, S-Southern). Redrawn from Iddon and Edmonds [2020]. (b) Mt Takahe, Marie Byrd Land, Antarctica. The summit caldera is ~8 km wide. (US Navy photograph TMA 1718 F33 022). (c) The Gomez Tuff, here ~100 m thick, overlying the darker Star Mountain Rhyolite lava. Little Aguja Canyon, Boy Scout Ranch, Texas. Photo courtesy of Professor Don Parker. (d) Mayor Island, pictured from the northeast, with New Zealand in the background. The caldera is 3 km wide.

1977, Prestvik et al., 1999]. Ascension Island lies close to the Ascension fracture zone, a right-lateral offset of the Mid-Atlantic Ridge; it may overlie a local mantle melting anomaly or "hotspot" [Evangelidis et al., 2004]. The island has erupted comendites [Weaver et al., 1996, Kar et al., 1998, Jicha et al., 2013].

The Rallier-du-Baty Peninsula forms the southwestern part of the Kerguelen Archipelago (Indian Ocean); magmatic activity, which included comenditic trachyte, is related to the long-lived Kerguelen plume [Gagnevin et al., 2003]. Easter Island is located on the Easter hotspot, on the Nazca plate ~350 km east of the East Pacific Rise. Its products include comendites [Haase et al., 1997]. Due to its tectono-magmatic features, including low eruptive rate, scat-tered rift zones and scarce lateral collapses, Vezzoli and Acocella [2009] considered it to represent an end-member type of hotspot volcano. The island of Socorro, Mexico, lies on the northern Mathematician Ridge which defines the location of a mid-ocean ridge spreading centre, abandoned at 3.5 Ma when activity shifted to the East Pacific Rise [Bohrson and Reid, 1995].

2.3. *Subduction-related settings*

Peralkaline silicic rocks also occur in various settings in what can broadly be considered collisional zones, formed either during active subduction or post-collision. They usually occupy local extensional

zones in such settings; we are unaware of any formed in a purely contractional setting, perhaps because shallow magma reservoirs tend not to form there. The Mayor Island volcano, which is dominated by pantelleritic eruptives [Barclay et al., 1996], lies offshore from the North Island of New Zealand (Figure 2d). Its location is controlled by localized extension related to a back-arc rift onto the edge of the New Zealand continental crust [Cole, 1990, Houghton et al., 1992]. Like Mayor Island, the volcanic rocks, including comendites, of the D'Entrecasteaux Islands, Papua New Guinea, are broadly related to the subduction of the Pacific Plate under the Australian Plate [Smith, 1976, Smith et al., 1977]. The islands lie west of a spreading centre which has been propagating into the Australian continent and thus represent an early stage of continental breakup.

Miocene peralkaline volcanism in west-central British Columbia, Canada, has been linked to lithospheric fracturing above the northern edge of the subducted Juan de Fuca plate [Bevier et al., 1979]. Further north, in northern British Columbia, the Mount Edziza Volcanic Complex, which includes comenditic eruptives, is thought to have formed in a late Caenozoic extension zone related to transcurrent motion along the adjacent continental margin [Souther and Hicks, 1984, Souther et al., 1984]. There are extensive peralkaline occurrences in the western sector of the Trans-Mexican Volcanic Belt [Mahood, 1980, 1981a,b, Mahood et al., 1985, Nelson and Hegre, 1990, Aguirre-Diaz and Morton-Bermea, 2018, Sosa-Ceballos et al., 2018], perhaps related to extension created by an eastward jump of the East Pacific Rise during opening of the Gulf of California [Luhr et al., 1985]. In the central sector of the Belt, comendites were erupted at 7.3–6.6 Ma from the Amazcala caldera, although the centre is bracketed between subduction-related, calc-alkaline volcanism [Aguirre-Diaz and Morton-Bermea, 2018]. The Acoculco Caldera Complex is located in the eastern part of the Belt and shows the unusual, possibly unique, feature of mixing between mildly peralkaline and calc-alkaline magmas in the post-caldera volcanism [Sosa-Ceballos et al., 2018]. At the Nemrut volcano, Lake Van, Turkey, some peralkaline units show evidence that magmas from the neighbouring, subalkaline Süphan volcano have occasionally entered the Nemrut system [Sumita and Schmincke, 2013a,b]. Yan et al. [2018] argued that the late Cretaceous tectonic setting of SE China, when peralkaline rhyolites were formed in the Yunshan caldera complex, was changed from a collisional to an extensional environment, perhaps related to the rollback of the subducting palaeo-Pacific plate.

Comendites occur on Palmarola Island (Tyrrhenian Sea, Italy) which is located along the boundary between the Italian continental shelf and the opening Tyrrhenian Sea. Geochemically, the volcanic rocks have a collisional imprint but also have features consistent with having been erupted in a within-plate setting [Cadoux et al., 2005]. The formation of Early Miocene peralkaline rhyolites on Sardinia, the type locality of comendite, was related to the subduction of an oceanic plate beneath the European continental plate, although details of the subduction process remain unresolved [Morra et al., 1994, Lustrino et al., 2013].

It appears, therefore, that the formation of peralkaline silicic rocks is not critically dependent on tectonic environment or crustal thickness; the main requirement is that the setting is extensional, with the proviso that there are periods of tectonic quiescence and low magma flux so that strongly evolved magmas can be generated in the upper parts of the magma reservoirs [Bohrson and Reid, 1997, Hutchison et al., 2018, Siegburg et al., 2018].

3. Nature of mantle sources

There is a consensus that peralkaline magmas evolve from melts generated in the mantle, but less agreement on the nature of the source mantle. The source that produces alkali basalts parental to silicic peralkaline rocks has been variably attributed to metasomatically enriched mantle [Di Bella et al., 2008, Markl et al., 2010], asthenospheric mantle enriched by "primitive" material from a deep mantle plume [Civetta et al., 1998, Rogers et al., 2000, Halldórsson et al., 2014], or mantle enriched by recycled Mid-Ocean Ridge Basalt (MORB) [Esperança and Crisci, 1995, Avanzinelli et al., 2014, White et al., 2020]. This section examines whether the nature of the source mantle is an important factor in promoting peralkalinity. Information on the mineralogy and composition of the mantle sources and on melting processes within the mantle can be inferred from the composition of the primary basalts at each centre, where a primary magma is the melt which was in equilib-

rium with the residual crystalline assemblage in the upper mantle region where melting took place. There are, however, remarkably few records of rocks potentially representing primary magmas in peralkaline-oversaturated suites. A picritic basalt from the Emuruangogolak volcano, Kenya Rift Valley, with a magnesium number (Mg-number = 100 ∗ Mg/(Mg + Fe), with all Fe as Fe^{2+}) of 69 and a Ni content of 259 ppm, was shown by Weaver [1977] to be olivine-cumulitic. A "picritic basalt" from the Erta'Ale Range, Ethiopia, has Mg-number 61 and Ni 75 [Barberi et al., 1974] and is a magnesian basalt. The primary magmas of peralkaline suites have clearly experienced high-pressure fractionation histories and have reached final equilibration at crustal pressures.

Information on the composition of primary magmas has to come, therefore, *via* geochemical modelling. Few studies have attempted to estimate the nature of the primary melt and degree of melting of the mantle source required to generate the primary magmas. Using rare earth element (REE) inversion, Neave et al. [2012] calculated that for Pantelleria melt generation was by ~1.7% melting of a light REE (La-Gd; LREE)-enriched peridotitic source at depths of 60–100 km, to produce a primary magma with Mg-number 69. The parental Pantelleria alkali basalts were then formed by 35% fractional crystallization of the primary melts. White et al. [2020] argued that the Pantescan magmas formed from a higher degree of partial melting (~6%) of a Depleted MORB Mantle (DMM)-dominated mantle enriched with a component of recycled MORB. For Gedemsa volcano, Giordano et al. [2014] argued that the primary magmas were formed by 7% partial melting of a complex mantle source with mantle-derived and crust-derived components.

Trace element modelling, mainly using REE and based on the compositions of parental basalts, generally indicates that the partial melting takes place either in the garnet facies [Lowenstern et al., 2006, Mahood and Baker, 1986] or over the spinel/garnet facies transition [e.g., Kenya Rift Valley—Latin et al., 1993, Macdonald, 1994, Macdonald et al., 2001] and Pantelleria [White et al., 2009, 2020, Neave et al., 2012]. Depending on the geothermal gradient, the depth range for the transition is 60–100 km, although LeMasurier et al. [2011] estimated a rather deeper source, 110–140 km, for primary magmas of Marie Byrd Land, Antarctica. White et al. [2020] suggested

that partial melting beneath Pantelleria may have been imitated at depth of 120–130 km, which they attributed to the presence of abundant fusible eclogitic material in the mantle.

Various mantle components have been invoked, even for the same suite. Esperança and Crisci [1995] suggested that the primary magmas of the Pantescan basalts were formed in lithosphere made fertile by long-term reworking of continental lithosphere by asthenosphere-derived melts and mixed with present-day MORB-type melts. Civetta et al. [1998] argued that the mantle sources under Pantelleria are heterogeneous and involve at least two geochemical components, a relatively depleted (MORB-like) component and an enriched High-μ (HIMU)-like component, with the possible involvement of a third, Enriched Mantle 1-type component. On the basis of Sr–Nd–Pb and U-series isotopic data, Avanzinelli et al. [2014] argued that mafic magmas on Pantelleria originated in the asthenospheric mantle with little or no interaction with either the subcontinental lithospheric mantle (SCLM) or continental crust. Certain hawaiites, however, had a different origin: they were either related to interaction with partial melts of the SCLM or were formed in a mantle source enriched by recycled crustal material. White et al. [2013] suggested that the high Ti–P and low Ti–P series on the island originated from asthenospheric spinel lherzolite and that the high Ti–P primary magmas formed at greater depths (92.2 ± 4.4 km) than those of the low Ti–P series (76.1 ± 7.8 km). White et al. [2020] argued that both suites were derived from a DMM-dominated mantle enriched with a component of recycled MORB and possibly other components. The Pantescan case is a rather good example of the non-uniqueness of isotopic data in identifying precisely the nature of the mantle sources.

Using geochemical and Sr–Nd–Pb isotope data, Giordano et al. [2014] suggested that mafic eruptives of the Gedemsa and Fanta'Ale (Fantale; Fentale) volcanoes, Main Ethiopian Rift, were formed by 7% modal batch melting of mantle comprising 12% subcontinental lithospheric mantle and 88% depleted mantle. In contrast, the high ^{3}He/^{4}He values of several centres, including Gedemsa, support the presence of the "C" mantle component, common to ocean islands. Yan et al. [2018] suggested that the source for peralkaline rhyolites of the Yunshan caldera complex, SE China, was a subduction zone-

enriched mantle wedge which had interacted with depleted asthenospheric melts. Generally speaking, although isotope and trace element data strongly indicate that peralkaline magmas are ultimately derived from enriched mantle sources, they are equivocal on the nature of the enrichment even at the same volcanic centre. However, the simple but critical point in terms of the future attainment of peralkalinity in a suite is that the mantle source must be fertile and capable of generating alkali basalt on partial melting.

4. Petrographic and geochemical features

4.1. *Petrography*

The most commonly occurring phenocryst phases in peralkaline trachytes and rhyolites are alkali feldspar, quartz, olivine, clinopyroxene, ilmenite, magnetite, aenigmatite, amphibole and less commonly biotite. Accessory microphenocrysts include zircon, fluorapatite, fluorite, pyrrhotite and chevkinite-(Ce). Dozens of combinations of these phases have been recorded in the literature but generally the dominant assemblage in trachytes and comendites is alkali feldspar + fayalitic olivine + hedenbergite + ilmenite + fluorapatite, and that in pantellerites is alkali feldspar + hedenbergite + aenigmatite ± quartz ± amphibole. White et al. [2005] proposed a generalized "reaction series" for pantelleritic rocks with increasing peralkalinity, decreasing temperature (~950 to 700 °C), and increasing oxygen fugacity relative to the fayalite-magnetite-quartz (FMQ) buffer: (1) augite + fayalite + ilmenite + magnetite (P.I. < ~1.4) (2) augite + fayalite + ilmenite (~1.4 < P.I. < ~1.5); (3) sodian augite or hedenbergite + fayalite + ilmenite + aenigmatite (~1.5 < P.I. < ~1.7); (4) sodian hedenbergite or aegirine-augite + ilmenite + aenigmatite ± amphibole (~1.7 < P.I. < ~1.9); and (5) aegirine-augite + aenigmatite ± amphibole (P.I. > ~1.9).

Macdonald et al. [2011] have reviewed the distribution of the phenocrysts over the compositional range of peralkaline trachytes and rhyolites and have also considered the stability relationships between them. Aspects of these relationships are discussed in various sections below. Here, we enter a plea that all published chemical analyses of peralkaline extrusive rocks be accompanied by a list of phenocryst assemblages for *each* analysis. Such assemblages record important, often subtle, information on the conditions under which the host rock formed. Generalized assemblages may hide important relationships. For example, do aenigmatite and ilmenite phenocrysts coexist and at what specific bulk-rock composition did quartz join the crystallizing assemblage? These features can reveal evidence of, *inter alia*, the fO_2 and pH_2O under which the host magmas evolved.

4.2. *Geochemistry*

Peralkaline rocks are defined by their unusual major element geochemistry, with a greater abundance of alkalis (Na + K) than Al. Although this often implies a high concentration of Na_2O (up to ~8 wt%), it often also occurs because of very low concentrations of Al_2O_3 (down to ~6 wt%) that may also be accompanied by very high concentrations of FeO* (up to ~9 wt%) despite SiO_2 > 69 wt%. This peculiar major element geochemistry is also reflected in the unusually high abundances of halogens and incompatible trace elements. Peralkaline silicic rocks generally contain high levels of F, Cl, high-field-strength elements (HFSE), REE and certain large ion lithophile elements (LILE), with relative abundances that typically demonstrate an Ocean Island Basalt (OIB) type pattern. The maximum abundances of these elements can certainly be very high: Cl > 1 wt% [Green Tuff, Pantelleria; Liszewska et al., 2018], F > 2 wt%, Zr > 6000 ppm and LREE (La–Sm) > 1500 ppm (Gold Flat Tuff, Nevada; Macdonald et al., 2019, and Rb > 1000 ppm [Olkaria complex, Kenya: Marshall et al., 2009]. However, the ranges are very large, e.g. Zr 10^2–10^3 ppm. Comparing the compilations of analytical data for peralkaline and metaluminous rhyolitic obsidians by Macdonald and Bailey [1973] and Macdonald et al. [1992], respectively, shows that the peralkaline types have concentrations of such elements as the LREE, Nb and Zr ten to 25 times greater than those in the metaluminous varieties. On the other hand, concentrations of Cl are only 5 to 10 times greater [Lowenstern, 1994]. While peralkaline silicic rocks can also show strong depletion in such incompatible elements as Ba and Sr, with levels commonly <10 ppm, these features are also found in subalkaline rhyolites and cannot be used as a distinguishing feature of peralkalinity.

Among the more important consequences of peralkaline compositions are (i) the effects of high halogen contents and high alkalinity on melt viscosity,

and (ii) the potential for the high abundances of certain rare metals to be concentrated into potential ore deposits.

4.3. *Viscosity*

Melt viscosity can strongly influence processes such as crystallization, crystal-melt separation, degassing and the dynamics of eruption, the main controls on viscosity being temperature and melt composition. It has long been inferred from geological evidence that peralkaline silicic magmas have lower viscosities than their metaluminous counterparts [Schmincke, 1974, Mahood, 1984], resulting from the higher volatile contents and lower degrees of melt polymerization. While there is a general correlation between P.I. and melt viscosity, the relationship is not linear; Stabile et al. [2016] showed that the Fe oxidation state has an effect on viscosity, decreasing Fe^{2+}/Fe^* resulting in increasing viscosity.

The viscosities of peralkaline silicic melts have been determined experimentally [Stevenson and Wilson, 1997, Stevenson et al., 1998, Di Genova et al., 2013, Stabile et al., 2016] and the results have been incorporated into various models of melt viscosity [Dingwell et al., 1998, Giordano et al., 2008]. The results have confirmed that peralkaline silicic melts have lower viscosities than their metaluminous equivalents, by as much as 2–3 orders of magnitude, e.g., 10^{10}–10^{11} Pa·s, Stevenson and Wilson, 1997; $10^{9.6}$–$10^{13.6}$ Pa·s, Stabile et al., 2016, 2021]. On Pantelleria, for example, the volcanological consequences of the low viscosities include the ubiquity of welded and rheomorphic pumice falls and high-grade to extremely high-grade ignimbrites [Rotolo et al., 2021]. Eruption columns are inferred to have been low [Mahood and Hildreth, 1986], which minimizes cooling of particles during fountaining and facilitates extensive welding. In later sections, we discuss the role of melt viscosity in such topics as magma chamber dynamics, the speed of development of zoned magma reservoirs, and the efficiency of magma mixing.

5. Geothermometry and geobarometry

In the following sections, we shall often refer to estimates of the crystallization conditions of peralkaline silicic magmas. First, we describe here the various methods used in the geothermometric and geobarometric estimates.

5.1. *Geothermometry*

Several techniques have been used to estimate the temperatures at which the phenocryst assemblages formed. In principle, the geothermometers could, when carefully tied to petrographic features, track the changes in temperature during the crystallization of individual magma batches from liquidus to near-solidus conditions.

As noted earlier, the use of two-oxide geothermometry in peralkaline silicic rocks is commonly hampered by the absence of coexisting oxides. A further constraint may be analytical imprecision due to very low Mg contents of the oxides, leading to relatively large errors in calculating Mg/Mn ratios and thus to failure in passing the Bacon and Hirschmann [1988] Mn–Mg partitioning test for equilibrium. Also, the uncertainties associated with the method [±30 °C; cf. Blundy and Cashman, 2008] may limit the identification of temperature variations in zoned deposits. Different calculation schemes are used, including Andersen et al. [1993], Ghiorso and Evans [2008] and Sauerzapf et al. [2008], but where tested on the same rocks appear to give similar results [Jeffery et al., 2017, Macdonald et al., 2019]. The oxides re-equilibrate over short timescales and most probably reflect the final pre-eruptive temperatures.

In the Quartz-Ulvospinel-Ilmenite-Fayalite (QUILF) thermobarometer [Andersen et al., 1993] temperature is calculated from Fe–Mg–Ca exchange between olivine and clinopyroxene; it cannot, therefore, be used in the most evolved pantellerites where olivine is typically absent. Several studies have presented QUILF temperatures, with the following ranges: peralkaline trachytes 709–865 °C; [Ren et al., 2006, D'Oriano et al., 2017]; comendites 680–740 °C [White et al., 2006, Marshall et al., 2009]; pantellerites 668–748 °C [Ren et al., 2006, Parker and White, 2008, Macdonald et al., 2019]. Trachytes parental to comendite and pantellerite typically have temperatures >790 °C [Romano et al., 2020]; lower temperatures are recorded in trachytes with high P.I. (>1.3) that are thought to have evolved via fractional crystallization of as assemblage of alkali feldspar + quartz from peralkaline rhyolite [Ren et al., 2006].

Temperature estimates based on equilibrium pyroxene–glass pairs have been proposed by Putirka [2008] and Masotta et al. [2013]. For these models, the pressure of equilibration and the melt water con-

tent must be known or assumed. Also, the pyroxenes must have a jadeite component. The models were applied to the peralkaline rhyolites of the Nemrut volcano, Turkey, by Macdonald et al. [2015] giving the range 808–862 °C ± 45 °C (Putirka model) and 721–881 °C ± 18.2 °C (Masotta et al., model).

The alkali feldspar-melt geothermometer of Putirka [2008] was used by Zou et al. [2010] to calculate the magmatic temperatures at the comenditic Changbaishan-Tianchi volcano. Rocks from two localities gave 741 °C and 752 °C (±30 °C). Neave et al. [2012] used the geothermometer to estimate the temperature for the Cuddia di Mida pantellerite on Pantelleria as 802 ± 23 °C, assuming a depth of 1.5 kbar and an H_2O content of 4 wt% based on SIMS data. The same methodology was applied by D'Oriano et al. [2017] to the comenditic trachyte component of the Lajes Ignimbrite, Terceira Island, and gave 850–900 °C ± 23 °C. Shortly before eruption, pantelleritic magmas at Aluto were in the narrow temperature range 718–765 °C [Gleeson et al., 2017]. Jeffery et al. [2017] found alkali feldspar-melt temperatures for various peralkaline trachyte ignimbrites of Terceira lying between 912 and 857 °C. These temperatures are higher than those from two-oxide thermometry, perhaps reflecting the earlier crystallization of the feldspars.

As far as we know, the only study to apply the Ti-in-zircon method [Watson et al., 2006] to a peralkaline extrusive rock is that by Zou et al. [2010] to the Changbaishan-Tianchi comendites. A TiO_2 activity was assumed (0.5) and the resulting average temperatures for two rocks were 702 ± 28 °C and 702 ± 43 °C, within the uncertainties of those estimated by the alkali feldspar-melt technique.

Appreciating that Petrogeny's Residua System (Q–Or–Ab) does not accurately represent the compositions of peralkaline silicic rocks, Thompson and MacKenzie [1967] determined phase relationships in the system Q–Or–Ab–H_2O with added acmite (4.5%) and Na-metasilicate (4.5%), designed to simulate pantelleritic melts. They proposed the existence of a low-temperature zone towards, and along, which peralkaline melts evolve, broadly analogous to the zone in the non-peralkaline system. Parker and White [2008] and Liszewska et al. [2018] estimated the equilibration temperatures of the Gomez Tuff, Texas, and Green Tuff, Pantelleria, respectively, by plotting them into projections of the experimental
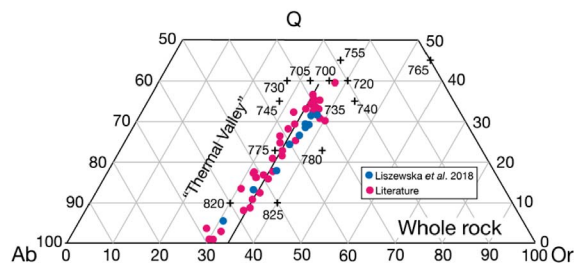

Figure 3. Whole-rock analyses of Green Tuff (Pantelleria) projected into the Q–Or–Ab plane in the Q–Or–Ab–Ac–Ns system at P_{H_2O} = 1000 bar [modified from Liszewska et al., 2018]. The crosses mark temperatures on the alkali feldspar liquidus surface [Carmichael and MacKenzie, 1963].

system Q–Or–Ab–H_2O–Ac–Ns. For the Gomez Tuff, the temperature was ~750 °C; for the Green Tuff, the lowest temperatures were ~700 °C (Figure 3).

Significant information on temperatures of equilibration has come from high temperature–pressure experiments [Mahood and Baker, 1986, Scaillet and Macdonald, 2001, 2003, 2006b, Di Carlo et al., 2010, Romano et al., 2018, 2020, 2021]. The main results are discussed below (Section 11) but one of the most important is that peralkaline rhyolites can achieve (near)liquidus temperatures lower than 700 °C. Experimental information on solidus temperatures is hampered by the difficulty of crystallizing minerals at near-solidus conditions. In experiments on pantellerites, Scaillet and Macdonald [2001] and Di Carlo et al. [2010] estimated solidus temperatures of ~660 °C.

The combination of thermodynamic estimates and experimental results has meant that the temperature ranges over which peralkaline trachytes and rhyolites equilibrate are rather well established, even for individual eruptive units. For example, Martel et al. [2013] estimated that the metaluminous to peralkaline trachytes of the Chaîne des Puys evolved in a reservoir (or reservoirs) where the temperatures increased from 700 to 825 °C downwards. The range within the reservoir that erupted the Green Tuff, Pantelleria, was ~900–700 °C [Liszewska et al., 2018].

5.2. *Geobarometry*

Low pressures of formation of peralkaline silicic rocks are commonly inferred from geological

evidence, such as the close association of caldera volcanoes and high-level intrusions [Mahood, 1984, Lowenstern et al., 2006, Wei et al., 2013]. More quantitative approaches use water solubility models, thermodynamic modelling and constraints imposed by experiments.

(a) The depth of a magma storage system can be estimated using water solubility models, such as those of Di Matteo et al. [2004] and Papale et al. [2006]. If the magma water content can be estimated, from, for example, melt inclusions, and water saturation is assumed, then the minimum pressure of the system can be calculated. Lanzo et al. [2013] used the Papale et al. [2006] model and a measured water content of 4.2 wt% to show that the Green Tuff, Pantelleria, had a saturation pressure of 65 MPa, equivalent to ~2.5 km depth. According to Romano et al. [2021] and Stabile et al. [2021], the Papale et al. model tends to slightly overestimate water solubility in such melt compositions. On the basis of new experimental determinations of water solubility in trachytic and pantelleritic rocks from Pantelleria, Romano et al. [2021] estimated the depth of the felsic reservoirs on the island to deepen from 2.4 to 3.5 km. Using the Di Matteo et al. formulation and a water content of 4.2 wt%, Jeffery et al. [2017] found that the minimum equilibration pressure of the magma system on Terceira which generated a suite of peralkaline ignimbrites was ~80 MPa (~3 km depth).

(b) Thermodynamic modelling involves the use of thermodynamic data from the literature, e.g., for the activity of the silica and ilmenite components and attempts to determine the stability of possible mineral phases over ranges of $P–T–f\mathrm{O}_2$. Magmatic differentiation in peralkaline systems has been modelled using the MELTS algorithm [Ghiorso and Sack, 1995] and the updated version rhyolite-MELTS [Gualda et al., 2012]. For isobaric systems, MELTS minimizes Gibbs free energy to determine phase equilibrium relationships, given the $P–T–f\mathrm{O}_2$ conditions. It then removes the equilibrium assemblage from the melt to produce a new melt; the model then proceeds stepwise.

White et al. [2009] used MELTS to model the origin of Pantescan pantellerites from an alkali basalt parent. They found that at low pressure (0.1 GPa) fractional crystallization of basalt with 1.0–1.5 wt% H_2O) at $f\mathrm{O}_2$ < FMQ produced a metaluminous trachyte with P.I. 0.89–0.97 and water contents 3.34–4.06 wt%.

No MELTS model, however, successfully resulted in a pantelleritic melt.

The various approaches have almost all shown that the transition from trachyte to rhyolite normally occurs at high crustal levels, in the range 2–5 km. However, the majority of petrogenetic models link these high-level reservoirs to deeper reservoirs, often down to the crust–mantle boundary; aspects of these broader magmatic systems are discussed below (Sections 13–15).

5.3. *Oxygen fugacity*

Estimates of the $f\mathrm{O}_2$ under which peralkaline rhyolites crystallize have been made using coexisting oxides [Nicholls and Carmichael, 1969, White et al., 2005, Beier et al., 2006, Jeffery et al., 2017], QUILF equilibria, and by imposing the redox conditions during high-$P–T$ experiments [Mahood and Baker, 1986, Scaillet and Macdonald, 2001, 2003, 2006b, Di Carlo et al., 2010, Jeffery et al., 2017, Romano et al., 2018, 2019, 2020, 2021]. Using the 750 °C temperature estimated by projection into the Q–Or–Ab–Ac–Ns–H_2O system and QUILF equilibria and assuming a pressure of 2 kbar, Parker and White [2008] found log $f\mathrm{O}_2$ values in the range −17.24 to −17.78 for the Gomez Tuff. Liszewska et al. [2018] used thermodynamic modelling to show that the temperature range in the Green Tuff, Pantelleria, ranged from 900 °C (comenditic trachytes) to 700 °C (pantellerites), with $f\mathrm{O}_2$ FMQ −1.5 to FMQ −0.5, and $a\mathrm{SiO}_2$ relative to quartz saturation of 0.74–1.00.

Most studies have shown that the magmas evolve under conditions close to the FMQ buffer (FMQ ± 1), i.e., they are relatively reduced (Figure 4). Exceptions include lavas of Ascension Island where the range is FMQ −1.8 to FMQ −2.4 [Chamberlain et al., 2016]. Beier et al. [2006] found that certain trachytes of the Sete Cidades volcano, São Miguel, Azores, are more oxidized, with $f\mathrm{O}_2$ values approaching the HM buffer. They related this to high volatile contents of the magmas, perhaps a result of the assimilation of crustal rocks.

6. Magmatic lineages

This section outlines the various liquid lines of descent along which peralkaline suites evolve, pointing out differences between them and relating the
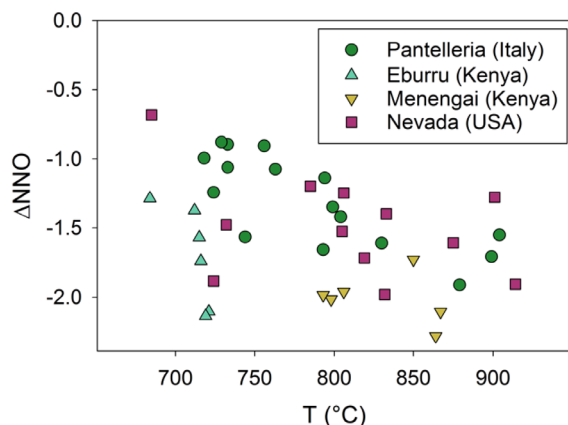
Figure 4. Plot of temperature (*T*) versus oxygen fugacity (*f*O_2) relative to the nickel–nickel oxide buffer at 100 MPa [ΔNNO; O'Neil and Pownceby, 1993, Pownceby and O'Neil, 1994] for representative samples from Pantelleria [Mahood and Stimac, 1990, White et al., 2005, 2009, Liszewska et al., 2018, Romano et al., 2018, 2019, 2020], Eburru [Ren et al., 2006], Menengai [Macdonald et al., 2011], and the Black Mountain volcanic centre, Nevada [Macdonald et al., 2019].

differences to the crystallizing assemblages and the external parameters which controlled them. Our approach is that the majority of peralkaline suites are essentially basalt-driven systems, in the sense that basalt has been the parental magma from which more evolved rocks have been derived or has provided the heat source for partial melting of various crustal rocks [Mahood and Baker, 1986, Bohrson and Reid, 1997, Macdonald, 2012]. The review acknowledges, therefore, the primary role of basalt and attempts to evaluate the various factors which lead to peralkaline silicic end points, particularly their polybaric fractionation histories.

The following section is divided into (i) the recognition of parental basalts; and (ii) one-stage models, where basaltic magma fractionates more or less continuously to trachytic or rhyolitic endmembers. We mainly use ten selected suites which we consider to be representative of the main types of basalt–peralkaline rhyolite sequences (Table 1), although other suites are introduced where particularly relevant. Suites come from continental and oceanic settings, have different assemblages of rock types, may

or may not show composition gaps, range from sodic to mildly potassic, and followed different evolutionary paths.

6.1. *Parental basalts*

The most primitive (generally most magnesian) basalts at peralkaline centres are taken to be potential parental magmas, with the caveat that for any system there is no unique primary, and thus parental, magma. The coexisting basalt in coeval eruptions and mixed magmas may *represent* the parental magma but cannot *be* it. Significant variation in the composition of putative parental basalts is found in individual centres, ranging from four derivative (?) suites on Ascension Island [Weaver et al., 1996] through three on Terceira, Azores [Self and Gunn, 1976, Mungall and Martin, 1995] and Socorro Island [Bohrson and Reid, 1995], to at least two on Pantelleria [Civetta et al., 1998, White et al., 2009, 2020, Avanzinelli et al., 2014]. Thus, treating each of our chosen units as one magmatic lineage is a simplification.

Table 2 lists analyses of rocks inferred by the original authors to represent, or be close to, the parental magmas to basalt–trachyte/rhyolite suites. The basalts range from mildly nepheline-normative to mildly hypersthene-normative and may be described as alkali to transitional basalts. Mg-numbers vary from 50 to 65. The ranges represent the degree of fractionation encountered between mantle source and the point of initial equilibration of each suite within the crust. There is significant variation in most major elements; for example, at 6 wt% MgO, K_2O, TiO_2 and P_2O_5 show ranges of more than ×2 Table 3. Na_2O contents are in the relatively narrow range 3–4 wt%. K_2O values in 9 of the representative suites are between 0.8 and 1.2 wt%; those from Easter Island and Nandewar are 0.4 and 1.9 wt%, respectively. Na_2O/K_2O ratios reflect mainly the variation in K_2O contents and range from 2 to ~7. The next section explores whether the diversity of peralkaline silicic extrusive rocks is derived from differing parental basalts, is a result of different fractionation histories, or is a combination of both factors.

6.2. *One-stage models: magmatic lineages*

Numerous studies have concluded that the peralkaline trachytes and rhyolites are ultimately formed by

Table 1. Representative basalt–peralkaline rhyolite suites

Suite	Nature	Rock types	Composition gap (SiO$_2$ range, wt%)	References
Boina	EARS	B, M, Be, T, P	X	1, 2
Erta'Ale	EARS	B, H, M, Be, Pt, C	X	3
Gedemsa	EARS	B, M, Be, Mt, Ct, Pt, P	X	4, 5
Olkaria	EARS	B, H, M, Be, Mt, Ct, C	X	6, 7
Pantelleria	Rifted margin	B, M, Mt, Ct, Pt, P	50–62	8, 9, 10
Ascension	Atlantic ocean	B, H, M, Be, Mt, Ct, C	X	11
Easter hotspot	Pacific ocean	B, M, Be, T, C	62–66	12
Socorro	Pacific ocean	B, H, M, Ct, Pt, P	54–61	13, 14
Terceira	Atlantic ocean	B, H, M, Be, Ct, C, P	60–65	15
Nandewar	Cont. intraplate	H, Ta, Tr, Mt, Ct, C	51–58	16

B, basalt; Be, benmoreite; C, comendite; Ct, comenditic trachyte; H, hawaiite; M, mugearite; Mt, metaluminous trachyte; P, pantellerite; Pt, pantelleritic trachyte; Ta, trachyandesite; Tr, trachyte. EARS, East African Rift System. References: 1, Barberi et al., 1975; 2, Field et al., 2012; 3, Barberi et al., 1974; 4, Peccerillo et al., 2003; 5, Giordano et al., 2014; 6, Macdonald et al., 2008; 7, Marshall et al., 2009; 8, Civetta et al., 1998; 9, White et al., 2009; 10, Neave et al., 2012; 11, Weaver et al., 1996; 12, Haase et al., 1997; 13, Bohrson and Reid, 1995; 14, Bohrson and Reid, 1997; 15, Mungall and Martin, 1995; 16, Stolz, 1985.

Table 2. Rocks identified as parental basalts in representative suites

Suite	Boina	Erta'Ale	Gedemsa	Olkaria	Pantelleria	Ascension	Easter Is.	Socorro	Terceira	Nandewar
wt%										
SiO$_2$	46.75	48.10	48.19	47.04	46.00	47.53	47.77	48.52	47.92	46.63
TiO$_2$	2.30	1.45	2.01	1.83	3.50	2.67	2.45	2.97	3.03	2.21
Al$_2$O$_3$	13.93	13.20	16.90	15.73	14.90	15.8	15.32	15.94	13.75	13.84
FeO*	10.96	10.31	9.91	11.07	11.30	11.50	10.65	10.82	11.27	10.78
MnO	0.19	0.17	0.20	0.18	0.18	0.17	0.17	0.17	0.20	0.15
MgO	9.75	10.13	8.47	7.77	7.01	6.65	8.58	6.78	7.71	9.66
CaO	10.08	12.06	9.19	11.85	11.00	10.35	9.82	9.67	10.66	8.37
Na$_2$O	2.70	2.45	2.75	2.41	3.50	2.81	2.98	3.43	3.20	3.12
K$_2$O	0.80	0.35	0.89	0.44	1.44	0.65	0.61	1.07	0.98	1.05
P$_2$O$_5$	0.35	0.24	0.39	0.24	0.99	0.59	0.31	0.58	0.62	0.60
LOI/H$_2$O$^+$	0.78	1.04	0.79	−0.13	—	−0.44	—	—	0.0	2.60
Total	98.59	99.50	99.69	98.43	99.82	98.28	98.66	99.95	99.34	99.01
Norm ne	—	—	6.0	—	5.7	—	—	0.12	0.80	—
Norm hy	2.7	3.8	—	3.0	—	10.5	5.3	—	—	0.48
Mg-no.	61.3	63.6	60.4	55.6	52.5	50.7	62.8	52.8	54.9	65.2
Cr (ppm)	—	—	227	71	—	156	269	146	268	277
Ni (ppm)	70	210	127	37	—	97	155	92	93	169

FeO*, all Fe as Fe^{2+}. Dash, no data. LOI, loss on ignition. Pantelleria data for high-Ti basalt suite. Terceira for rift-related suite.

Table 3. Selected geochemical features of peralkaline suites

	Maximum value (at MgO in brackets)				Concentration at 6 wt% MgO				P.I.*
	FeO*	TiO$_2$	Al$_2$O$_3$	P$_2$O$_5$	Al$_2$O$_3$	Na$_2$O	K$_2$O	FeO*	MgO
	(MgO value in brackets)								
Boina	16 (5.0)	3.4 (5.0)	16 (6.0)	0.7 (3.5)	16.0	3.1	1.1	15.0	≈0.1
Erta'Ale	17 (4.8)	3.1 (5.0)	16 (11)	1.2 (3.2)	15.5	3.1	0.8	14.0	1.2
Gedemsa	10 (8.0)	2.1 (5.1)	19 (4.2)	0.6 (5.0)	17.5	3.1	1.2	11.0	0.8
Olkaria	13 (5.0)	3.2 (3.5)	16 (8.0)	1.1 (3.5)	15.0	3.0	1.0	12.5	0.4
Pantelleria	14 (5.0)	4.0 (5.3)	16 (6.2)	1.3 (6.8)	16.0	3.5	1.0	11.5	0.3
Ascension	14 (7.0)	3.2 (4.5)	18 (3.5)	1.3 (3.5)	15.5	3.2	0.9	13.0	0.1
Easter hotspot	14 (6.0)	3.5 (5.5)	17 (8.0)	0.5 (7.5)	16.0	3.1	0.4	14.0	≈0.1
Socorro	14 (3.5)	4.2 (4.7)	16 (6.5)	1.8 (4.0)	16.0	3.8	1.0	11.5	0.2
Terceira-1	14 (4.0)	3.5 (4.0)	18 (3.5)	0.9 (2.8)	16.0	3.5	0.9	12.0	0.3
Terceira-2	13 (5.0)	4.0 (6.0)	17 (2.0)	1.5 (4.0)	14.0	3.7	1.0	12.5	0.3
Nandewar	13 (6.7)	3.0 (6.0)	17 (1.3)	1.6 (5.8)	15.0	3.5	1.9	12.0	0.5

P.I.*, peralkalinity index (mol. (Na$_2$O + K$_2$O)/Al$_2$O$_3$) achieved at given MgO value. Terceira-1 is comendite trend; Terceira-2 is pantellerite trend.

protracted fractional crystallization of alkali basalt magmas, along liquid lines of descent which include ferrobasalt, mugearite, benmoreite and metaluminous trachyte [Barberi et al., 1975, Weaver, 1977, Novak and Mahood, 1986, Mungall and Martin, 1995, Civetta et al., 1998, Peccerillo et al., 2003, Lowenstern et al., 2006, Macdonald et al., 2008, Parker and White, 2008, White et al., 2009, Ronga et al., 2010, Rooney et al., 2012, Hutchison et al., 2016a, Gleeson et al., 2017, Jeffery et al., 2017]. Although all these sequences generated peralkaline silicic endmembers, the evolutionary paths were all to some extent unique. As noted above, ten extrusive suites are used here to illustrate the range of magmatic lineages (Table 1). The lineages are presented in Figure 5, using MgO as a differentiation index. To avoid overcrowded plots, we use four *illustrative* suites for each oxide. Important geochemical markers for all suites are given in Table 3.

The suites all show a rather similar pattern of a gentle increase in SiO$_2$ abundances until ~3 wt% MgO, when SiO$_2$ is ~50 wt%, and then a sharper rise to values >70 wt%. For Al$_2$O$_3$, differentiation normally results in peaked trends, with maximum abundances being reached over a considerable range of MgO values, 0.5–8 wt%, and at variable maximum Al$_2$O$_3$ abundances, 16–19 wt% (Table 3). At So-

corro, however, Al$_2$O$_3$ levels decrease continuously [Bohrson and Reid, 1995]. In the "flat"/decreasing trends, plagioclase is reported to be the modally dominant phenocryst in the basalts [Weaver, 1977, Nelson and Hegre, 1990, Bohrson and Reid, 1995, Gioncada and Landi, 2010]. Interestingly, however, Al shows peaked behaviour even in suites where plagioclase is a phenocryst phase in the basalts (Tables 2, 3), implying that it has not been a significant fractionating phase in the basaltic magmas. Perhaps the crystals were not dense enough to separate from melt efficiently. Plagioclase formation is dependent on the Al/(Mg + Fe) ratio of the melt and on the pH$_2$O in the melt: low pH$_2$O tends to promote early crystallization [Gaetani et al., 1993].

As far as we are aware, only two extrusive peralkaline suites have passed through a two-feldspar stage, where plagioclase and alkali feldspar phenocrysts coexisted in equilibrium; where plagioclase is reported, it invariably forms cores in alkali feldspar and is residual from a higher-temperature stage [Barberi et al., 1974, White et al., 2009, Romengo et al., 2012]. The two exceptions are the Chopine trachyte from the Massif Central in France [Martel et al., 2013] and the Katenmening trachytes, Silali volcano, Kenya [Macdonald et al., 1995]. In a later section (Section 11), we examine the experimental information
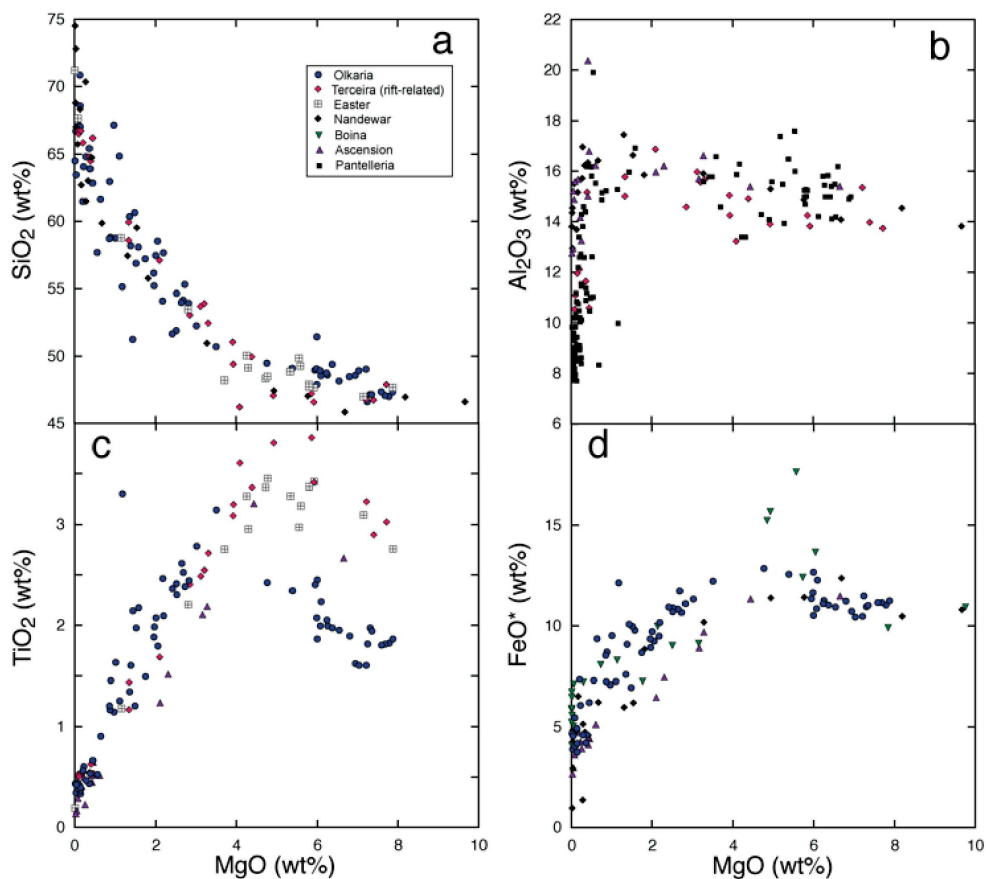
Figure 5. Plots of SiO$_2$ against MgO for selected oxides for basalt–peralkaline rhyolite suites. Each box contains data for four suites, chosen to represent different behaviours. In the Terceira case only data for the rift-related basalt–pantellerite sequence is used; for Ascension, analyses are from the intermediate Zr/Nb sequence. Data sources: Ascension—Weaver et al. [1996]; Boina—Barberi et al. [1975]; Easter Island—Haase et al. [1997]; Nandewar—Stolz [1985]; Olkaria—Macdonald et al. [2008], Marshall et al. [2009]; Pantelleria—Mahood and Baker [1986], Civetta et al. [1998], Avanzinelli et al. [2004], Ferla and Meli [2006], White et al. [2009]; Socorro—Bohrson and Reid [1995, 1997]; Terceira—Mungall and Martin [1995].

for the stability relationships of the Chopine trachyte and its significance for the development of peralkalinity. At Silali, the two-feldspar trachytes fit compositionally between mugearites and trachytes and have been modelled as part of the liquid line of descent.

Early plagioclase crystallization usually results in CaO increasing in residual melts until clinopyroxene joins the assemblage when abundances fall (e.g., at 6 wt% MgO; Nandewar and Easter). The order of appearance of plagioclase and clinopyroxene is dependent on melt Ca/(Mg + Fe) ratio and on pH$_2$O. As noted above, high water activities reduce plagio-

clase stability, resulting in melts with higher Al$_2$O$_3$ contents [Gaetani et al., 1993], e.g., as suggested for Aluto magmas by Gleeson et al. [2017]. Crystallization of clinopyroxene can affect the composition of residual melts in several ways. It depletes the melt in CaO and increases the FeO*/MgO ratio. If the pyroxene is nepheline-normative, it may exacerbate the trend towards silica saturation. More importantly, significant entry of Al into pyroxene will promote the peralkalinity of the residual melts; Bryan [1976] and Weaver [1977] invoked aluminous titanaugite as effective in promoting peralkalinity in the Socorro

and Emuruangogolak suites, respectively. Mahood and Baker [1986] crystallized Al- and Ti-rich clinopyroxenes in their experimental study of Pantescan basalts, affecting both the degree of silica saturation and the peralkalinity. In contrast, in their crystallization experiments of comendites from the Olkaria complex, Scaillet and Macdonald [2003] found that the crystallization of calcic clinopyroxene in slightly peralkaline rhyolites inhibited the increase in melt peralkalinity by counteracting the effects of feldspar.

In most suites, FeO* and TiO_2 show a peaked behaviour, with maximum values in the range 5–7 wt% MgO. In contrast, at Gedemsa, both show continuous decreases with decreasing MgO content. Many authors have ascribed the peaked trends to build-up of Fe and Ti in the melt until FeTi-oxides join the fractionating assemblage, when they are then removed from the melt. The point at which they appear as phenocrysts is dependent, *inter alia*, on fO_2; more reduced magmas will delay oxide crystallization. The trends are normally consistent with phenocryst assemblages, which show oxides appearing in the intermediate (hawaiitic–mugearitic) magmas. The Fe–Ti-depletion trends at Gedemsa [Peccerillo et al., 2003] and Nemrut [Macdonald et al., 2015] have been explained, on the basis of geochemical modelling, by FeTi-oxides joining the fractionating assemblage in the basaltic magmas, yet in neither case was oxide reported as a phenocryst phase in the basalts. Another problem can be the high proportions of oxides required by geochemical modelling which are greater than the observed proportions [e.g., on Pantelleria: White et al., 2009, Neave et al., 2012]. Neave et al. [2012], whose models required 12% magnetite to reproduce the liquids, appealed to preferential settling of oxides prior to eruption but this is not consistent with the common occurrence in these rocks of oxide–clinopyroxene clusters.

Na_2O levels increase to the trachyte stage, but then either increase or decrease towards rhyolitic compositions as feldspars become more sodic. In the Olkaria suite, considerable scatter in the rhyolites is related to Na loss on devitrification or secondary hydration. All suites show general increases in K_2O abundances, although at variable rates. In some suites, e.g., the rate increases at 3–4 wt% MgO (Olkaria); in others (Boina) the rate is rather constant. In both the Ascension and Nandewar suites K_2O levels

fall in the most evolved rocks (MgO <1 wt%). Gleeson et al. [2017] found that at the Aluto volcano crystallization of sanidine resulted in K depletion in residual melts, as predicted by rhyolite-MELTS modelling.

The series showing peaked Fe–Ti trends almost invariably show a similar behaviour of P. Maximum P_2O_5 concentrations are, however, usually achieved at lower MgO levels (Table 3). The peak concentrations for P reflect the appearance of apatite in the fractionating assemblage although this is not always noted petrographically. For example, apatite is not listed as a phenocryst phase in the mafic Gedemsa rocks [Peccerillo et al., 2003]. It is not clear what stabilizes apatite crystallization; the peak concentrations range from 0.6 to 1.8 wt% P_2O_5 (Table 3), so it cannot simply be P activity.

A notable feature of apatite compositions in the suites is the variable degrees of britholite (REE + Si) enrichment. Macdonald et al. [2012] suggested that the controlling factor might be the F/Cl ratio of the host rocks, britholite enrichment being stronger in magmas with F > Cl (e.g. Menengai and Olkaria) than in those with Cl > F (Pantelleria). The suggestion needs to be tested with data from more suites.

6.3. *Status of minor mafic phases*

It is important to establish whether minor sodic phases can fractionate from peralkaline rhyolites because their appearance would slow down the increase in peralkalinity of residual melts. Mbowou et al. [2012] and Renna et al. [2013] have invoked arfvedsonite fractionation in comendites from Lake Chad and Corsica, respectively, but the process was not satisfactorily modelled. Indeed, we know of no natural extrusive suite where a strong case for fractionation of either aegirine or sodic amphibole has been made.

The case for aenigmatite is more equivocal. White et al. [2009], for example, referred to aenigmatite as being part of the fractionating assemblage from metaluminous trachyte to pantellerite on Pantelleria but none of the models presented contained aenigmatite. In their modelling of the rhyolite array at the Main Ethiopian Rift volcanoes, Iddon and Edmonds [2020] proposed a fractionating assemblage including 19% aenigmatite, yet aenigmatite occurs only in minor modal amounts in pantellerites, usually <3%. Gleeson et al. [2017] argued that aenigmatite is not

accurately modelled because of a lack of experimental data to constrain its thermodynamic properties. Liszewska et al. [2018] have argued that a subgroup of melts in the Green Tuff on Pantelleria evolved along a quartz–alkali feldspar–aenigmatite cotectic. Such a trend would be open to experimental testing. Of course, aenigmatite usually appears very late during magma evolution when crystal separation may be hampered by melt viscosity, and thus has little real effect on the liquid trend [Mungall and Martin, 1995, Gleeson et al., 2017].

Perhaps the most fully documented occurrence of biotite phenocrysts in comendites is from the Olkaria complex, Kenya Rift Valley [Macdonald et al., 1987, Marshall et al., 2009], where it occurs as subhedral to euhedral crystals 0.5–1.5 mm long. Geochemical modelling by Macdonald et al. [1987] did not find a role for biotite in the differentiation of the comendites and it must be assumed that it was, at least in this case, a non-fractionating phase. Jeffery et al. [2016] found minor amounts of biotite phenocrysts in comenditic trachytes of the Furnas volcano, São Miguel, Azores, and using rhyolite-MELTS calculated that there was ~1% biotite fractionation in the latest evolutionary stages. In contrast, Jeffery et al. [2017] reported biotite phenocrysts in the comenditic trachytes of the Grota de Vale Ignimbrite Formation on Terceira but found no evidence from geochemical modelling that it was a fractionating phase. Gleeson et al. [2017] reported biotite forming <2% of the phenocryst assemblage in peralkaline rhyolites of the Aluto volcano but did not identify it in their modelled fractionating assemblages. In contrast, using major element mass balance calculations White et al. [2006] found that biotite was part of the fractionating assemblage in the comenditic Emory Peak Rhyolitic Member in the Pine Canyon caldera, Trans-Pecos Texas, accompanying alkali feldspar, quartz, magnetite, zircon and monazite. Further study of biotite–phyric suites can continue to test the efficacy of biotite fractionation but on current evidence its role seems normally to be minor.

6.4. *Status of kaersutite and orthopyroxene fractionation*

This section discusses the potential role of "unseen", usually higher pressure, phases in magma evolution. Two recent studies have focused attention on the possible role of kaersutite in the differentiation of alkali basalt to trachyte. Nekvasil et al. [2004] experimentally simulated incremental crystal fractionation of a *hy*-normative hawaiite towards sodic rhyolite. The experimental conditions were pressure 9.3 kbar, temperatures 1250–860 °C, bulk water content of the hawaiite > ~0.5 wt% and fO$_2$ ~1.5 log units below FMQ. The most evolved residual melts generated were trachytic, with SiO$_2$ ~64 wt%, relatively low Na$_2$O/K$_2$O ratios (~1), and compositions on the peraluminous/metaluminous boundary (mol. Al$_2$O$_3$/(CaO + Na$_2$O + K$_2$O) ≈ 1). The earliest stages were dominated by olivine–clinopyroxene crystallization but at 1060 °C kaersutite joined the assemblage and was the dominant phase down to 900 °C. An important result was an acceleration of silica enrichment and production of trachytic residual melts, the "mafic rhyolites" of Nekvasil et al. [2004]. The experiments outlined, therefore, a possible role for kaersutite fractionation at deep crustal pressures, although they did not proceed as far as producing peralkaline melts.

In the unusual, perhaps unique, case of the Marie Byrd Land province, West Antarctica, LeMasurier et al. [2011] proposed that pantellerites were derived by fractional crystallization of basanite magma. Their model suggested that basanite was generated within the asthenosphere at depths >50 km and then fractionated within the lithosphere (~30–35 km) to form metaluminous trachyte. The critical mechanism for crossing the thermal divide from silica-undersaturated to silica-saturated melts was fractionation of kaersutite, which LeMasurier et al. [2011] were able to model geochemically. Note the consistency between the inferred depth of kaersutite crystallization and the experimental results (9.3 kbar) of Nekvasil et al. [2004]. The trachytic melts then rose to high crustal levels (≤5 km), where fractionation under low fO$_2$ and low P_{H_2O} favoured a high plagioclase/clinopyroxene ratio and generation of pantelleritic magmas. Kaersutite phenocrysts were not recognized in the suite, which LeMasurier et al. [2011] ascribed to complete resorption during ascent from mantle depths. Geochemical modelling also showed the possibility that the pantellerites could have been derived by crystallization of an *ol-hy*-normative basalt but such rocks are not known in association with the pantellerites. The interesting dilemma, then, was to invoke a major fractionating

phase which is not seen, or a hypothetical parent magma which is not seen, in the actual rocks.

Other studies have invoked, on the basis of geochemical modelling, amphibole crystallization from the intermediate members of peralkaline suites. Mungall and Martin [1995] found that including amphibole in the fractionating assemblage was necessary in order to model the transition from mugearite to felsic magma in the peralkaline suites of Terceira, Azores. In contrast, Jeffery et al. [2017] found, from least-squares mass balance models, that inclusion of amphibole resulted in model failure. During modelling of the basalt–comenditic trachyte suite from the Rallier-du-Baty Peninsula, Kerguelen, Gagnevin et al. [2003] suggested that certain aspects of the HFSE distribution could be explained by crystallization of amphibole at an intermediate stage. Field et al. [2012] referred to disequilibrium amphibole occurring in a Dabbahu (Boina) pantellerite, which may be relict from an earlier fractionation stage. The potential role of amphibole in the evolution of peralkaline silicic suites seems to be a real possibility if, for the moment, not robustly documented.

Orthopyroxene phenocrysts have been reported in the comenditic Shungura Tuff, Kenya [Martz and Brown, 1981], comenditic ignimbrites of the Black Mountain volcanic centre, Nevada [Vogel et al., 1987], the comenditic Wild Horse Mesa Tuff, California [McCurry, 1988], and comendites of the Nemrut volcano, Turkey [Macdonald et al., 2015]. Sumner and Wolff [2003] recorded hypersthene phenocrysts in trachytes and comendites of the "TL" ignimbrite, Gran Canaria, the hypersthene reacting to clinopyroxene and magnetite in the comendite. Using MELTS modelling, Rooney et al. [2012] showed that comendites of the Chefe Donsa suite, Ethiopia, could have been formed by 70% fractionation from trachyte magma of an assemblage including orthopyroxene; however, no orthopyroxene phenocrysts were recorded in the rocks.

As far as we are aware, no experimental study of a peralkaline silicic rock has yet generated orthopyroxene and its stability range in peralkaline magmas is far from clear. It cannot, however, be precluded that some peralkaline suites pass through the orthopyroxene stability field at high pressure, the mineral normally being resorbed at lower pressure. Orthopyroxene was described in the trachyandesite to sodic trachyte portion of the composite P1 ig-

nimbrite at Gran Canaria, Canary Islands [Freundt and Schmincke, 1995], where it occurs in equilibrium with clinopyroxene, plagioclase, ilmenite, and magnetite that suggest higher temperatures (900–815 °C), more oxidizing conditions (fO$_2$ > FMQ), and potentially higher pressures (340 ± 150 MPa) that are described for most peralkaline systems. Orthopyroxene was also reported in alkalic (but metaluminous) rhyolite from the Kane Wash Tuff [Kane Springs Wash Caldera, Nevada; Novak and Mahood, 1986], where the equilibrium mineral assemblage also provides evidence of higher temperatures (>820 °C) and pressures (~480 MPa) with oxygen fugacities at or slightly above the FMQ buffer.

7. The peralkaline silicic endpoint(s)

Silicic suites reach peralkalinity, in the sense of having a molecular excess of (Na$_2$O + K$_2$O) over Al$_2$O$_3$, when SiO$_2$ contents are in the range 62–70 wt% (MgO ~1 wt%), i.e., in the trachyte–rhyolite range. They enter "peralkaline space" at different points and then follow different trends (Figure 6). In detail, in many centres the magmas follow more than one trend. On Pantelleria, for example, almost all the eruptive episodes followed slightly different trends [Jordan et al., 2021]. On Terceira two trends are discernible from mafic to silicic: one follows a slightly lower Al, higher Fe trend and ends up as pantellerites; the other follows a slightly higher Al, lower Fe trend and produces comenditic trachytes and comendites [Mungall and Martin, 1995]. The two trends were a result of different primary basalts and the timing and extent of FeTi-oxide fractionation. The different trends must be a result of different fractionating assemblages and therefore of initial compositional differences and/or variable conditions of crystallization. LeMasurier [2019] used mass balance modelling to show that comendites and pantellerites of Marie Byrd Land followed separate pathways *via* fractional crystallization. The pathway to comendites involved fractionating a relatively large proportion of FeTi-oxides and a low plagioclase/pyroxene ratio; that to pantellerites involved lower proportions of FeTi-oxides and higher plagioclase/pyroxene ratios.

All trends, including those of glasses produced experimentally from pantellerites, tend to converge on a small range of compositions, the endpoints of
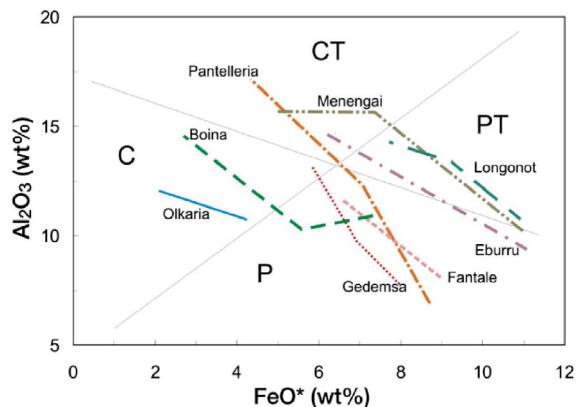
Figure 6. Trends of selected peralkaline suites on an FeO*–Al$_2$O$_3$ plot [after Macdonald et al., 2011]. Rock types: C, Comendite; CT, Comenditic Trachyte; P, Pantellerite; PT, Pantelleritic Trachyte.

which have FeO* ~13 wt% and Al$_2$O$_3$ ~5 wt% (Figure 7a). Macdonald et al. [2012] referred to these endpoints as the effective minima compositions (EMC) for peralkaline silicic magmas. The use of the term *effective* alluded to the fact that melts more evolved than this are highly unlikely to separate from their crystal mush hosts. The relatively high density due to the high Fe contents and their normal occurrence as low melt fractions are also likely to inhibit crustal ascent and they remain trapped at depth. Possible extruded exceptions are a pantellerite obsidian (lava?) from Fantale, Ethiopia [Lacroix, 1930] and a lava from the Mt Takahe volcano, Marie Byrd Land [LeMasurier et al., 2018]. It is important to note that, at least at Boseti, the highly evolved compositions were reached by the fractionation of alkali feldspar + fayalite + hedenbergite + oxide ± quartz assemblages, the dominant assemblage in the associated pantellerites.

Increasing fractionation, as measured by P.I., is accompanied by Si enrichment until P.I. reaches about 2.00, when the trend reverses to Si decrease (Figure 7b). It is as yet unclear what mineral assemblage has generated the Si-depletion trend, although quartz fractionation may have been involved. In two extraordinary cases, the melt evolved significantly beyond the EMC. A matrix glass from the Boseti volcano, Ethiopia, has 2.2 wt% Al$_2$O$_3$ and 16.99 wt% FeO* [Macdonald et al., 2012], and interstitial glass from the Mt Takahe pantellerite has 1.70 wt% Al$_2$O$_3$,
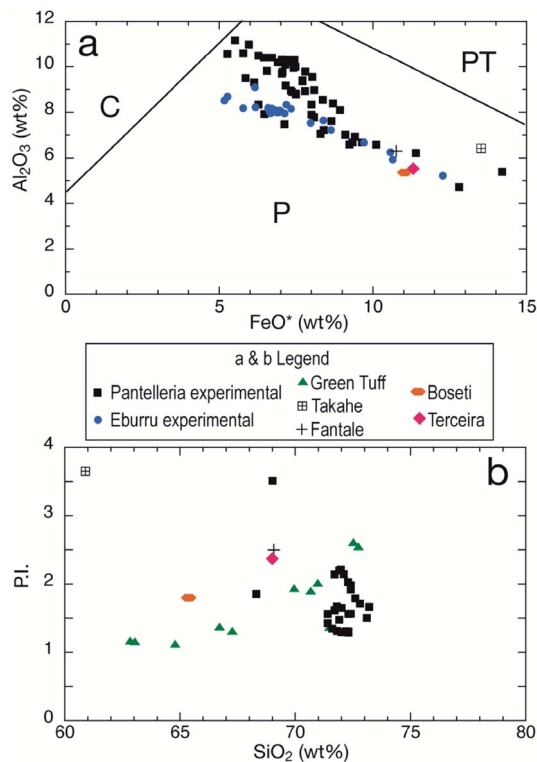

Figure 7. (a) FeO*–Al$_2$O$_3$ plot of highly evolved pantelleritic compositions. Data for Eburru and Pantelleria are for glasses produced experimentally from Eburru and Pantescan pantellerites by Scaillet and Macdonald [2006b] and Di Carlo et al. [2010], respectively. Fantale: obsidian from the Fantale volcano, Ethiopia [Lacroix, 1930]. Boseti: average lighter matrix glass in sample B375, Boseti volcano, Ethiopia [Macdonald et al., 2012]. Melt inclusion in fayalite, Terceira Island, Azores [Mungall and Martin, 1995]. Mt Takahe, lava from Mt Takahe volcano, Marie Byrd Land [LeMasurier et al., 2018]. (b) SiO$_2$–Peralkalinity Index (P.I.) plot for selected suites and rocks. Data sources: Green Tuff, Pantelleria—Liszewska et al. [2018]; Boseti, Fantale, Takahe and Terceira—as for Figure 7. Experimental glasses determined on Pantescan pantellerite at P = 25–150 MPa, T = 680–800 °C, fO_2 ≤ NNO, and H$_2$O$_{melt}$ up to 6 wt% [Di Carlo et al., 2010]. Experimental glasses from Eburru—Scaillet and Macdonald [2006b]. Rock types: C, Comendite; P, Pantellerite; PT, Pantelleritic Trachyte.

16.25 wt% FeO* and a P.I. of 13.6 [LeMasurier et al., 2018]. It plots in the trachyte field in the TAS classification. Presumably these compositions were a result of massive feldspar crystallization; this would be consistent with the observation that alkali feldspar is the only phenocryst in the Takahe host rock.

An unresolved question is whether there is, in fact, more than the small range of EMC in the natural systems shown in Figures 7a and b. We noted earlier (Section 5) the presence in the Q-Ab-Or-Ac-Ns system of a low-temperature zone, equivalent to the low-temperature valley in the granite system, towards which peralkaline silicic melts migrate during fractional crystallization. This would seem to be consistent with the convergence of natural and experimental melts towards the EMC on Figures 7a and b. However, on the basis of alkali feldspar–liquid relationships in Menengai trachytes, Macdonald et al. [2011] argued that there might in fact be more than one such low-temperature zone, with, in particular, certain pantelleritic trachytes following different trend(s) to comendites and pantellerites. For the Menengai melts to reach the EMC a sharp decrease in FeO*/Al_2O_3 ratios would be required (Figure 6). A set of experiments comparable to those by Scaillet and Macdonald [2006b] and Di Carlo et al. [2010] would help to resolve this issue.

Whether a given suite reaches the minimum composition(s) is simply a function of the degree of fractionation achieved. All peralkaline silicic suites have the *potential* to generate pantellerites given suitable tectonic and thermal conditions and assuming that the lowest-temperature melts can be satisfactorily separated from crystals.

8. Geochemical modelling

A major approach to using the analytical data base of peralkaline silicic rocks is geochemical modelling, where various mathematical and thermodynamic models are used to test the viability of petrogenetic processes, such as fractional crystallization, partial melting and magma mixing. This section outlines the most commonly employed models, commenting on their strengths and weaknesses.

The MELTS and rhyolite-MELTS models [Gualda et al., 2012] have been increasingly widely used to investigate the role of fractional crystallization under variable $P–T–fO_2$ conditions, and with variable starting water contents [Peccerillo et al., 2003, Ronga et al., 2010, White et al., 2009, Çubukçu et al., 2012, Rooney et al., 2012, Macdonald et al., 2015, Jeffery et al., 2017, Hutchison et al., 2018]. Generally, the models have been successful at predicting the liquid lines of descent and the mineral assemblages and compositions. Rhyolite-MELTS does not, however, model accurately the formation of hydrous phases such as amphibole, biotite, and apatite [Gualda et al., 2012]. Rooney et al. [2012] found that rhyolite-MELTS tends to overestimate melt P_2O_5 concentrations, as a result of deficiencies in the apatite solubility model. In their modelling of fractional crystallization in peralkaline ignimbrites of Terceira, Jeffery et al. [2017] noted that rhyolite-MELTS failed to model conditions at temperatures <850 °C, especially the feldspar compositions.

One result of the geochemical modelling is the information it has provided on the existence, or otherwise, of the so-called Daly Gap. In the next section, the modelling results are incorporated with other lines of evidence to explore the significance of the gap in peralkaline silicic systems.

9. Significance of the Daly Gap

In some peralkaline-oversaturated suites, marked by crosses in Table 1, there is an essentially complete series of *melt* compositions between basalt and trachyte, although intermediate members, roughly corresponding to mugearites and benmoreites, are usually volumetrically minor, especially in continental volcanoes. Other suites, however, show composition gaps, albeit over different SiO_2 ranges (Table 1). The absence or scarcity of intermediate magmas is the basis of the Daly Gap, the significance of which has exercised the minds of petrologists since the days of Bunsen [1851] without a completely satisfactory resolution. The majority of recent studies on peralkaline silicic suites have ascribed the formation of the trachyte and rhyolite members to protracted fractional crystallization of basaltic magma and several mechanisms to explain the Daly Gap have been proposed.

9.1. *Physical controls*

The apparent absence of intermediate eruptives has been related to various physical controls. Weaver [1977], for example, suggested that high density

and/or crystal content prevented their eruption at Emuruangogolak volcano, Kenya, and Mungall and Martin [1995] and Jeffery et al. [2017] attributed their absence from Pico Alto, Terceira, at least partly to similar controls. Rooney et al. [2012] have proposed that, at Ethiopian Rift volcanoes, intermediate melts are not extracted from crystal–liquid mushes because there has been insufficient crystallization to form a rigid framework, generally at about 50–60% crystallinity. Siegburg et al. [2018] also argued that mafic magmas cannot dynamically ascend through low-density felsic reservoirs.

9.2. *Rapid differentiation through a short crystallization interval*

In some suites evolving from basalt to peralkaline rhyolite, geochemical modelling has shown that SiO_2 values do not change linearly. There are stages, especially in intermediate compositions, where the values can change rapidly over a short temperature interval [Mushkin et al., 2002]. White et al. [2009] and Gleeson et al. [2017] have proposed this mechanism to explain the Daly Gaps at Pantelleria and Aluto volcanoes, respectively. Figure 8 shows the rate of change of SiO_2 during fractional crystallization at Aluto volcano modelled by Gleeson et al. [2017] for assumed wall-rock temperatures of 500 and 300 °C. The gap, or a relative scarcity of intermediate magmas, occurs at broadly similar SiO_2 values, e.g., 50–62 wt% at Pantelleria and 50–64 wt% at Aluto, reflecting the broadly similar fractionating assemblages in these peralkaline systems.

9.3. *Plutonic xenoliths*

Some studies have suggested that the missing intermediate rocks are represented by plutonic xenoliths. Comagmatic hypabyssal xenoliths of intermediate composition fill the compositional gap in the lavas of the Santa Barbara and Pico Alto volcanoes, Terceira [Mungall and Martin, 1995]. Freundt-Malecha et al. [2001] considered monzonitic and syenitic xenoliths in the rhyolite–trachyte–basalt composite ignimbrite P1 on Gran Canaria to be the "missing links" in the bimodal suite. Boulders of amphibole-bearing monzonites and monzogabbros in the Rallier-du-Batty Peninsula, Kerguelen are thought by Gagnevin et al.
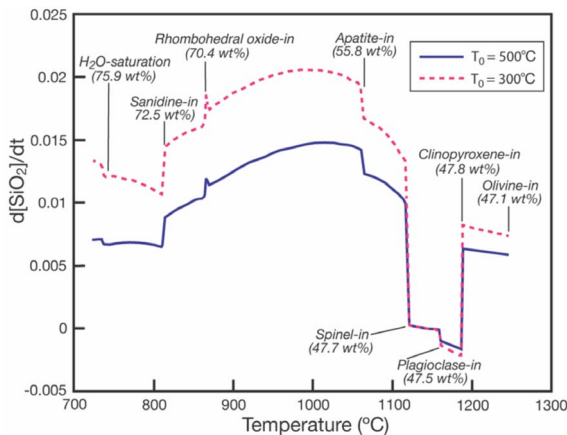

Figure 8. SiO_2 variation as a function of time $(d[SiO_2]/dt)$ in silicate melt during fractional crystallization, plotted against magmatic temperature. Two wall-rock temperatures (T_o) were assumed in the modelling (500 and 300 °C). Order of phenocryst appearance inferred for Aluto volcano, Ethiopia. Note the sharp increases in $d[SiO_2]/dt$ when FeTi-oxides, and to a lesser extent apatite, crystallize. Modified from Gleeson et al. [2017].

[2003] to represent intermediate magmas formed at depth but not erupted. Syenitic xenoliths are common in the Green Tuff, Pantelleria (Figure 9a). Ferla and Meli [2006] reported syenogabbroic and syenodioritic xenoliths in trachytic lavas of Pantelleria which compositionally fill the gap between basalts and trachytes on the island. However, they concluded from mineralogical and geochemical evidence that they had formed by the mixing of hawaiitic and trachytic magmas. Detailed petrographical study is clearly required to determine the origin of plutonic xenoliths.

9.4. *Magmatic enclaves*

Many studies have recorded the presence in the salic members of enclaves representing chilled melts of intermediate composition, e.g. trachybasaltic inclusions on Mayor Island [Ewart et al., 1968, Rutherford, 1978], leucoandesites in Caenozoic comendites of SW Sardinia [Morra et al., 1994]; mafic enclaves at Pantelleria [Ferla and Meli, 2006], trachyandesitic inclusions in the Gold Flat pantellerite, Nevada [Mac-
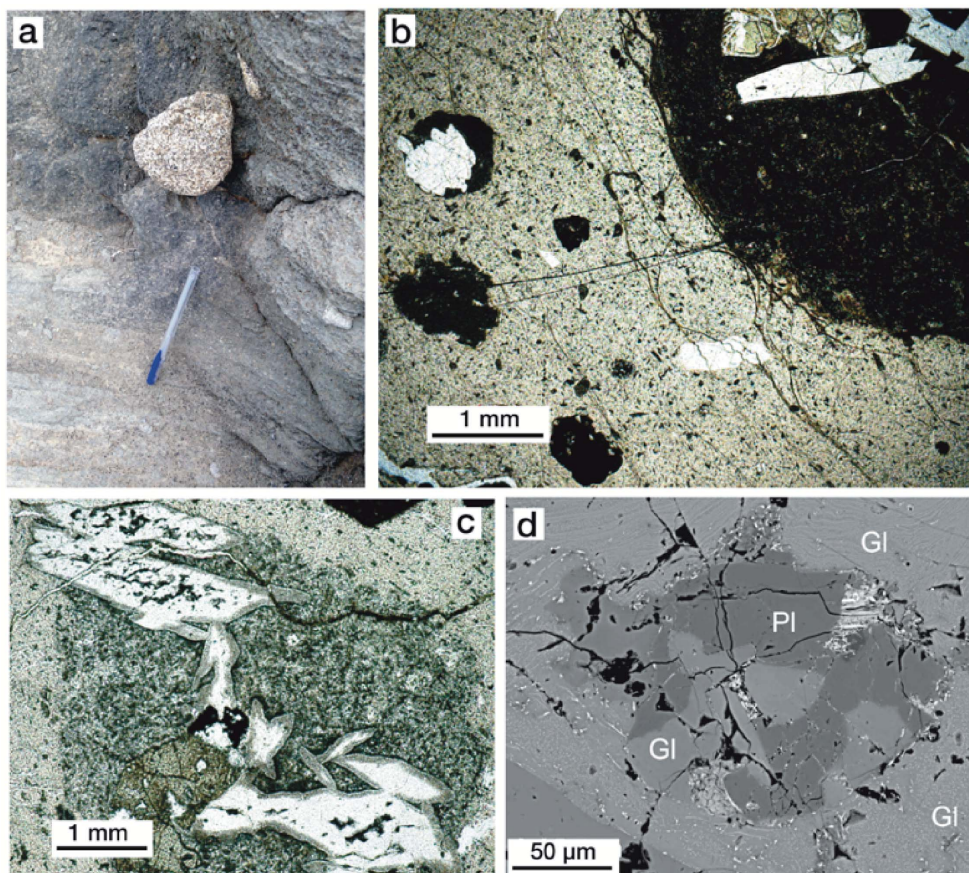
Figure 9. (a) Syenite nodule in pantelleritic Green Tuff, Pantelleria. (b) Mafic inclusions (dark) in comendite (light brown). Largest inclusion contains a disaggregated gabbroic xenolith; inclusion at top right contains a partially resorbed alkali feldspar xenocryst. (c) Disaggregating syenite xenolith in magmatic inclusion of intermediate composition in comendite host. (b) and (c), from Greater Olkaria Volcanic Complex, Kenya [based on Macdonald et al., 2008]. (d) Highly resorbed plagioclase (Pl) antecryst (An_{26-23}) with glass (Gl) in pantellerite, Gold Flat Tuff, Nevada [Macdonald et al., 2019].

donald et al., 2019] and mafic enclaves in comendites of the Olkaria Complex [Figure 9b; Macdonald et al., 2008]. While apparently providing strong evidence for the presence of intermediate magmas in the system, some studies have interpreted them as the products of mixing between basalt and trachyte magmas [Ferla and Meli, 2006, Romengo et al., 2012]. As noted for the plutonic xenoliths, petrographic and mineral chemical studies are needed to determine the mode of origin. The sample shown in Figure 9c shows a complex assemblage of a disaggregating syenite xenolith in a magmatic inclusion of intermediate composition in a comendite host from the Olkaria Complex [Macdonald et al., 2008].

9.5. *Phenocryst assemblages*

Megacryst assemblages in peralkaline trachytes and rhyolites often provide evidence for the crystallization of magmas of intermediate composition, for example plagioclase cores to alkali feldspar phenocrysts and forsteritic cores to olivine phenocrysts in rhyolites [White et al., 2009, Macdonald et al., 2012, 2019, Jeffery et al., 2017, Liszewska et al., 2018, Iddon et al., 2019, Parker, 2019, Neave, 2020]. The crystals are not in equilibrium with their host melts and are taken to be residual from an earlier stage of crystallization and from less evolved magmas (Figure 9d).
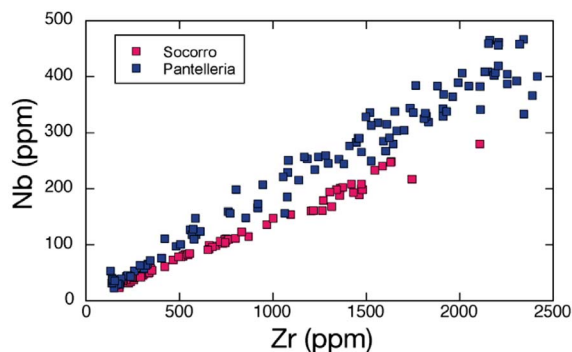
Figure 10. Zr–Nb plot for eruptive suites of Pantelleria and Socorro. Data sources: Pantelleria, Avanzinelli et al. [2004], Civetta et al. [1998], White et al. [2009]; Socorro, Bohrson and Reid [1997].

Figure 11. Partial melting of syenite xenolith (residual sanidine crystal (Sa) at top left) to form a pale glass with perlitic cracks (P) and a darker glass with feldspar microlites and vermicular quartz. Olkaria complex, Kenya, BSE image. After Macdonald et al. [2008].

9.6. *Geophysical evidence for intermediate magmas at depth*

Based on a positive gravity anomaly beneath Pantelleria, Mattia et al. [2007] suggested that it may be a result of high-density intermediate magmas trapped deep in the system. Similarly, a positive gravity anomaly in the shallow crust beneath Aluto caldera may provide evidence for the density filtering of intermediate magmas forming a Daly Gap [Iddon et al., 2019]. The anomalies do not, however, provide unequivocal evidence for the nature of the source rocks; they could, for example, be hawaiitic or mixed magma rocks.

9.7. *The need for a full petrographic basis*

We discuss here one aspect of composition gaps which highlights the need for detailed petrographic information to accompany the geochemical data. The basalt–peralkaline rhyolite suites of Socorro Island and Pantelleria are in many ways closely similar (Figure 10). The range of lithologies is from alkali basalt through hawaiite to trachyte to comenditic trachyte (±pantelleritic trachyte) to pantellerite. The major and trace element compositions of the main components are broadly similar. A Zr–Nb plot (Figure 11) shows strongly positive relationships in both suites, with slightly different Zr/Nb ratios. The continuous nature of the trends could be taken to point
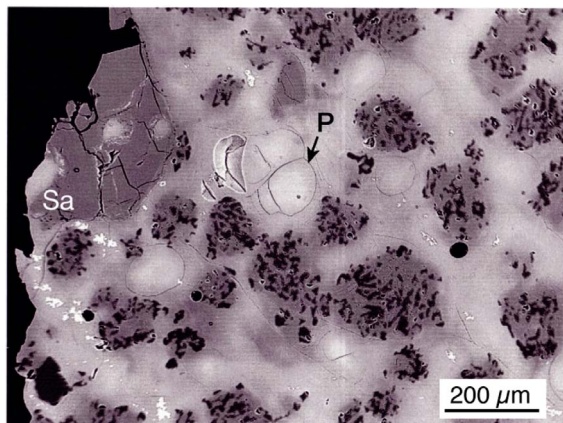
to crystal fractionation as the dominant differentiation mechanism. However, the Zr–Nb plot disguises the fact that there is, as noted above, a major composition gap in both series, SiO_2 ~54–61 wt% on Socorro and 50–62 wt% on Pantelleria. In both suites, trachytic rocks have certain trace element contents overlapping those in mafic rocks, the overlap being partly used to propose two different petrogenetic histories.

For Pantelleria, White et al. [2009] showed that the gap is at least partly filled by feldspar-accumulitic trachytes, with, *inter alia*, lower incompatible trace elements (ITE) and higher Ba contents than the non-accumulitic equivalents, thus confirming the existence of the Daly Gap in *magmatic* compositions. They were, however, able to model compositional variation in the suite as dominated by fractional crystallization, suggesting that the compositional gap was a result of rapid crystallization. Such a model cannot be applied to Socorro, where the rocks are aphyric or sparsely phyric. Bohrson and Reid [1995, 1997] used the overlapping trace element evidence to suggest that the mafic and silicic rocks on Socorro had independent origins, the salic rocks having been formed by partial melting of alkali basalts or gabbros. Thus, the essentially continuous nature of the Zr–Nb relationships masks, for Pantelleria, the existence

of a composition gap, and, for Socorro, may relate to independently evolving magmas. The point to be stressed from this example is that the significance of composition gaps can be properly assessed only on the basis of full petrographic information.

In summary, we take the view that in the majority of peralkaline silicic suites the bulk of petrological and geochemical evidence points to fractional crystallization having produced an essentially continuous range of melts, some of which were prevented from being erupted through physical or thermodynamic discrimination.

10. Role of crust

In this section, three processes involving crustal rocks are considered: (i) two-stage models, where mafic rocks are partially melted to form peralkaline melts or their parental melts; (ii) partial melting of continental crust; and (iii) crustal contamination.

10.1. *Two-stage models*

Two-stage models for the origin of peralkaline silicic rocks usually involve partial melting of mafic rocks (underplated?) to form trachyte, followed by fractional crystallization of the trachyte to form peralkaline rhyolites [Pantelleria: Lowenstern and Mahood, 1991, Avanzinelli et al., 2004; Socorro: Bohrson and Reid, 1997; Ethiopia; Trua et al., 1999]. The models have been developed partly to explain the volumetric excess in many peralkaline provinces of felsic rocks over mafic rocks, and the absence or scarcity of intermediate compositions as explanations for the Daly Gap. Other factors invoked include trace element features inconsistent with a fractional crystallization hypothesis but compatible with partial melting [Bohrson and Reid, 1997, Trua et al., 1999], the relatively low water contents of pantellerites [Lowenstern and Mahood, 1991] and evidence from clinopyroxene chemistry, where compositional trends in pyroxenes in mafic and silicic rocks indicate different parental magmas [Avanzinelli et al., 2004]. The [Lowenstern and Mahood, 1991] model fails, however, to take account of polybaric degassing episodes at Pantelleria [White et al., 2009], whilst White et al. [2009] showed that clinopyroxene chemistry at Pantelleria is actually more compatible with fractional crystallization than partial melting.

Major element geochemical modelling has been used to confirm the potential viability of the partial melting of the alkali basalt/gabbro model. Bohrson and Reid [1997] calculated that moderate degrees (5–10%) of modal equilibrium melting of Socorro alkali basalts could generate magmas compositionally similar to the Socorro felsic rocks. Using equilibrium melting models, Peccerillo et al. [2003] found that about 10–30% melting of a basalt/gabbro could generate the Gedemsa felsic rocks. However, as White et al. [2009] have stressed, major element mass balance models cannot effectively discriminate between (Rayleigh) fractional crystallization and equilibrium batch melting, a point acknowledged by Peccerillo et al. [2003] and Bohrson and Reid [1997].

Syenogabbroic and syenodioritic xenoliths in trachytic lavas from Pantelleria contain glass which varies in composition from metaluminous trachyte to peralkaline quartz trachyte to pantellerite. The glasses are thought to have formed by partial melting of the hosts [Ferla and Meli, 2006]. However, in detail they are not similar to other Pantescan pantellerites. Comendites of the Olkaria complex, Kenya Rift Valley, contain syenitic xenoliths in basalts which also experienced partial melting [Macdonald et al., 2008]. The glasses range from ±c-normative to ac-normative. In one example (Figure 11), partial melting produced a pale, peralkaline glass and a darker glass containing vermicular quartz and feldspar microlites. It is poorer in SiO_2, TiO_2, FeO*, MnO and CaO, and richer in Al_2O_3, Na_2O and K_2O than the peralkaline variety. This is consistent with an increasing ratio of alkali feldspar to mafic components in the residual solid as melting proceeded. The peralkaline glasses are comenditic but compositionally distinct from the host comendites, as in the Pantescan case above. It appears, then, that although peralkaline melts may be generated locally by the partial melting of xenoliths, they do not generally follow the main liquid line of descent.

As noted by Scaillet and Macdonald [2003] and Caricchi et al. [2006], no experimental study has yet produced peralkaline melts by partial melting of crustal rocks, ranging from underplated basalts and gabbros to higher-level, more salic lithologies. Such a process would need volatile fluxing, as suggested by Bailey [1980], Bailey and Macdonald [1987] and Scaillet and Macdonald [2003], but that has not been demonstrated experimentally either.

10.2. *Partial melting of continental crust*

Here we discuss models of the formation of peralkaline silicic rocks by the partial melting of continental crust; basalt may be the heat source promoting the melting. Recourse to crustal melting models has commonly been made to explain the large volumes of silicic rocks in some provinces compared to the associated basalts. However, models of crust–basalt interactions have shown that the amount of basalt needed to generate a given amount of silicic magma by melting via enthalpy transport is broadly similar to that needed for crystal fractionation [Barboza and Bergantz, 2000, Dufek and Bergantz, 2005].

Through comparison of the major element compositions of the comendites of the Olkaria (Naivasha) complex with phase equilibria in the system Na_2O–K_2O–Al_2O_3–SiO_2, Bailey and Macdonald [1970] suggested that the comendites represent a path of increasing partial melting of crustal rocks in the presence of an alkali-bearing vapour. Macdonald et al. [1987] also invoked a model for the Olkaria rocks of partial melting of heterogeneous crustal source rocks, followed by variable amounts of fractional crystallization, calling on an important role for volatiles in promoting peralkalinity and in controlling trace element distribution patterns. Davies and Macdonald [1987] showed that whereas Sr–Nd isotope relationships are consistent with formation of the Olkaria rhyolites by fractionation of the associated basalts by ACF, Pb isotopic systematics showed that the basalts and rhyolites are not cogenetic. They proposed that the rhyolites represent crustal melts formed at ~6 km depth. U-series disequilibria and Th-isotopes were used by Black et al. [1997] to confirm the crustal origin of the rhyolites. More recently, Macdonald et al. [2008] presented evidence from matrix glasses in the trachytes that the rhyolites are in fact the products of crystal fractionation of basalt, but they did not offer an explanation for the differences in Pb isotope compositions.

The Pine Canyon caldera, Trans-Pecos Magmatic Province, Texas, erupted peralkaline quartz trachyte, rhyolite and high-silica rhyolite lavas and ash-flow tuffs about 32–33 Ma [White et al., 2006]. The trachytes and rhyolites can be related to associated basalts and mugearites by fractional crystallization, but the peralkaline high-silica rhyolite is thought to have formed by ~5% partial melting of mafic gran-

ulite at <25 km depth, melting having been promoted by heat from basaltic intrusions coupled with metasomatism by a F-rich volatile phase. High-silica comendite associated with the Pine Canyon system are strongly depleted in incompatible trace elements compared to the trachyte-low silica rhyolite series and have much lower Zr/Hf, Nb/Ta, and Ce/Yb ratios consistent with a crustal origin [Joachum et al., 1986, Green, 1995, White and Urbanczyk, 2001]. This conclusion was supported by a major element mass balance model with good results ($\Sigma r^2 = 0.370$) and a geologically reasonable residual assemblage that requires a similar amount of high-silica comenditic melt (~4%) as trace element models (~5%).

10.3. *Role of crustal contamination*

Many studies have invoked a role for crustal contamination, and specifically Assimilation–Fractional Crystallization (AFC), in the evolution of peralkaline rhyolitic suites. The evidence always comes from trace element and isotopic data which are shown to be incompatible with closed-system evolutionary models. Few (if any) papers have dealt with the mechanism of contamination, e.g. by incorporation of partially melted host rock, or by some sort of selective diffusive process.

Transitional basalts of the Olkaria (Naivasha) complex, Kenya, are thought to have assimilated variable amounts of Proterozoic amphibolite facies crust Davies and Macdonald [1987]. Bohrson and Reid [1995] argued that the alkali basalts of the Socorro suite assimilated small amounts of Fe-oxyhydroxides, an important constituent of metalliferous sediments, in small magma chambers located in the shallow oceanic crust or within the volcanic edifice. Contamination of peralkaline trachytes on São Miguel, Azores, by syenites altered by seawater was proposed by Snyder et al. [2004]. Alkali basalt at the Pine Canyon caldera, Trans-Pecos Texas, evolved by ~60–70% fractional crystallization coupled with significant assimilation of shale wall rock (M_a/M_c (mass assimilated/mass crystallized) = 0.3–0.4) to produce peralkaline quartz trachyte [White et al., 2006].

Mafic magmas in various suites of the Main Ethiopian Rift experienced variable degrees of contamination at various depths in the heterogeneous Pan-African crust [Rooney et al., 2012, Trua et al.,

1999]. Fractional crystallization of the Gedemsa magmas was accompanied by small amounts of assimilation of crustal material (M_a/M_c < 0.1) [Peccerillo et al., 2003]. Small degrees of contamination have also been invoked for the Marie Byrd Land suite (<3%; LeMasurier et al. [2011]. In contrast, Hutchison et al. [2016a, 2018] and Gleeson et al. [2017] argued that several volcanoes of the Main Ethiopian Rift which have erupted basalts and peralkaline rhyolites show evidence of no, or minimal, crustal assimilation. Hutchison et al. [2018] suggested that this might, at least partly, be because the crust becomes less fusible as rifts mature. White et al. [2020] also found that the basalts of Pantelleria experienced no significant crustal component. The Millennium eruption of the Changbaishan-Tianchi volcano apparently involved magmas showing no evidence of contamination [Wei et al., 2013].

An important question is whether the assimilation can significantly change the direction of the liquid line of descent of residual melts, in particular the transition from silica-undersaturation to silica-oversaturation. One possible example is from the Leyva Canyon volcano, Trans-Pecos Magmatic Province, Texas, where White and Urbanczyk [2001] found that mixing of ne-normative basaltic magma with a high-Al_2O_3 crustal component resulted, *inter alia*, with silica-oversaturated mildly peralkaline felsic rocks.

11. Experimental evidence for the origin of peralkaline silicic rocks

11.1. *Experiments on mafic compositions*

Mahood and Baker [1986] studied experimentally the least-evolved basalt from Pantelleria under anhydrous conditions at 1 atm along the FMQ buffer and at 8 kbar to determine the liquid line of descent. The 1 atm experiments reproduced more closely the natural trend. However, after even ~70% crystallization, the SiO_2 content of the melt was still 50 wt%, far removed from the trachytic members of the suite. Nekvasil et al. [2004] attempted to generate peralkaline salic melts by experimental simulation of incremental crystal fractionation of a hawaiitic magma. They suggested that the spectrum from hawaiite to rhyolite could be produced by fractionation at 9.3 kbar with bulk water contents (in the starting material)

of >~0.5 wt% at fO_2 ~1.5 log units below FMQ. The most evolved melt synthesized had 63.99 wt% SiO_2 and a P.I. of 0.89, i.e., it was a metaluminous trachyte. Caricchi et al. [2006] conducted an experimental study of a hydrous, transitional alkaline basalt at 0.5 to 1 GPa and 950 to 1100 °C. They found that melts in fractional crystallization experiments approached the natural rock trend leading to the transition from subaluminous to peralkaline residual melts. However, the most evolved melt had 61.94 wt% and a P.I. of 0.71, considerably removed from peralkalinity. Similar results were found by White et al. [2009] during geochemical modelling of the transition from basalt to trachyte; in this case, equilibrium crystallization models produced melts with low P.I. (0.62–0.78); fractional crystallization was required to generate peralkalinity.

The failure of the experiments to produce peralkaline silicic compositions probably reflects the fact that in nature the most peralkaline products represent only a very small fraction of the starting basalt, in the case of pantellerites <5%. Such small melt fractions would not normally be discernible in the experiments. Attempting to quantify conditions in intermediate compositions, Rondet et al. [2019] conducted high $P–T$ experiments on a trachyandesite from the Pavin Massif Central, France. The phenocryst assemblage was plagioclase, amphibole, clinopyroxene and Fe–Ti oxides. Matrix glass and melt inclusions had trachytic compositions, some being mildly peralkaline. The experiments constrained the pre-eruptive conditions as 970–975 °C, 150–200 MPa, NNO + 1.5, and 4.5–5.5 wt% melt H_2O. The experimental glasses, however, were trachytic but peraluminous.

11.2. *Metaluminous to peralkaline transition*

Evidence on the transition from metaluminous to peralkaline trachytes was provided by the experiments of Martel et al. [2013] on rocks from the Chaîne des Puys, French Massif Central. Rocks from seven intrusive bodies were studied at pressures between 200 and 400 MPa, temperatures between 700 and 900 °C, at water saturation and fO_2 of NNO + 1. Two of the intrusions can be used to exemplify the results, Chopine (P.I. 1.08) and Clierzou (P.I. 0.89). Chopine contains phenocrysts of plagioclase, alkali feldspar, FeTi-oxides, biotite and clinopyroxene; Clierzou has

plagioclase, FeTi-oxides and amphibole. The phenocryst assemblages were reproduced fairly well by the experiments. Given the nature of the mineral assemblage, particularly the plagioclase and biotite in the Chopine rock, it might be expected that residual melts would, with decreasing temperature, show increasing SiO_2 contents and increasing peralkalinity. However, in both cases increasingly evolved melts were *less* peralkaline. The authors had to make corrections to their Na_2O analyses, to allow for possible Na volatilization during the experiment, and it is possible that the values presented are lower than the true values, lowering the P.I. of the glasses. In their experimental study of a pantelleritic pumice from the Green Tuff, Romano et al. [2020] found that initially the P.I. became lower than in the starting material and then increased to 2.1, an effect not seen in the natural rocks [Liszewska et al., 2018].

Romano et al. [2018] used metaluminous trachytes from Pantelleria to examine the transition towards peralkalinity. Experimental conditions were 750–950 °C, 0.5–1.5 kbar, fO_2 < NNO and at fluid saturation (with X_{H_2O} between 0 and 1). The residual glasses after 80 wt% crystallization had comenditic trachyte composition, produced by a massive crystallization of alkali feldspar. The experiments thus provided sound evidence for the metaluminous to peralkaline transition.

11.3. *Experiments on peralkaline rhyolites*

High *P*–*T* experiments on comendites have been conducted by Scaillet and Macdonald [2001, 2003] and on pantellerites by Scaillet and Macdonald [2006b], Di Carlo et al. [2010] and Romano et al. [2020]. In most cases, the experiments reproduced the natural phase assemblages and liquid lines of descent fairly well [Romano et al., 2020]. Important general results were that (i) peralkaline silicic magmas can exist at temperatures below 700 °C; (ii) equilibration pressures are <5 kbar; (iii) most suites evolve at or just below FMQ; (iv) peralkaline silicic melts are normally water-rich (>4 wt%).

Despite considerable progress, certain problems remain. For example, the stability fields and compositions of amphibole are not well constrained. Romano et al. [2020] synthesized amphibole in the Green Tuff but it is absent in the natural rocks. The crystallization conditions of biotite have not been fully documented, the factors controlling the crystallization of quartz are poorly known, and the relationships between ilmenite and aenigmatite have still not been fully resolved. It appears that the stability ranges of the phases are highly sensitive to melt composition, and to even small variations in intensive parameters, as reviewed by Romano et al. [2020]. However, the experimental data can be used as a useful complement to thermodynamic modelling which, as noted above, is not always successful in peralkaline compositions.

12. Fluids and degassing

The presence of dissolved volatiles in silicate melts is fundamentally important. (i) Volatiles affect the abundances and compositions of phases crystallizing in magma and their subsequent stability. (ii) They affect the physical properties of the magma, such as density and viscosity, and thus magma chamber dynamics, including the role of convection. (iii) They also affect fractionation rates and thus the nature and extent of the liquid line of descent. (iv) On reaching saturation, volatiles exsolve as bubbles, potentially driving volcanic eruptions and influencing the volcanic eruptive style. In this section, we discuss aspects of the volatile concentrations in peralkaline magmas and certain of the effects of degassing on magma evolution.

12.1. *Volatile concentrations in peralkaline silicic magmas*

Various methods have been used to estimate the volatile contents of peralkaline magmas. Abundances in obsidians and matrix glasses can provide such estimates but they are almost always minimum values due to the degassing of the host magmas before, during and after eruption. Melt inclusions in phenocryst phases can contain true magmatic values but care must be taken to ensure that the inclusions have not leaked or undergone some postentrapment crystallization. For example, restored pre-eruptive melt H_2O contents of Olkaria comendites using δD and matrix H_2O values yielded values of up to 5.7 wt%, about twice the maximum found in the melt inclusions [Wilding et al., 1993]. Water values in the literature are in the range 3.5–5.8 wt%,

except for a value of 7.9 ± 0.5 wt% for a comenditic trachyte pumice from Puy Chopine, Massif Central, France [Martel et al., 2013]. In their review of studies of peralkaline magmatism in the Atlantic Ocean, Jeffery and Gertisser [2018] found that estimated melt water values ranged from 1.5 to 9.1 wt%. Although the situation varies from island to island, they noted that the highest values occur in the most peralkaline (evolved) rocks, suggesting that the H_2O concentrations are controlled largely by fractional crystallization.

Levels of CO_2 are usually low, <150 ppm [Lowenstern and Mahood, 1991, Gioncada and Landi, 2010, Field et al., 2012, Neave et al., 2012, Lanzo et al., 2013]. Such low values strongly suggest that most of the CO_2 is lost from the magmatic system during the pre-pantellerite evolutionary stages. Lowenstern [1994] suggested that the low CO_2 contents of Pantescan pantellerites (<100 ppm) are consistent with saturation with a mixed H_2O–CO_2 vapour at 50–100 MPa. Neave et al. [2012] used the H_2O and CO_2 contents to estimate a maximum equilibration pressure of 1.5 kbar (150 MPa). Iddon and Edmonds [2020] argued that basalts stored beneath the Main European Rift are saturated in CO_2 at up to 18 km in the upper crust, much of the CO_2 being lost by diffusive degassing.

Fluorine abundances in peralkaline rhyolites can be very high, e.g., ≤2.2 wt% in the pantelleritic Gold Flat ignimbrite in Nevada [Macdonald et al., 2019], or very low, e.g., ≤0.13 wt% in the Green Tuff, Pantelleria [Liszewska et al., 2018]. The high values are in part made possible by the tendency of F to partition into the melt during magma evolution [Webster et al., 1993, Barclay et al., 1996]. Fluorine can influence phase relationships in magmas, e.g., by affecting the point at which quartz joins the crystallizing assemblage, and by determining the stability and composition of amphibole. By forming complexes with various elements, e.g., Zr and REE, it may increase their solubility.

In peralkaline silicic magmas, Cl partitions between melt, vapour, and saline liquids. How it partitions determines, *inter alia*, when it is degassed from the melt. For example, high and constant levels of Cl (up to 1 wt%) in pantellerites are because they are saturated with H_2O–NaCl fluids at low pressures [Metrich and Rutherford, 1992, Lowenstern, 1994]. As an example of degassing, White et al. [2009] showed

that a Cl-rich aqueous phase exsolved in the transition pantelleritic trachyte to pantellerite on Pantelleria. Neave et al. [2012] noted that Cl abundances in melt inclusions in the pantellerites are consistent with partitioning of Cl into a subcritical hypersaline fluid at low pressures, while Lanzo et al. [2013] used combined H_2O and Cl data to estimate a confining pressure of ~50 MPa for Pantescan pantellerites.

An important source of information on volatile contents and behaviour has been through high P–T experiments where the imposed volatile contents can be assessed by their success in matching the observed mineral assemblages and compositions. The high-water values are consistent with experimental studies on peralkaline rhyolites ± trachytes [Scaillet and Macdonald, 2001, 2003, 2006b, Di Carlo et al., 2010, Romano et al., 2018]. The hydrous nature, along with the reduced nature indicated by the fO_2 values and low temperatures of equilibration (see above), prompted Macdonald [2012] to refer to peralkaline silicic magmatism as being of "cold-wet-reduced" type. This view was opposed to that of Bachmann and Berganz [2008] who proposed that in hotspot systems high-silica rhyolites are of hot-dry-reduced type.

Hydrocarbon-bearing fluid inclusions have been reported in alkaline rocks of both silica-oversaturated [Strange Lake Pluton: Salvi and Williams-Jones, 2006] and silica-undersaturated [Khibiny and Lovozero massifs: Nivin et al., 2005; Ilímaussaq complex: Krumrei and Markl, 2005] affinity. There is an active debate about the origin of the hydrocarbons: Salvi and Williams-Jones [2006], for example, ascribed their formation to wall rock alteration reactions, while Krumrei and Markl [2005] favoured a high-temperature magmatic origin for the hydrocarbons. As far as we know, nobody has reported hydrocarbons in a peralkaline silicic extrusive rock. If the absence is real, it is telling us something about the oxidation conditions during mantle melting or during magma transport.

12.2. *Degassing*

Simple mass balance calculations (and realistic amounts of fractional crystallization) indicate that if a primary basalt is generated with 1.5 wt% water and subsequently fractionates through to trachyte (where
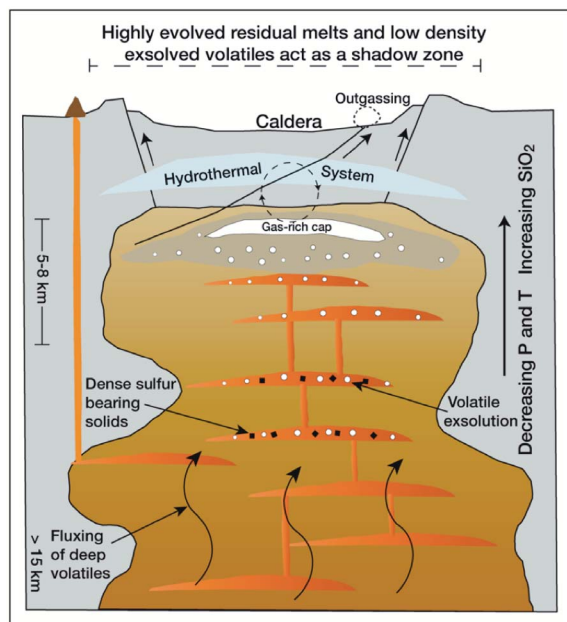
Figure 12. Cartoon of a magma system beneath the axial part of the Main Ethiopian Rift, stressing the behaviour of volatiles at various levels. Redrawn from Iddon and Edmonds [2020].

$F = 0.1$) in an essentially closed system with continuous partitioning of water into the melt, the trachyte magma will contain 15 wt% water. This is considerably higher than the maximum water solubility, ~8 wt%, determined experimentally in such magmas [Di Matteo et al., 2004, Martel et al., 2013]. Loss by degassing must occur. The question then arises: "At what level(s) did the various melts in the basalt–trachyte sequence degas?" Based on MELTS modelling of the basalt–pantellerite sequence on Pantelleria, White et al. [2009] inferred that exsolution of a halogen-rich aqueous fluid occurred when the melts had reached 59 wt% SiO_2 and then at 64 wt% SiO_2. In their study of peralkaline volcanoes of the Main Ethiopian Rift, Iddon and Edmonds [2020] suggested that at the Daly Gap the magma become saturated in sulphide and an exsolved volatile phase. There was then further degassing in shallow reservoirs (6–8 km), with a substantial exsolved volatile phase. Their model of the magma systems includes details of volatile behaviour down to at least 15 km (Figure 12).

The compositions of the degassed phases are dependent, *inter alia*, on the nature of the dissolved volatiles and on magma dynamics, particularly the rate of ascent. CO_2 is less soluble than H_2O, SO_2, F and Cl and will normally enter a volatile phase at higher pressures and be degassed. An absence or scarcity of CO_2 in the salic members of the sequence, as in the Pantescan pantellerites, is no guarantee that it did not play an important role in magma genesis. However, we are unaware of any direct occurrence of a peralkaline silicic suite with carbonatites; it may well be that significant amounts of CO_2 are not required for the formation of their primary mafic magmas.

13. The early evolutionary stages

13.1. *Initiation of magmatic activity*

The first stage involves the rise of mafic magmas from the mantle, first into lower crustal storage zones and then into holding zones at various crustal levels. In some centres, mafic magmas erupt onto the surface, e.g., the volcanoes of Marie Byrd Land, Antarctica [LeMasurier et al., 2011], and the Guilherme Moniz and Cinco Picos volcanoes on Terceira [Self and Gunn, 1976, Jeffery et al., 2017]. In other cases, the magmas ascend into the upper crust, generally to 1–5 km depth, and stall, allowing the development of the plumbing systems in which the peralkaline members form. Ongoing work on peralkaline systems has shown that they are all to some degree unique, as a perusal of cartoon models of their plumbing systems reveals, e.g., Dunkley et al. [1993], Macdonald et al. [1994, 2008], Troll and Schmincke [2002], Sumner and Wolff [2003], Marshall et al. [2009], Neave et al. [2012], Jeffery et al. [2016, 2017], Gleeson et al. [2017], Aguirre-Diaz and Morton-Bermea [2018], Andreeva et al. [2018], Hutchison et al. [2018], Liszewska et al. [2018], Sosa-Ceballos et al. [2018], Gottsmann et al. [2020], Neave [2020]. The magmatic systems vary in shape, size, depth, longevity and internal structure. Models involving single reservoirs range from balloon- or mushroom-shaped (Figures 13a and b), a series of stacked sills (Figure 13c), and the transcrustal model of Hammond et al. [2020; Figure 13d]. More complex models include that for Silali volcano, Kenya, where Macdonald et al. [1995] proposed a series of sill-like reservoirs, some of which had collapsed after eruption, allowing basaltic magmas to
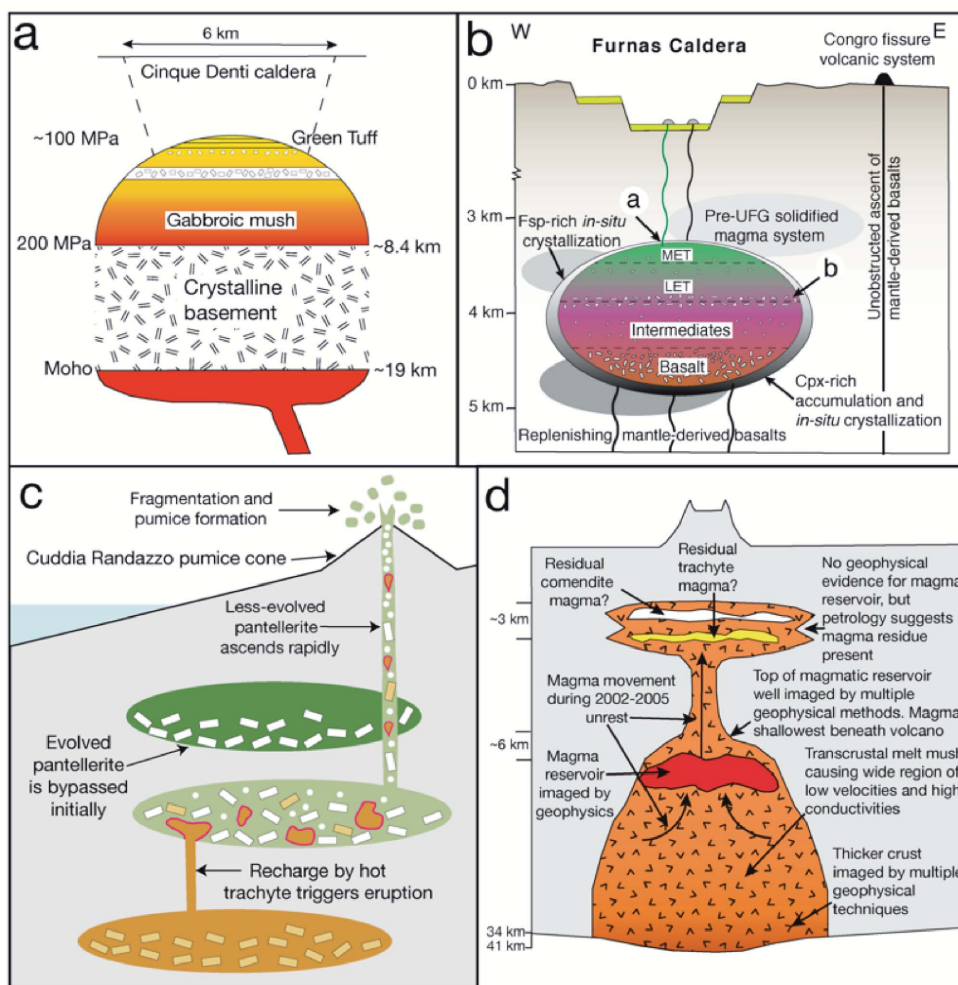
Figure 13. To show the diversity of peralkaline silicic magma systems. (a) The mushroom-shaped model inferred for the Pantescan system prior to eruption of the Green Tuff. Redrawn after Liszewska et al. [2018]. (b) Model of the shallow plumbing system of Furnas volcano shows a density-stratified reservoir with a cap of evolved trachytes (MET) overlying less evolved trachytes (LET). After Jeffery et al. [2016]. (c) Inferred reservoir structure of the Cuddia Randazzo–Khaggiar system, Pantelleria, when the pumice cone formed. Note the interconnections between the stacked bodies. Redrawn from Neave [2020]. (d) Cartoon model of the magma plumbing system beneath Changbaishan-Tianchi volcano, constructed from geophysical and petrological evidence. Note the thickened crust. Redrawn from Hammond et al. [2020].

pass through them. At the Olkaria centre, following a period of caldera collapse subsequent eruptions were from many small, partially interconnected reservoirs. Based on Interferometric Synthetic Aperture Radar (InSAR) data for Dabbahu volcano, Field et al. [2012] modelled the presence of a series of stacked sills (reservoirs) over a 1–5 km depth range. Clearly there is no "standard" model for the plumbing systems—their nature will depend on such factors as local tectonics, mechanism and rate of magma input from depth, and volatile contents and their effect on viscosity. In the following sections, we present

some of the evidence used in elucidating the nature of, and processes within, peralkaline magma systems.

13.2. *Geological information on depth of reservoirs*

Noting that peralkaline caldera volcanoes commonly contain lithic clasts from the volcanic edifice, including cognate syenites, but lack subjacent crustal lithologies, Mahood [1984] proposed that their magma reservoirs are shallow. The Alid volcanic centre in Eritrea is an elliptical structural dome, 5×7 km, formed during uplift caused by shallow intrusion of rhyolitic magma. Given that the intrusion formed at <2–3 km depth and had a diameter of 3 to 5 km, Lowenstern et al. [2006] calculated that the intrusion has a volume of between 7 and 65 km^3. Based on the distribution of mafic cones at the Changbaishan-Tianchi volcano, inferred as indicating the presence of a shadow zone, Wei et al. [2013] estimated that the subsurface comendite body could be ~20 km in diameter. Assuming a 10:1 diameter/thickness proportion [Jellinek and DePaolo, 2003], the resulting volume would be ~600 km^3.

Attempting to illustrate the relationship between the erupted deposits and the related reservoir, Macdonald et al. [2014] pictured the young trachytic Longonot volcano, Kenya, and the Mesoproterozoic syenitic complex Kûngnât, Greenland, as complementary magmatic systems and developed a model of a single trachytic centre throughout its life cycle. Many petrogenetic and volcanological features were shown to be shared by the two complexes, pointing to their similar development despite the great age difference.

13.3. *Petrological information*

From determination of volatiles, mainly H_2O and CO_2, in melt inclusions in phenocrysts, saturation pressures can be calculated using solubility models, such as those of Di Matteo et al. [2004] and Papale et al. [2006]. The pressure estimates are then converted to depth. The method relies on the magmas having been volatile-saturated prior to eruption and suitable crustal density models being available. Using the technique, Field et al. [2012] estimated that volatile saturation pressures for historic pantellerites of the Dabbahu volcano are in the range 43–207 MPa

and inferred that magma storage depths for these eruptions are ~1–5 km below sea level. Neave et al. [2012] also used H_2O and CO_2 data to estimate equilibration pressure for Pantescan pantellerites of up to 1.5 kbar. For the Green Tuff ignimbrite, Pantelleria, which is virtually CO_2-free, Lanzo et al. [2013] found a pressure interval of 45–65 MPa. Considering the possibility that some water may have been lost by degassing of the melt inclusions, they preferred a storage depth of 2.5 km. Jeffery et al. [2017] postulated that ignimbrites of Terceira were stored at pressures up to ~135 MPa, equivalent to 3.7 km depth.

A useful summary of magma storage conditions in various peralkaline systems, based on geochemical modelling and experimental evidence, has been presented by Gleeson et al. [2017; their Table 3].

14. Geophysical information on nature of reservoirs

The ways in which peralkaline reservoirs develop and evolve are dependent on many factors: the regional and local tectonics, their size and shape, magma compositions, volatile behaviour, and how open the system is. Geophysical techniques are increasingly being used to provide information on such aspects of magma plumbing systems as their shape and size, the distribution of zones of melt accumulation, and the paths of melt migration. A comprehensive review of the main techniques is provided by Magee et al. [2018]. Here we describe some results as applied to peralkaline silicic systems.

14.1. *Ground deformation*

One method of looking inside an active volcano is to measure surface deformation, resulting from subsurface magmatic or hydrothermal processes. The deformation can provide information on the levels of magma accumulation and migration and, sometimes, on conditions within the magma reservoir, such as cooling and contraction. Traditionally based on the placement of multiple sensors around the volcano, measurements can now be made globally using satellites and it is now known that over 220 volcanoes around the world were actively deforming in 2016 [Biggs and Pritchard, 2017].

Interferometric Synthetic Aperture Radar (InSAR) is a remote sensing technique using microwave

electromagnetic radiation to detect, *inter alia*, displacements of the Earth's surface. Mattia et al. [2007] used InSAR, and Electronic Distance Measurement (EDM) and levelling data, to identify the point source of ground deformation beneath the Pantelleria caldera. Their preferred model was of a simple spherical source at ~4 km beneath the island. Using InSAR, Biggs et al. [2009] detected episodic geodetic activity at four central volcanoes in the central Kenya Rift (Paka, Menengai, Longonot and Suswa) over the period 1997–2007. Inflation of Paka is shown in Figure 14a). InSAR data were used by Biggs et al. [2011] to quantify the amount of uplift and subsidence beneath four volcanoes in the Main Ethiopian Rift. They modelled the sources as penny-shaped cracks at depths of between <2.5 and ~5 km. In contrast, Field et al. [2012] modelled InSAR and seismic evidence from the Dabbahu volcano to show that a system of thin stacked sills in the depth range ~1 to 5 km best fits the ground deformation data. A period of inflation at Aluto in 2008 was explained by Hutchison et al. [2016a,b] as reflecting fluid injection into a magma reservoir at *ca.* 5.1 ± 0.5 km depth. Wei et al. [2013] interpreted the increased levels of seismicity and ground deformation (especially uplift) in mid-2002 at the Changbaishan-Tianchi volcano as reflecting an episode of magma recharge and/or volatile exsolution at depths of ~5 km, although the unrest did not culminate in an eruption. Iddon and Edmonds [2020] have noted that a high fraction of dissolved volatiles in the evolved melts can also have an effect on ground displacements.

14.2. *Gravimetry*

Gravimetric studies of volcanoes measure changes in the gravitational field caused by the subsurface distribution of magma. Several circular-shaped positive gravity anomalies have been identified along the northern Main Ethiopian Rift and some are associated with rhyolitic volcanoes, such as Gedemsa. In most, there is a density decrease from the bottom (~20 km) to the top (<4 km) of the anomaly. Peccerillo et al. [2003] interpreted the data as supporting the hypothesis that the silicic centres developed above large intrusions of mafic magma, crystallization of which as ultramafic to mafic rocks explains the gravimetric data. Mahatsente et al. [1999] located a positive gravity anomaly in the shallow crust beneath Aluto which Iddon et al. [2019] suggested may

provide evidence of crystallized intermediate magmas. A 2850 kg·m^{-1} body determined in the gravity survey of the Boset (Boseti) volcano by Cornwell et al. [2006] may represent the same chamber identified by Whaler and Hautot [2006] using magnetotellurics as a small, shallow, high conductivity low at <1 km depth beneath the volcano.

Based on the results of geodetic and gravimetric surveys, data modelling and other geophysical observations, Gottsmann et al. [2020] presented the model of the upper crustal plumbing system beneath the Corbetti caldera shown in Figure 14b. SBDTZ is the seismic brittle–ductile transition zone. The current magma intrusion lies within a crystal mush zone. A peralkaline rhyolitic system is thought to lie at the top of the intrusion and feeds the explosive magmatism at the centre. There is a hydrothermal system at 0.2–1.0 km depth (not shown).

14.3. *Seismic imaging*

Many studies of active volcanoes and volcanic regions have determined variations in seismic velocity. High velocity anomalies observed in shallow crustal regions beneath active volcanoes have commonly been interpreted as cooled magma bodies whereas low velocity anomalies have almost invariably been interpreted as areas of melt accumulation, often in the depth range 8–15 km [Lees, 2007, Masturyono et al., 2001]. The seismic imaging is consistent with the presence of no more than a few tens of percent of melt in a crystal mush model [Lees, 2007, Huang et al., 2015]. Sometimes, however, the various geophysical methods provide contrasting results. Iddon et al. [2019], for example, have noted that seismic and deformation data for the Aluto volcano point to the existence of a shallow magma reservoir, whereas magnetotelluric methods have failed to identify a volume of enhanced electrical conductivity in the crust which would be consistent with the presence of partial melt.

In their study of the seismic velocity structure of Aluto caldera, Wilks et al. [2020] concluded that volatiles exsolved from a deep melt-rich body (>10 km depth) migrated into a shallow volume of rock containing over-pressurized gas which is shown by abundant seismicity and low V_p/V_s (Figure 14c). This exchange of fluids causes the restless behaviour of Aluto. Using seismic records, Hammond et al.
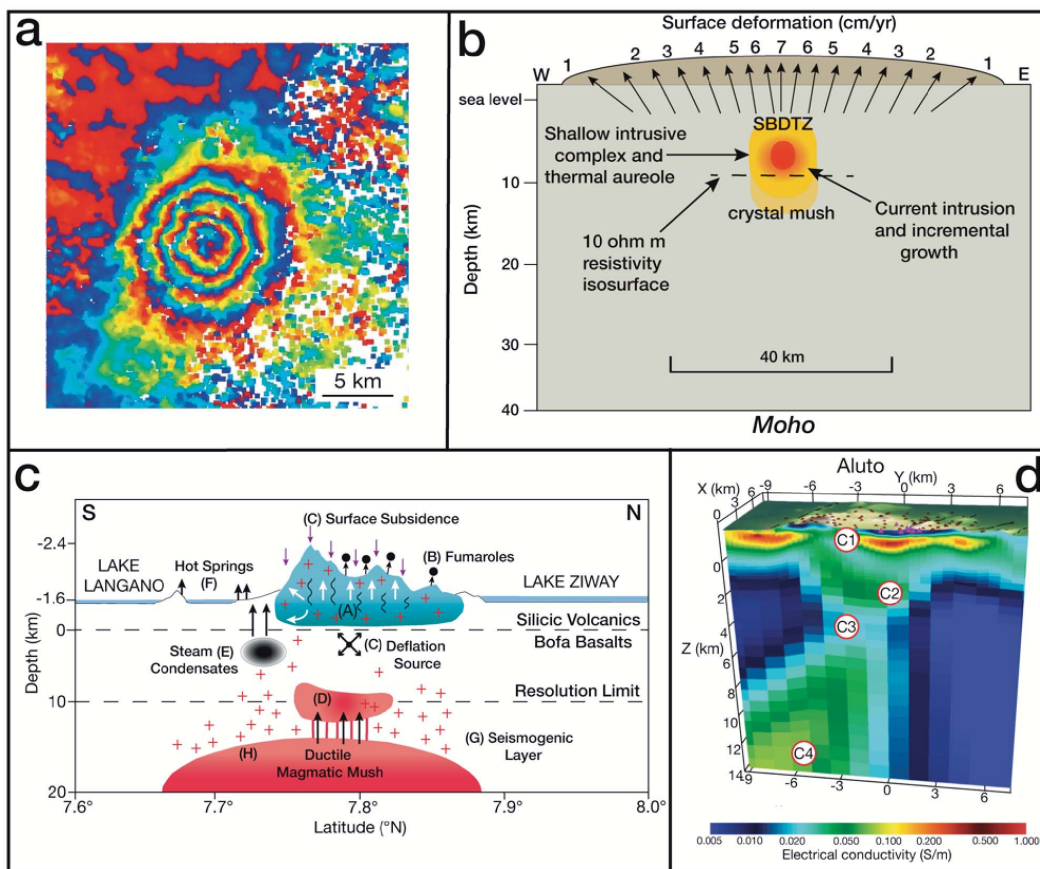
Figure 14. (a) Inflation episodes at Paka volcano, Kenya Rift Valley, 2006–2007. Each colour cycle represents 2.8 cm of displacement in the satellite line of sight. From Biggs et al. [2009]. (b) Upper crustal plumbing system beneath Corbetti caldera, modelled from geodetic and gravimetric data by Gottsmann et al. [2020]. (c) Subsurface structure of Aluto volcano, modelled by Wilks et al. [2020] from seismic data. Zone A exhibits high seismicity within a region of over-pressurized gas; B is a zone of fumarolic activity; Zone C exhibits surface deflation; D has a significant melt component derived from greater depth; Zone H is a reservoir of magmatic mush. (d) Electrical conductivity model of Aluto volcano [Samrock et al., 2021]. Conductors C1 to C4 are explained in the text.

[2020] found a significant velocity reduction at 4–8 km depth which they interpreted as a zone of partial melt. Interestingly, they also presented evidence that melt is present over a wide region of low velocities and high conductivities and extends through the crust as a "transcrustal mush zone" (Figure 14d). Although models of transcrustal magmatic systems are gaining in popularity [Annen et al., 2015, Cashman et al., 2017, Sparks and Cashman, 2017], this may be the first application to a peralkaline silicic system.

The total volumes and melt fractions of seismically inferred reservoirs are potentially important in providing information on the possibility of future eruptions. For example, Hammond et al. [2020] suggested that recharge of their seismically identified partial melt zone beneath Changbaishan-Tianchi volcano was responsible for the episode of unrest from 2002–2005.

14.4. *Magnetotelluric surveying*

Magnetotelluric (MT) surveying uses variations in the Earth's electromagnetic field to determine the distribution of electrical conductivity in the subsur-

face. In volcanic systems, the electrical conductivity is controlled by, *inter alia*, the presence of melt, magmatic or meteoric brine or hydrothermal zones [Samrock et al., 2021]. Applying the technique to the Aluto volcano in the Main Ethiopian Rift, Samrock et al. [2021] proposed the model shown in Figure 14d. The conductor C1 is a clay cap. Conductor C2, at depths of ~1–4 km, is interpreted as a magmatic heat source for a hydrothermal zone which lies between C1 and C2. The conducting zone C4 at depths >8 km is the lower crustal zone of melt accumulation and thus the parental magma reservoir. C3 represents magmatic pathways connecting C2 and C4. In their MT study of the Changbaishan-Tianchi volcano, Yang et al. [2021] identified three high conductivity zones at depths of 3–5, 10–16 and 40–60 km. They suggested that the deepest might be related to melting of the asthenospheric mantle, the middle crustal zone is a magma chamber, and the upper crustal anomaly is a porous saline zone.

The various geophysical techniques, especially when tied to petrological studies, are revealing in increasing detail the scale, structure, and dynamics of magmatic systems. Considerable insights are being made into how the plumbing systems work and the potential for future eruptions.

15. Establishment of zoned magma chambers

A majority of recent studies have shown that the upper crustal magma reservoirs are compositionally zoned. One of the strongest lines of evidence is the eruption of ignimbrites with variations in bulk-rock and phenocryst compositions and in estimated P–T–P_{volatile} conditions. The scale of the zonation is very variable and seems to be independent of eruptive volume. For example, the Green Tuff, Pantelleria, has a Dense Rock Equivalent (DRE) volume of ~10 km^3 and is zoned from comenditic trachyte to pantellerite. The comenditic Bracks Rhyolite, Trans-Pecos Texas, with a volume of 75 km^3, is compositionally homogeneous [Henry et al., 1990], and the pantelleritic Gomez Tuff, also in Trans-Pecos Texas, shows only minimal variation despite having a volume of ~220 km^3 [Parker and White, 2008].

A simplified model of zonation would show a rhyolitic cap overlying trachytic magmas which become progressively more feldspar-rich with depth in the reservoir, into a so-called mush zone, as proposed

for peralkaline silicic systems by Macdonald et al. [1994, 1995, 2019], Sumner and Wolff [2003], Marshall et al. [2009], White et al. [2009], Wolff et al. [2015], D'Oriano et al. [2017], Jeffery and Gertisser [2018], Iddon et al. [2019] and Gottsmann et al. [2020]. A further variation may be the presence of mixed magma layers, or layers with different phenocryst abundances. Boundaries between layers may be sharp or show evidence of crystal transport across them.

How quickly is compositional zonation established? After eruption of the Green Tuff ignimbrite, Pantelleria, the magmatic system had evolved from metaluminous trachytic to pantelleritic compositions in a few thousand years Mahood and Hildreth [1986]. Leat et al. [1984] argued for the Menengai caldera volcano that extensive compositional zonation developed through thicknesses exceeding 10^2 m in times of 10^2–10^3 years. At some centres in the Olkaria complex, compositional zonation developed rapidly, in a few thousand years at most [Marshall et al., 2009]. The rapidity of the processes in these systems was at least partly due to the very low melt viscosities.

16. Differentiation mechanisms

16.1. *Fractional crystallization*

In the majority of recent studies of peralkaline systems, geochemical modelling has established fractional crystallization as the dominant mechanism driving the transition basalt to trachyte/rhyolite [e.g., Novak and Mahood, 1986, Mungall and Martin, 1995, Peccerillo et al., 2003, Lowenstern et al., 2006, Flude et al., 2008, Jeffery and Gertisser, 2018, Macdonald et al., 2008, Parker and White, 2008, Marshall et al., 2009, Ronga et al., 2010, Neave et al., 2012, Giordano et al., 2014, Hutchison et al., 2016a,b, Jeffery et al., 2016, 2017, Gleeson et al., 2017, Aguirre-Diaz and Morton-Bermea, 2018, Iddon et al., 2019, Iddon and Edmonds, 2020]. The main magmatic lineages were discussed earlier (Section 6); in detail, they reflect the ambient P–T–$f\text{O}_2$–P_{volatile} conditions in each system, especially during the earlier stages of evolution. As Macdonald [2012], Gleeson et al. [2017], Jeffery and Gertisser [2018] and Romano et al. [2020] have shown, the crystallization conditions for peralkaline trachyte–rhyolite systems tend to be broadly similar. Ultimately this is reflected in

the observation, discussed above (Section 7), that all peralkaline silicic suites have the potential to evolve towards the effective minimum composition(s).

The efficiency of crystal fractionation in the crustal reservoirs is partly dependent on the rate at which crystals grow. Rogers et al. [2004] estimated that the fractionation rate (calculated by dividing the magma fraction crystallized by the time period of differentiation) for evolution of the hawaiite–trachyte sequence at the Longonot volcano, Kenya, was ~0.2×10^{-4}/year, whereas fractionation in the trachytes was more rapid, up to 3×10^{-4}/year. Lowenstern et al. [2006] found rather similar rates for the basalt–comendite suite at the Alid volcanic centre (2–3×10^{-5}/year). They further estimated that the production rate of comendite was 2×10^{-4} to 1.0×10^{-3} km^3/year, broadly similar to the value of 2.5×10^{-3} km^3/year proposed for the Olkaria comendites by Heumann and Davies [2002], which, they claim, are comparable to much larger metaluminous silicic systems.

16.2. *Magma mingling and mixing*

Magma mingling and mixing have been recognized in the majority of, if not all, peralkaline silicic systems. Macdonald [2012], for example, has listed several examples from the Kenya Rift Valley and Jeffery and Gertisser [2018] refer to occurrences in Atlantic Islands. The evidence takes several forms, including compositionally banded pumice fiamme and pumice clasts; quenched enclaves; and disequilibrium phenocryst assemblages (Figure 15). Various lithological combinations are found. Macdonald et al. [2008] recorded two-, three- and four-component mixes of basalt, mugearite, benmoreite, trachyte and rhyolite in comendites of the Olkaria complex, Kenya. An important feature of these rocks is that they can reveal the presence in the plumbing system of magmas that were never erupted as discrete units.

One of the most remarkable examples of mixing is the Miocene P1 ignimbrite (14.1 Ma) on Gran Canaria [Freundt and Schmincke, 1995, Schmincke and Sumita, 2010]. The body has a volume of ~43 km^3 and comprises four components: crystal-poor to highly phyric rhyolite, sodic trachyandesites through mafic to evolved trachytes, Na-poor trachyandesites, and two varieties of basalt. The rocks record two contemporaneous fractionation series and some rocks were modified by selective contamination of alkali feldspar. The components were then intensely mixed during eruption.

Younger ignimbrites on Gran Canaria also point to complex processes in the reservoir. Troll and Schmincke [2002] recorded in Ignimbrite "A" (13.63 ± 0.3 Ma) a complex history of magma mixing, feldspar resorption and inter-magma batch transport. Ignimbrite "TL" (13.4 Ma) contained three magma compositions, comendite, trachyte and benmoreite, which were involved in mixing before during withdrawal [Sumner and Wolff, 2003]. An interesting conclusion was that intrusion of benmoreite magma into the chamber occurred over several months to years.

In some suites, intermediate composition magmas were formed only by mingling of mafic and felsic magmas [Novak and Mahood, 1986, Ferla and Meli, 2006, Lowenstern et al., 2006, Flude et al., 2008, Romengo et al., 2012]. At Silali, Kenya [Macdonald et al., 1995], Gedemsa, Ethiopia [Peccerillo et al., 2003], Olkaria, Kenya [Macdonald et al., 2008] and Nemrut volcano, Turkey [Çubukçu et al., 2012], mixed magma intermediates occur in addition to non-mixed rocks.

16.3. *Resorption/remobilization of cumulates*

The recognition that the magmatic reservoirs can contain feldspar-rich layers, and thus the possibility of feldspar-cumulitic layers, led to suggestions that the compositions of magmas may be affected by crystal resorption [Sumner and Wolff, 2003, Macdonald et al., 2008, White et al., 2009, Wolff et al., 2015, Jeffery et al., 2017, Iddon et al., 2019]. Most recently, Wolff et al. [2020] used Ba and Eu enrichments to suggest that many compositionally zoned felsic tuffs, including the Green Tuff, Pantelleria, show crystal-scale evidence for formation of magma by thermal rejuvenation of high-crystallinity (>50%) mush (Figure 16). One consequence is to blur the distinction between the compositions of evolved melts and crystal mushes. Cumulate remelting is clearly a viable process in peralkaline magmatic systems and must be considered in petrogenetic models. This is particularly pertinent in the light of the suggestion of Hutchison et al. [2018, p. 215] that 16–30% of the volume generated by crustal extension beneath a silicic complex would be filled by magmatic cumulates.
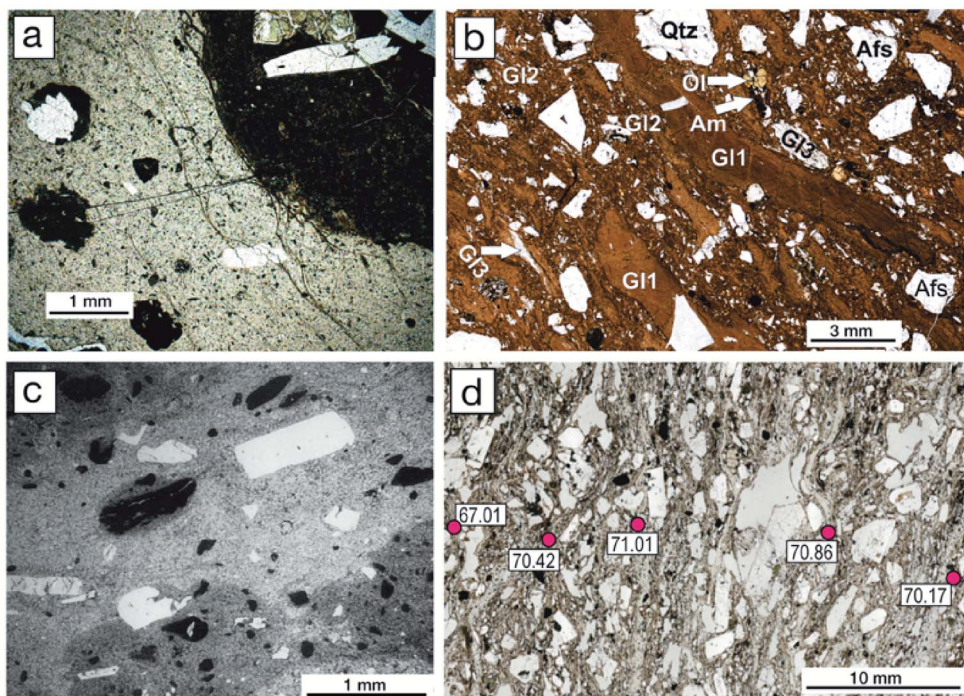
Figure 15. (a) Mingling of basalt (dark) and comendite (light brown), Greater Olkaria Volcanic Complex. The grey material to left may be a third component. From Macdonald et al. [2008, Figure 3d]. (b) Mingling of two pantelleritic melts (Gl1 and Gl2) and comenditic melt (Gl3), also marked are alkali feldspar (Afs), amphibole (Am), olivine (Ol), and quartz (Qtz), Gold Flat Tuff, Nevada [Macdonald et al., 2019]. (c) Mingling of trachyte (darker) and comendite (lighter) in ignimbrite "TL", Gran Canaria. The trachyte encloses dense, angular benmoreite globules. Based on Sumner and Wolff [2003]. (d) Streaky mingling of trachytic and pantelleritic magmas at the micron scale, values are wt% SiO_2 Green Tuff, Pantelleria [Liszewska et al., 2018].

17. Evacuating the reservoir

Various mechanisms have been proposed to initiate eruption. Differentiation of an initially water-poor silicic magma can yield highly fractionated, low-density magmas with high water contents. The uppermost parts of the reservoir can become oversaturated in water, causing an excess pressure which can lead to eruption [Blake, 1984, Gioncada and Landi, 2010, Landi and Rotolo, 2015, Gleeson et al., 2017]. Alternatively, the trigger may be mafic magma recharge, for which there is strong evidence in the presence of mixed magma rocks [Sumner and Wolff, 2003, Flude et al., 2008, Pan et al., 2017, Macdonald et al., 2019, Neave, 2020]. In an interesting variant, Pimentel et al. [2016] showed that the eruption of comenditic trachytes in 1761 CE on Terceira Island

was triggered by stresses related to contemporaneous trachybasalt eruption but with no mixing of the magmas.

The modes of eruption from compositionally zoned high-level reservoirs are very variable. Drawdown may be simple, with progressively deeper layers being incorporated [Blake and Ivey, 1986]. In Figure 17a, the eruption of an ash-flow tuff from the Menengai volcano, Kenya, tapped through several compositional layers in the reservoir [Macdonald et al., 1994]. During the eruption of ignimbrite "TL" on Gran Canaria, mingling of comenditic and trachytic magmas with benmoreitic globules and a feldspar-rich trachytic layer occurred (before and) during eruption [Figure 17b; Sumner and Wolff, 2003]. Mahood et al. [1985] described, in the Guadalajara Ignimbrite, Mexico, the simultaneous
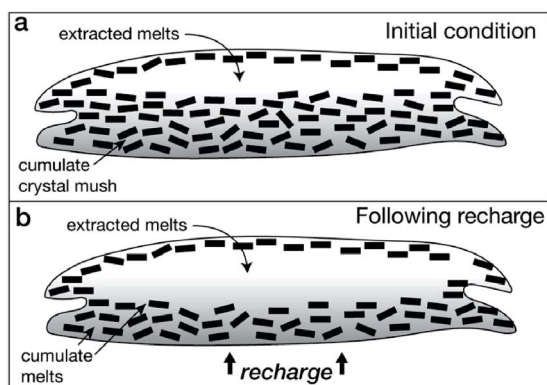
Figure 16. (a) Initial condition of a hypothetical system containing a cumulate mush. (b) After recharge by less evolved magma, the cumulates are partially melted. Based on Wolff et al. [2020].

eruption of two comenditic magmas of slightly different composition. The basal member of the Gold Flat Tuff, Nevada, contained pantelleritic and comenditic melts derived from separate reservoirs. which were mixed during eruption [Macdonald et al., 2019].

18. Timescales of growth and eruptive periodicity

Peralkaline silicic volcanoes can grow and evolve rapidly. For example, Menengai and Longonot in the Kenya Rift, and Mayor Island, New Zealand, developed shield volcanoes, followed by two periods of caldera collapse, over periods in the range 130–400 ka. Based on the Kenyan examples, Hutchison et al. [2016a] inferred that the edifice-building phase at Aluto lasted for 150–400 ka, followed by major ignimbrite eruptions at 310 ka, a period of repose lasting 250 ka and then episodic post-caldera activity after 60 ka. Activity at Aluto was, therefore, episodic on a variety of scales. On Pantelleria perhaps as many as five caldera collapses have occurred in the past 190 ka [Jordan et al., 2018]. The trachytic–rhyolitic cone of Changbaishan-Tianchi has been growing for 1.12 Ma [Andreeva et al., 2018]. On the basis of evidence from the Alid volcanic centre, Eritrea, Lowenstern et al. [2006] estimated that extraction of basalt from the mantle source through to the
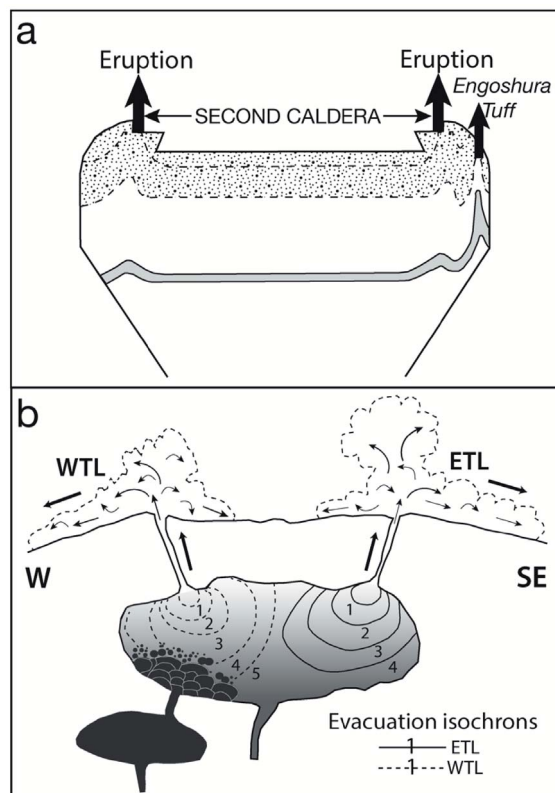

Figure 17. Reservoir evacuation processes. (a) Eruption of the second caldera-forming ash-flow tuff, Menengai volcano, Kenya. Dashed lines represent isochemical surfaces. The Engoshura Tuff (Eng. Tuff) was perhaps erupted from a vent tapping a zone of strong compositional gradient, tapping into a Ba-rich layer. Redrawn from Macdonald et al. [1994]. (b) Ignimbrite "TL", Gran Canaria. Eruptions from the western lobe (WTL) tapped into a layer of intrusive benmoreite which was absent beneath the eastern lobe (ETL). Redrawn from Sumner and Wolff [2003].

formation of comenditic rhyolites took some 30,000–50,000 years.

Information is accumulating on the eruption periodicities of peralkaline systems, allowing some insights into magmatic processes. For example, Iddon et al. [2019] presented a model to show that eruption intervals for post-caldera pantellerites at Aluto were greater than the upper limits calculated for melt segregation from their crystal mush, providing

no obstacle to a fractional crystallization origin. On Mayor Island, the mean eruption interval is around 4000 years [35 events in ~130 ka: Houghton et al., 1992]. At the Nemrut volcano, Turkey, major eruptions of silicic magmas for the past ~190 ka appear to have occurred at intervals spaced some 20,000–40,000 years apart, which Sumita and Schmincke [2013a] interpreted as being the incubation times for the silicic magmas to build into large eruptible volumes. Based on the style and volume of recent eruptions, Hutchison et al. [2016a] suggested that silicic eruptions at Aluto volcano, Main Ethiopian Rift, occur at an average rate of 1 per 1000 years. McNamara et al. [2018] suggested that the volcano has erupted at least 24 times in the Holocene, most eruptions occurring in three bursts at 11 ka, 6.1 ka and ~3.5 ka. The three main felsic episodes over the last 230 ka at the Boset-Bericha Volcanic Complex, also in the Main Ethiopian Rift, occurred at ~230 ka, ~119 ka, and since ~16 ka, may indicate an overall frequency of around 100 ka [Siegburg et al., 2018]. The mean eruption intervals for post-caldera pantellerites at Aluto have been estimated at 300–400 years by Iddon et al. [2019]. The magma system of Terceira has erupted at least seven ignimbrites and several smaller-scale eruptions over the past ~60 ka, typical eruption volumes (DRE) being ~1–2 km^3 [Jeffery et al., 2017].

The increasing recognition that magmatic systems contain significant volumes of mush zones that are transitional into solid rock has made it difficult to distinguish the so-called volcanic and plutonic stages in their evolution. What information is available on the age of the last eruption of a peralkaline system (i.e., the end of the volcanic stage) and its entering a phase where its future will be dominated by cooling-induced crystallization (the plutonic stage)? Certain aspects of Pantelleria may suggest that it will not erupt again. (i) In the last ~190 ka, there have been two, and possibly five, episodes of caldera collapse [Jordan et al., 2018]. (ii) After formation of the last caldera at 46 ± 1 ka, a resurgent dome formed on the caldera floor. (iii) The most peralkaline products were erupted at the time of the formation of the second caldera. (iv) On the basis of new $^{40}Ar/^{39}Ar$ dating and geodetic evidence of deflation and subsidence of the most recent caldera floor, Scaillet et al. [2011] proposed that the intracaldera system, in stasis since 7 ka, is on the wane and that there is no evidence of a forthcoming eruption in the next 2 ka. (v) This is perhaps consistent with the results of a seismic survey in 2006–2007 and of signals recorded during 2010–2014 that Pantelleria has a very low rate of seismicity [Spampinato et al., 2017]. Nevertheless, renewed input of mafic magma into the system could result in its rejuvenation.

19. Volcanic hazards

Several peralkaline silicic volcanoes have the potential to erupt in the near future. One of the most spectacular is the Changbaishan-Tianchi volcano, China/North Korea. When it erupted around 946 CE, it deposited ~100 km^3 of comendite–trachyte ejecta which spread as far as northern Japan, a distance of some 1000 km, where some 4–5 cm of ash were deposited [Horn and Schmincke, 2000, Wei et al., 2013, Pan et al., 2017]. With a Volcanic Explosivity Index (VEI) of 7, the eruption is one of the two largest Holocene eruptions on Earth. From 2002–2005, there were marked increases in seismicity, deformation and the hydrogen and helium contents of spring waters, causing regional concern. The unrest did not result in an eruption, but it stressed the need for complete and continuous monitoring, especially since millions of people live close to the volcano [Wei et al., 2013]. The magmas of the Millennium Eruption may have been stored in the crust for 10,000–20,000 years before eruption [Zou et al., 2010, Wei et al., 2013]; future eruptions may not be imminent.

Throughout the East African Rift System, it appears that shallow magmatic processes are currently operating on a decadal timescale [Biggs et al., 2011]. In the Kenya sector, three centres (Paka, Menengai and Longonot) showed signs of inflation or deflation over the period 1997–2008, as determined by InSAR [Biggs et al., 2009]. The Olkaria volcano complex, associated with the caldera centres, is a multi-centred comenditic dome field which last erupted at 180 ± 50 yBP [Clarke et al., 1990]. Menengai, Olkaria and Longonot are located in densely populated areas and present important hazards to life and property. Further north, in the Main Ethiopian Rift, four volcanic centres (Aluto, Corbetti, Bora and Haledebi) experienced deformation from 1993 to 2010 [Biggs et al., 2011, Gleeson et al., 2017; see also Fontijn et al., 2018]. As in Kenya, the hazard implications are significant; for example,

6.8 million people live within 100 km of Aluto. On the basis of a newly developed probabilistic volcanic hazard assessment methodology, Clarke et al. [2020] argued that numerous settlements, amenities and economically valuable geothermal infrastructure lie within the most hazardous regions of the Aluto caldera. More than 250,000 people could be endangered by an even modest-scale eruption (0.5 km^3 of magma) from the Corbetti Volcanic system [Rapprich et al., 2016].

In an earlier phase of magmatic activity, layers of tephra 15–20 cm thick and compositionally similar to the Oligocene Ethiopian plateau ignimbrites have been found in the central Indian Ocean ~2600 km away from the ignimbrites. Ayalew et al. [2002] speculated that the tephra layers represent distal fallout from the Ethiopian ignimbrite-forming eruptions.

On Pantelleria, ash from the eruption of the Green Tuff ignimbrite [45.7 ± 1.0 Ma; Scaillet et al., 2013] reached as far as the Dodecanese, 1300 km away [Margari et al., 2007]. As noted above, there is much uncertainty about the volcano's future eruptive potential, but careful monitoring is necessary. Mayor Island is the emergent portion of a compound lava shield built predominantly of peralkaline rhyolites. A caldera formed during two or three collapse periods some 6300 years ago. The most recent eruption is thought to have occurred 500–1000 years ago [Houghton et al., 1992]. Ash from the caldera-forming event produced tephra deposits up to 70 cm thick on mainland North Island, New Zealand.

Nemrut volcano, adjacent to Lake Van in Turkey, is the country's most active volcano. Magmatism for ~570,000 years has been dominated by peralkaline trachytes and rhyolites [Macdonald et al., 2015], the most recent eruption, ~500 years ago, being of comenditic lava flows in a rift valley on the northern flank of the volcano [Peretyazhko et al., 2015]. The active Furnas central volcano on São Miguel, Azores, is considered to be one of the most hazardous in the archipelago. There have been ten young (<5 ka) sub-Plinian eruptions of comenditic trachyte [Jeffery et al., 2016], the latest occurring in 1761 CE [Pimentel et al., 2016]. Pimentel et al. [2021] describe the potentially devastating effects on the 55,000 inhabitants of a future ignimbrite-forming eruption of Pico Alto volcano, Terceira.

A further, and perhaps underestimated, hazard is the emission of CO_2 and radon from active sys-

tems. For example, D'Alessandro et al. [2018] have estimated that the total CO_2 output of the volcanic/geothermal system of Pantelleria is 24.2 tons per day and have pointed to areas on the island which are at high risk to human health from indoor concentrations exceeding European Union threshold values. It is perhaps inevitable that such high concentrations also characterize other systems and detailed monitoring is required.

20. Environmental impact

On the basis of experimental data, Scaillet and Macdonald [2006a] showed that the fluid/melt partitioning of S in peralkaline rhyolites is lower than in metaluminous rhyolites, i.e., less S enters the fluid phase, especially under CO_2-rich conditions. Sulphur, ultimately derived from basaltic parents, can concentrate in the melt, eventually to be lost to the atmosphere during eruption. The estimated volume of the peralkaline rhyolites associated with the Ethiopian Trap flood sequences is 60,000 km^3 DRE [Ayalew et al., 2002]. Assuming that the rhyolites were derived from alkali basalt with 1 wt% melt water and 1000 ppm S, and that the derivative melts had 5–6 wt% dissolved water coexisting with 4–6 wt% fluid with up to 1 wt% S, then eruption of the rhyolites could have released 10^{17} g of S into the atmosphere. These are amounts comparable to estimated releases from the basaltic members of the flood activity. The flood sequences coincided with a worldwide cooling event and Ayalew et al. [2002] and Scaillet and Macdonald [2006a] speculated that the S released from the rhyolites was an important contributor to the cooling.

Using a broadly similar technique, Neave et al. [2012] estimated that the total S yield from the explosive eruption of the Green Tuff, Pantelleria (45.7 ± 1 ka; ~7 km^3 DRE) was 80–160 Mt which almost certainly had at least local environmental effects. Claessens et al. [2016] recorded a 1.8 Ma period of Late Miocene pantelleritic magmatism in central Kenya. They noted that their eruption coincided with a period of aridity in East Africa, with vegetation being pushed towards a more grass-dominated type. Using the Scaillet and Macdonald [2006a] and Neave et al. [2012] results as a model, Claessens et al. [2016] speculated that very significant amounts of S entered the atmosphere, producing such environmental effects as a surface temperature decrease, the direct

effect of acid rain on the fauna and flora, and acidification of lakes. Iddon and Edmonds [2020] estimated that an explosive, caldera-forming eruption (VEI > 5) in the Main Ethiopian Rift could outgas, in addition to 6 Mt of CO_2, 390 Mt of S into the lower troposphere or stratosphere. Ayalew et al. [2002] noted that eruption of the Ethiopian plateau ignimbrites coincided with a long-term Oligocene global cooling and may have accelerated the shift towards glacial conditions. The coincidence at least draws attention to the potential for Ethiopian Oligocene volcanism, and indeed any major peralkaline eruption, to have caused environmental stress.

However, the magnitude of an eruption may not by itself have global impact. Xu et al. [2013] found no stratospherically loaded sulphate spike associated with the Millennium eruption of Changbaishan-Tianchi in the volcanism record from the GISP ice core. They reasoned that the sulphate aerosols were not transported to the Arctic region, probably due to its relatively low stratospheric sulphur emission. The eruption probably had limited regional climatic effects.

21. Ore deposit potential

Critical elements and/or materials are defined as those elements for which a marked increase in usage has emerged, relative to past consumption. These elements or materials are usually listed as strategic based on assessed risks to their supply and/or impact to potential supply restrictions. Although the particular element list varies as a function of assessor, country, or economic union, they have many things in common. The critical elements include two general groups: (1) traditional commodities that have either very limited occurrences or supply such as Co and Sn and/or are involved in new technologies such as Mn and Sb, (2) and elements such as REE, Y, Nb, Ta that are used in new technologies such as electric vehicles, smartphones, wind power generation, and superalloys for jet engines and turbine blades.

The magmatic processes that yield peralkaline magmas enrich the final products in incompatible elements such as REE, HFSE, etc. [e.g., Mahood and Stimac, 1990]. The concentration of these elements can be further enhanced by late-stage magmatic and hydrothermal fluids, and supergene processes. Peralkaline intrusives have been explored and mined for these elements for many decades (e.g., Bokan Mountain, Alaska, USA, Strange Lake, Canada, Lovozero, Russia, Siwana Complex, India, and Norra Kärr, Sweden). As of this writing, we know of only one active mine in peralkaline extrusives, although there is and has been much exploration. We will restrict our discussion to REE and U as examples of the ore deposit potential of peralkaline extrusives.

In the last 100 years, the world's REE production went through three stages, placer mining of mainly monazite, the bastnäsite-rich Mountain Pass carbonatite, California, USA, and from the early 1990s, in China from the Bayan Obo deposit and ion-adsorption clay deposits. Currently, China accounts for >85% of the world's REE production [Schulz et al., 2017]. With the rapidly increasing use of REE in modern technology, current REE deposit exploration considers all potential sources. Mungall and Martin [1996] described a peralkaline rhyolite, Terceira, Azores, with extreme enrichment of HFSE in the glass and suggest that this occurrence is analogous to the Strange Lake, CA intrusive; however, mining in the Azores is improbable. Chandler and Spandler [2020] report active exploration in a peralkaline rhyolite complex in the Peak Range volcanics in central Queensland, Australia that is extremely enriched in REE and HFSE. The secondary ore mineral assemblage and REE redistribution observed is interpreted to be due to a combination of hydrothermal alteration by fluids derived from subjacent devolatilizing magma bodies, and late-stage supergene processes. They speculate that hydrothermal alteration is pervasive in the region and that deposits with high grades are likely.

Uranium is included in some critical element lists due to military, medical isotope and energy production, and satellite–energy uses. The Streltsovka caldera hosts the largest U mine and reserves in Russia. The ore developed through an extensive hydrothermal system that mobilized U from both the Late Jurassic peralkaline volcanics as well as from the Hercynian subalkaline granitic basement [Chabiron et al., 2003]. Castor and Henry [2000] describe exploration of large U deposits in Tertiary volcanics in Nevada and Oregon, USA. The peralkaline McDermitt and Virgin Valley calderas host rhyolites with U contents up to 15 ppm; much of the ore is hydrothermal with high Zr contents. Also of considerable importance, the largest Li deposit in the USA (~2 Mt)

occurs in basins adjacent to the McDermitt caldera. The Li has been leached from peralkaline rhyolite lavas and ash by hydrothermal and meteoric fluids [Benson et al., 2017] and is bound in clay in ash-rich sediments. The Cumberland Hill (New Brunswick, CA) peralkaline rhyolite is highly enriched in incompatible elements including U (up to ~20 ppm). Gray et al. [2010] suggest that the combination of a high U content and the probable supergene remobilization into the host sedimentary basin would create an area with high U ore potential.

The interplay of various factors makes a mineral deposit economic, such as tonnage and grade, amenability to mining and processing, acceptable low values of deleterious components, the impact on the environment, and market demand and price. Peralkaline extrusives with the requisite tonnage and grade, would be good candidates for mining mainly due to their surficial position conducive to open pit mining and their relative ease of beneficiation. Exploration targets should also observe the potential for hydrothermal and/or meteoric fluid element mobilization to nearby sedimentary hosts.

22. Final remarks

What exciting developments do we foresee for studies of peralkaline silicic extrusives? Some examples are: (i) Combined petrological/geophysical approaches to understanding reservoir processes will guide us to identifying the important signals of impending eruptions and to assessing the environmental hazards related to S and CO_2 emissions. (ii) Many large peralkaline provinces remain understudied, such as the Black Mountain Volcanic Centre, SW Nevada [Sawyer et al., 1994], the Marie Byrd Land Province, Antarctica [LeMasurier et al., 2018], and the Davis Mountains volcanic field, Trans-Pecos Texas [Parker, 2019]. (iii) The increasing demand for rare metals and the diversifying of sources means that peralkaline extrusive will become legitimate exploration targets, assuming all social and environmental issues can be resolved satisfactorily. (iv) Studies of the most highly evolved peralkaline melts are providing new insights into the extremes of magmatic processes. (v) On a personal note, we look forward to a further understanding of the dimensions and genesis of the reservoirs that fed the huge Ethiopian ignimbrite fields.

Conflicts of interest

Authors have no conflict of interest to declare.

References

Aguirre-Diaz, G. d. J. and Morton-Bermea, O. (2018). Geochemistry of the Amazcala Caldera, Querétaro, Mexico: An unusual peralkaline center in the central Mexican Volcanic, Belt. *Bol. Soc. Geol. Mex.*, 70, 731–760.

Andersen, D. J., Lindsley, D. H., and Davidson, P. M. (1993). A Pascal program to assess equilibria among Fe–Mg–Mn–Ti oxides, pyroxene, olivine, and quartz. *Comput. Geosci.*, 19, 1333–1350.

Andreeva, O. A., Yarmolyuk, V. V., Andreeva, I. A., and Borisovskiy, S. E. (2018). Magmatic evolution of Changbaishan Tianchi volcano, China–North Korea: evidence from mineral-hosted melt and fluid inclusions. *Petrology*, 26, 515–545.

Annen, C., Blundy, J. D., Leuthold, J., and Sparks, R. S. J. (2015). Construction and evolution of igneous bodies: Towards an integrated perspective of crustal magmatism. *Lithos*, 230, 206–221.

Avanzinelli, R., Bindi, L., Menchetti, S., and Conticelli, S. (2004). Crystallization and genesis of peralkaline magmas from Pantelleria Volcano, Italy: an integrated petrological and crystal-chemical study. *Lithos*, 73, 41–69.

Avanzinelli, R., Braschi, E., Marchioni, S., and Bindi, L. (2014). Mantle melting in within-plate continental settings: Sr–Nd–Pb and U-series isotope constraints in alkali basalts from the Sicily Channel (Pantelleria and Linosa Islands, Southern Italy). *Lithos*, 188, 113–129.

Ayalew, D., Barbey, P., Marty, B., Reisberg, L., Yirgo, G., and Pik, R. (2002). Source, genesis and timing of giant ignimbrite deposits associated with Ethiopian continental flood basalts. *Geochim. Cosmochim. Acta*, 66, 1429–1448.

Bachmann, O. and Bergantz, G. W. (2008). Rhyolites and their source mushes across tectonic settings. *J. Petrol.*, 40, 2277–2285.

Bacon, C. R. and Hirschmann, M. M. (1988). Mg/Mn partitioning as a test for equilibrium between co-existing Fe–Ti oxides. *Am. Mineral.*, 73, 57–61.

Bailey, D. K. (1980). Volcanism, Earth degassing and replenished lithosphere mantle. *Philos. Trans. R. Soc. Lond. A*, 297, 309–322.

Bailey, D. K. and Macdonald, R. (1970). Petrochemical variations among mildly peralkaline (comendite) obsidians from the oceans and continents. *Contrib. Mineral. Petrol.*, 28, 340–351.

Bailey, D. K. and Macdonald, R. (1987). Dry peralkaline felsic liquids and carbon dioxide flux through the Kenya Rift dome. In Mysen, B. O., editor, *Magmatic Processes: Physiochemical Principles*, pages 91–105. Geological Society, London, Special Publications.

Barberi, F., Ferrara, G., Santacroce, R., Treuil, M., and Varet, J. (1975). A transitional basalt-pantellerite sequence of fractional crystallization, the Boina Centre (Afar, Ethiopia). *J. Petrol.*, 16, 22–56.

Barberi, F., Santacroce, R., and Varet, J. (1974). Silicic peralkaline volcanic rocks of the Afar Depression (Ethiopia). *Bull. Volcanol.*, 38, 755–790.

Barboza, S. A. and Bergantz, G. W. (2000). Metamorphism and anatexis in the mafic complex contact aureole, Ivrea Zone, northern Italy. *J. Petrol.*, 41, 1307–1327.

Barclay, J., Carroll, M. R., Houghton, B. F., and Wilson, C. J. N. (1996). Pre-eruptive volatile content and degassing history of an evolving peralkaline volcano. *J. Volcanol. Geotherm. Res.*, 74, 75–87.

Beier, C., Haase, K. M., and Hansteen, T. H. (2006). Magma evolution of the Sete Cidades volcano, São Miguel, Azores. *J. Petrol.*, 47, 1375–1411.

Benson, T. R., Coble, M. A., Rytuba, J. J., and Mahood, G. A. (2017). Lithium enrichment in intracontinental rhyolite magmas leads to Li deposits in caldera basins. *Nat. Commun.*, 8, 1–9.

Bevier, M. L., Armstrong, R. L., and Souther, J. G. (1979). Miocene peralkaline volcanism in west-central British Columbia—its temporal and plate-tectonics setting. *Geology*, 7, 389–392.

Biggs, J., Anthony, E. Y., and Ebinger, C. J. (2009). Multiple inflation and deflation events at Kenya volcanoes, East African Rift. *Geology*, 37, 979–982.

Biggs, J., Bastow, I. D., Keir, D., and Lewt, E. (2011). Pulses of deformation reveal frequently recurring shallow magmatic activity beneath the Main Ethiopian Rift. *Geochem. Geophys. Geosyst.*, 12, 1–11.

Biggs, J. and Pritchard, M. E. (2017). Global volcano monitoring: what does it mean when volcanoes deform? *Elements*, 13, 17–22.

Black, S., Macdonald, R., and Kelly, M. R. (1997). Crustal origin for peralkaline rhyolites from Kenya: evidence from U-series disequilibria and Th-isotopes. *J. Petrol.*, 38, 277–297.

Blake, S. (1984). Volatile oversaturation during the evolution of silicic magma chambers as an eruption trigger. *J. Geophys. Res.*, 89, 8237–8244.

Blake, S. and Ivey, G. N. (1986). Density and viscosity gradients in zoned magma chambers, and their influence on withdrawal dynamics. *J. Volcanol. Geotherm. Res.*, 27, 153–178.

Blundy, J. and Cashman, K. (2008). Petrologic reconstruction of magmatic system variables and processes. *Rev. Mineral. Geochem.*, 69, 179–239.

Bohrson, W. A. and Reid, M. R. (1995). Petrogenesis of alkaline basalts from Socorro Island, Mexico: Trace element evidence for contamination of ocean island basalt in the shallow ocean crust. *J. Geophys. Res.*, 100, 24555–24576.

Bohrson, W. A. and Reid, M. R. (1997). Genesis of silicic peralkaline volcanic rocks in an ocean island setting by crustal melting and open-system processes: Socorro Island, Mexico. *J. Petrol.*, 38, 1137–1166.

Bryan, W. B. (1976). A basalt-pantellerite association from Isla Socorro, Islas Revillagigedo, Mexico. In Aoki, H. and IIzuka, S., editors, *Volcanoes and Tectonosphere*, pages 78–91. Tokai University Press, Tokyo, Japan.

Bunsen, R. (1851). Über die Prozesse der vulkanischen Gesteinsbildungen Islands. *Ann. Phys. Chem.*, 83, 197–272.

Cadoux, A., Pinti, D. L., Aznar, C., Chieso, S., and Gillot, P.-Y. (2005). New chronological and geochemical constraints on the genesis and geological evolution of Ponza and Palmarola Volcanic Islands (Tyrrhenian Sea, Italy). *Lithos*, 81, 121–151.

Caricchi, L., Ulmer, P., and Peccerillo, A. (2006). A high-pressure experimental study on the evolution of the silicic magmatism of the Main Ethiopian Rift. *Lithos*, 91, 46–58.

Carmichael, I. S. E. and MacKenzie, W. S. (1963). Feldspar-liquid equilibria in pantellerites: an experimental study. *Am. J. Sci.*, 261, 382–396.

Cashman, K. V., Sparks, R. S. J., and Blundy, J. D. (2017). Vertically extensive and unstable magmatic systems: A unified view of igneous processes. *Science*, 355, article no. eaag3055.

Castor, S. B. and Henry, C. D. (2000). Geology, geochemistry, and origin of volcanic rock-hosted uranium deposits in northwestern Nevada and southeastern Oregon, USA. *Ore Geol. Rev.*, 16(1–2), 1–40.

Chabiron, A., Cuney, M., and Poty, B. (2003). Possible uranium sources for the largest uranium district associated with volcanism: the Streltsovka caldera (Transbaikalia, Russia). *Miner. Depos.*, 38(2), 127–140.

Chamberlain, K. J., Barclay, J., Preece, K., Brown, R. J., and Davidson, J. P. (2016). Origin and evolution of silicic magmas at ocean islands: perspectives from a zoned fall deposit on Ascension Island, South Atlantic. *J. Volcanol. Geotherm. Res.*, 327, 349–360.

Chandler, R. and Spandler, C. (2020). The Igneous Petrogenesis and Rare Metal Potential of the Peralkaline Volcanic Complex of the Southern Peak Range, Central Queensland, Australia. *Lithos*, 358, article no. 105386.

Civetta, L., D'Antonio, M., Orsi, G., and Tilton, G. R. (1998). The geochemistry of volcanic rocks from Pantelleria Island, Sicily Channel: petrogenesis and characteristics of the mantle source region. *J. Petrol.*, 39, 1453–1491.

Claessens, L., Veldkamp, A., Schoorl, J. M., Wijbrans, J. R., van Gorp, W., and Macdonald, R. (2016). Large scale pantelleritic ash flow eruptions during the Late Miocene in central Kenya and evidence for significant environmental impact. *Glob. Planet Change*, 145, 30–41.

Clarke, B., Tierz, P., Calderm, E., and Yirgu, G. (2020). Probabilistic volcanic hazard assessment for pyroclastic density currents from pumice cone eruptions at Aluto volcano, Ethiopia. *Front. Earth Sci.*, 8, article no. 348.

Clarke, M. C. G., Woodhall, D. G., Allen, D., and Darling, G. (1990). *Geological, Volcanological and Hydrogeological Controls on the Occurrence of Geothermal Activity in the Area Surrounding Lake Naivasha, Kenya*. Ministry of Energy, Nairobi, Kenya.

Cole, J. W. (1990). Structural control and origin of volcanism in the Taupo Volcanic Zone, New Zealand. *Bull. Volcanol.*, 52, 445–459.

Cornwell, D. G., MacKenzie, G. D., England, R. W., Maguire, P. K. H., Asfaw, L. M., and Oluma, B. (2006). Northern main Ethiopian rift crustal structure from new high-precision gravity data. In Yirgu, G., Ebinger, C. J., and Maguire, P. K. H., editors, *The Afar Volcanic Province Within the East African Rift System*, volume 259, pages 307–321. Geological Society, London, Special Publications, London, UK.

Çubukçu, H. E., Ulusoy, I., Aydar, E., Ersoy, O., Şen, E., Gourgaud, A., and Guillou, H. (2012). Mt. Nemrut volcano (Eastern Turkey): Temporal petrological evolution. *J. Volcanol. Geotherm. Res.*, 209–210, 33–60.

D'Alessandro, W., Brusca, L., Cinti, D., Gagliano, A. I., Longo, M., Pecoraino, G., Pfanz, H., Pizzino, L., Raschi, A., and Voltattorni, N. (2018). Carbon dioxide and radon emissions from the soils of Pantelleria island (southern Italy). *J. Volcanol. Geotherm. Res.*, 362, 49–63.

Davies, G. R. and Macdonald, R. (1987). Crustal influences in the petrogenesis of the Naivasha basalt-comendite complex: combined trace element and Sr–Nd–Pb isotope constraints. *J. Petrol.*, 28, 1009–1031.

Di Bella, M., Russo, S., Petrelli, M., and Peccerillo, A. (2008). Origin and evolution of the Pleistocene magmatism of Linosa Island (Sicily Channel, Italy). *Eur. J. Mineral.*, 20, 587–601.

Di Carlo, I., Rotolo, S. G., Scaillet, B., Buccheri, V., and Pichavant, M. (2010). Phase equilibrium constraints on pre-eruptive conditions of recent felsic explosive volcanism at Pantelleria Island, Italy. *J. Petrol.*, 51, 2245–2276.

Di Genova, D., Romano, C., Hess, K. U., Vona, A., Giordano, D., Dingwell, D. B., and Behrens, H. (2013). The rheology of peralkaline rhyolites from Pantelleria island. *J. Volcanol. Geotherm. Res.*, 249, 201–216.

Di Matteo, V., Carroll, M. R., Behrens, H., Vetere, F., and Brooker, R. A. (2004). Water solubility in trachytic melts. *Chem. Geol.*, 212, 187–196.

Dingwell, D. B., Hess, K.-U., and Romano, C. (1998). Extremely fluid behavior of hydrous peralkaline rhyolites. *Earth Planet. Sci. Lett.*, 158, 31–38.

D'Oriano, C., Landi, P., Pimentel, A., and Zanon, V. (2017). Magmatic processes revealed by anorthoclase textures and trace element modelling: The case of the Lajes Ignimbrite eruption (Terceira Island, Azores). *J. Volcanol. Geotherm. Res.*, 347, 44–

63.

Dufek, J. D. and Berganz, G. W. (2005). Lower crustal magma genesis and preservation: A stochastic framework for the evaluation of basalt-crust interaction. *J. Petrol.*, 46, 2167–2195.

Dunkley, P. N., Smith, M., Allen, D. G., and Darling, W. G. (1993). *The geothermal activity and geology of the northern sector of the Kenya Rift Valley*, volume SC93/1 of *British Geological Survey research report*.

Esperança, S. and Crisci, G. M. (1995). The island of Pantelleria: A case for the development of DMM-HIMU isotopic compositions in a long-lived extensional setting. *Earth Planet. Sci. Lett.*, 136, 167–182.

Estrade, G., Salvi, S., Béziat, D., Rakotovao, S., and Rakotondrazafy, R. (2014). REE and HFSE mineralization in peralkaline granites of the Ambohimira-havavy alkaline complex, Ampasindava peninsula, Madagascar. *J. Afr. Earth Sci.*, 94, 141–155.

Evangelidis, C. P., Minshull, T. A., and Henstock, T. J. (2004). Three-dimensional crustal structure of Ascension Island from active source seismic tomography. *Geophys. J. Int.*, 159, 311–325.

Ewart, A., Taylor, S. R., and Capp, A. C. (1968). Geochemistry of the pantellerites of Mayor Island, New Zealand. *Contrib. Mineral. Petrol.*, 17, 116–140.

Ferla, P. and Meli, C. (2006). Evidence of magma mixing in the Daly Gap of alkaline suites: a case study from the enclaves of Pantelleria (Italy). *J. Petrol.*, 47, 1467–1507.

Field, L., Blundy, J., Brooker, R. A., and Wright, T. (2012). Magma storage conditions beneath Dabbahu Volcano (Ethiopia) constrained by petrology, seismicity and satellite geodesy. *Bull. Volcanol.*, 74, 981–1004.

Flude, S., Burgess, R., and McGarvie, D. W. (2008). Silicic volcanism at Ljósufjöll, Iceland: Insights into evolution and eruptive history from Ar–Ar dating. *J. Volcanol. Geotherm. Res.*, 169, 154–175.

Fontijn, K., McNamara, K., Tadesse, A. Z., Pyle, D. M., Dessalegn, F., Hutchison, W., Mather, T. A., and Yirgu, G. (2018). Contrasting styles of post-caldera volcanism along the Main Ethiopian Rift: implications for contemporary volcanic hazards. *J. Volcanol. Geotherm. Res.*, 356, 90–113.

Freundt, A. and Schmincke, H.-U. (1995). Petrogenesis of rhyolite-trachyte-basalt composite ignimbrite P1, Gran Canaria, Canary Islands. *J. Geophys. Res.*, 100, 455–474.

Freundt-Malecha, B., Schmincke, H.-U., and Freundt, A. (2001). Plutonic rocks of intermediate composition on Gran Canaria: The missing link of the bimodal volcanic suite. *Contrib. Mineral. Petrol.*, 141, 430–445.

Gaetani, G. A., Grove, T. L., and Bryan, W. B. (1993). The influence of water on the petrogenesis of subduction-related igneous rocks. *Nature*, 365, 332–334.

Gagnevin, D., Ethien, R., Bonin, B., Moine, B., Féraud, G., Gerbe, M. C., Cottin, J. Y., Michon, G., Tourpin, S., Mamias, G., Perrache, C., and Giret, A. (2003). Open-system processes in the genesis of silica-oversaturated alkaline rocks of the Rallier-du-Batty Peninsula, Kerguelen Archipelago (Indian Ocean). *J. Volcanol. Geotherm. Res.*, 123, 267–300.

Ghiorso, M. S. and Evans, B. W. (2008). Thermodynamics of rhombohedral oxide solid solutions and a revision of the Fe–Ti two-oxide geothermometer and oxygen-barometer. *Am. J. Sci.*, 308, 957–1039.

Ghiorso, M. S. and Sack, R. O. (1995). Chemical mass transfer in magmatic proceeses: IV. A revised and internally consistent thermodynamic model for the interpolation and extrapolation of liquid–solid equilibria in magmatic systems at elevated temperature and pressure. *Contrib. Mineral. Petrol.*, 119, 197–212.

Gioncada, A. and Landi, P. (2010). The pre-eruptive volatile contents of recent basaltic and pantelleritic magmas at Pantelleria (Italy). *J. Volcanol. Geotherm. Res.*, 180, 191–201.

Giordano, A., Russell, D. K., and Dingwell, D. B. (2008). Viscosity of magmatic liquids: a model. Earth Planet. *Sci. Lett.*, 271, 123–134.

Giordano, F., D'Antonio, M., Civetta, L., Tonarini, S., Orsi, G., Ayalew, D., Yirgu, G., Dell'Erba, F., Di Vito, M. A., and Isaia, R. (2014). Genesis and evolution of mafic and felsic magmas at Quaternary volcanoes within the Main Ethiopian Rift: Insights from Gedemsa and Fanta'Ale complexes. *Lithos*, 188, 130–144.

Gleeson, M. L. M., Stock, M. J., Pyle, D. M., Mather, T. A., Hutchison, W., Yirgu, G., and Wade, J. (2017). Constraining magma storage conditions at a restless volcano in the Main Ethiopian Rift using phase equilibria models. *J. Volcanol. Geotherm. Res.*, 337, 44–61.

Gottsmann, J., Biggs, J., Lloyd, R., Biranho, Y., and Lewi, E. (2020). Ductility and compressibility accommodate high magma flux beneath a silicic con-

tinental rift caldera: insights from Corbetti caldera (Ethiopia). *Geochem. Geophys. Geosyst.*, 21, article no. e2020GC008952.

Gray, T., Dostal, J., McLeod, M., Keppie, D., and Zhang, Y. (2010). Geochemistry of Carboniferous peralkaline felsic volcanic rocks, central New Brunswick, Canada: examination of uranium potential. *Atl. Geol.*, 46, 173–184.

Green, T. H. (1995). Significance of Nb/Ta as an indicator of geochemical processes in the crust-mantle system. *Chem. Geol.*, 120, 347–359.

Gualda, G. A., Ghiorso, M. S., Lemons, R. V., and Carley, T. L. (2012). Rhyolite-MELTS: a modified calibration of MELTS optimized for silica-rich, fluid-bearing magmatic systems. *J. Petrol.*, 53, 875–890.

Haase, K. M., Stoffers, P., and Garbe-Schönberg, C. D. (1997). The petrogenetic evolution of lavas from Easter Island and neighbouring seamounts, near-ridge hotspot volcanoes in the SE Pacific. *J. Petrol.*, 38, 785–813.

Halldórsson, S. A., Hilton, D. R., Scarsi, P., Abebe, T., and Hopp, J. (2014). A common mantle plume source beneath the entire East African Rift System revealed by coupled helium-neon systematics. *Geophys. Res. Lett.*, 41, 2304–2311.

Hammond, J. O. S., Wu, J.-P, Ri, K.-S., Wei, W., Yu, J.-N., and Oppenheimer, C. (2020). Distribution of partial melt beneath Changbaishan/Paektu volcano, China/Democratic People's Republic of Korea. *Geochem. Geophys. Geosyst.*, 21, article no. e2019GC008461.

Henry, C. D., Price, J. G., Rubin, J. N., and Laubach, S. E. (1990). Case study of an extensive silicic lava: the Bracks Rhyolite, Trans-Pecos Texas. *J. Volcanol. Geotherm. Res.*, 43, 113–132.

Heumann, A. and Davies, G. R. (2002). U–Th disequilibrium and Rb–Sr age constraints on the magmatic evolution of peralkaline rhyolites from Kenya. *J. Petrol.*, 43, 557–577.

Hildenbrand, A., Weis, D., Madureira, P., and Marques, F. O. (2014). Recent plate re-organization at the Azores Triple Junction: evidence from combined geochemical and geochronological data on Faial, S. Jorge and Terceira volcanic islands. *Lithos*, 210, 27–39.

Hoernle, K. A., Zhang, Y. S., and Graham, D. (1995). Seismic and geochemical evidence for large-scale mantle upwelling beneath the eastern Atlantic and western and central Europe. *Nature*, 374, 34–39.

Horn, S. and Schmincke, H.-U. (2000). Volatile emission during the eruption of Baitoushan Volcano (China/North Korea) ca. 969 AD. *Bull. Volcanol.*, 61, 537–555.

Houghton, B. F., Weaver, S. D., Wilson, C. J. N., and Lanphere, M. A. (1992). Evolution of a Quaternary peralkaline volcano: Mayor Island, New Zealand. *J. Volcanol. Geotherm. Res.*, 51, 217–236.

Huang, H.-H., Lin, F.-C., Schmandt, B., Farrell, J., Smith, R. B., and Tsai, V. C. (2015). The Yellowstone magmatic system from the mantle plume to the upper crust. *Science*, 348(6236), 773–776.

Hutchison, W., Biggs, J., Mather, T. A., Pyle, D. M., Lewi, F., Yirgu, G., Caliro, S., Chiodini, G., Clor, I. F., and Fischer, T. P. (2016b). Causes of unrest at silicic calderas in the East African Rift: New constraints from InSAR and soil-gas chemistry at Aluto volcano, Ethiopia. *Geochem. Geophys. Geosyst.*, 17, 3008–3030.

Hutchison, W., Mather, T. A., Pyle, D. M., Boyce, A. J., Gleeson, M. L. M., Yirgu, G., Blundy, J. D., Ferguson, D. J., Vye-Brown, C., Millar, I. L., Sims, K. W. W., and Finch, A. A. (2018). The evolution of magma during continental rifting: New constraints from the isotopic and trace element signatures of silicic magmas from Ethiopian volcanoes. *Earth Planet. Sci. Lett.*, 489, 203–218.

Hutchison, W., Pyle, D. M., Mather, T. A., Yirgu, G., Biggs, J., Cohen, B. E., Barfod, D. N., and Lewi, F. (2016a). The eruptive history and magmatic evolution of Aluto volcano: new insights into silicic peralkaline volcanism in the Ethiopian rift. *J. Volcanol. Geotherm. Res.*, 328, 9–33.

Iddon, F. and Edmonds, M. (2020). Volatile-rich magmas distributed through the upper crust in the Main Ethiopian Rift. *Geochem. Geophys. Geosyst.*, 21, article no. e2019GC08904.

Iddon, F., Jackson, C., Hutchison, W., Fontijn, K., Pyle, D. M., Mather, T. A., Yirgu, G., and Edmonds, M. (2019). Mixing and crystal scavenging in the Main Ethiopian Rift revealed by trace element systematics in feldspars and glasses. *Geochem. Geophys. Geosyst.*, 20, 230–259.

Imsland, P., Larsen, J. G., Prestvik, T., and Sigmond, E. M. (1977). The geology and petrology of Bouvetøya, south Atlantic Ocean. *Lithos*, 10, 213–234.

Javoy, M. and Courtillot, V. (1989). Intense acidic volcanism at the Cretaceous-Tertiary boundary. *Earth Planet. Sci. Lett.*, 94, 409–416.

Jeffery, A. J. and Gertisser, R. (2018). Peralkaline felsic magmatism of the Atlantic islands. *Front. Earth Sci.*, 6, article no. 145.

Jeffery, A. J., Gertisser, R., O'Driscoll, B., Pacheco, J. M., Whitley, S., Pimentel, A., and Self, S. (2016). Temporal evolution of a post-caldera, mildly peralkaline magmatic system: Furnas volcano, São Miguel, Azores. *Contrib. Mineral. Petrol.*, 171, article no. 42.

Jeffery, A. J., Gertisser, R., Self, S., Pimentel, A., O'Driscoll, B., and Pacheco, J. M. (2017). Petrogenesis of the peralkaline ignimbrites of Terceira, Azores. *J. Petrol.*, 58, 2365–2402.

Jellinek, A. M. and DePaolo, D. J. (2003). A model for the origin of large silicic magma chambers: precursors of caldera-forming eruptions. *Bull. Volcanol.*, 65, 363–381.

Jicha, B. R., Singer, B. S., and Valentine, M. J. (2013). $^{40}Ar/^{39}Ar$ geochronology of subaerial Ascension Island and a re-evaluation of the temporal progression of basaltic to rhyolitic volcanism. *J. Petrol.*, 54, 2581–2596.

Joachum, K. P., Seufert, H. M., Spettel, B., and Palme, H. (1986). The solar-system abundances of Nb, Ta, and Y, and the relative abundances of refractory lithophile elements in differentiated planetary bodies. *Geochem. Cosmochem. Acta*, 50, 1173–1183.

Jordan, N. J., Rotolo, S. G., Williams, R., Speranza, F., McIntosh, W. C., Branney, M. J., and Scaillet, S. (2018). Explosive eruptive history of Pantelleria, Italy: repeated caldera collapse and ignimbrite formation at a peralkaline volcano. *J. Volcanol. Geotherm. Res.*, 349, 42–73.

Jordan, N. J., White, J. C., Macdonald, R., and Rotolo, S. G. (2021). Evolution of the magma system of Pantelleria (Italy) from 190 ka to present. *C. R. Géosci.*, 353, 1–17.

Jørgensen, K. A. (1980). The Thorsmörk ignimbrite: an unusual comenditic pyroclastic flow in southern Iceland. *J. Volcanol. Geotherm. Res.*, 8, 7–22.

Kar, A., Weaver, B., Davidson, J., and Colucci, M. (1998). Origin of differentiated volcanic and plutonic rocks from Ascension Island, South Atlantic Ocean. *J. Petrol.*, 39, 1009–1024.

Kovalenko, V. I., Yarmolynk, V. V., Kovatch, D. V., Kovalenko, D. V., Kozlovsku, A. M., Andreeva, I. A., Kotov, A. B., and Sal'nikova, E. B. (2009). Variations in isotope composition and of critical ratios of in-

compatible trace elements as reflections of source mixing for alkaline granitoids and basites from the Khaldzan Buregtey massif and of the rare-metal deposit there. *Petrology*, 17, 249–275.

Krumrei, T. V. and Markl, G. (2005). Fluid inclusions in sodalite from the peralkaline Ilimaussaq complex, South Greenland: an indicator of fluid composition changes. In *Peralkaline Rocks: Sources, Economic Potential and Evolution from Alkaline Melts*, pages 59–60. PERALK Workshop on Peralkaline Rocks, Tuebingen, Germany. Abstract.

Kynicky, J., Chakmouradian, A. R., Xu, C., Krmicek, J., and Galiova, M. (2011). Distribution and evolution of zirconium mineralization in peralkaline granites and associated pegmatites of the Khan Bogd complex, southern Mongolia. *Can. Mineral.*, 49, 947–965.

Lacroix, A. (1930). Les roches hyperalcalines du Massif du Fantale et du col de Balla. *Mém. Soc. Géol. Fr.*, 14, 89–102.

Landi, P. and Rotolo, S. G. (2015). Cooling and crystallization recorded in trachytic enclaves hosted in pantelleritic magmas (Pantelleria, Italy): Implications for pantellerite petrogenesis. *J. Volcanol. Geotherm. Res.*, 301, 169–179.

Lanzo, G., Landi, P., and Rotolo, S. G. (2013). Volatiles in pantellerite magmas: A case study of the Green Tuff Plinian eruption (Island of Pantelleria, Italy). *J. Volcanol. Geotherm. Res.*, 262, 153–163.

Latin, D., Norry, M. J., and Tarzey, R. J. E. (1993). Magmatism in the Gregory Rift, East Africa: evidence for melt generation in a plume. *J. Petrol.*, 34, 1007–1027.

Le Bas, M. J., Le Maitre, R. W., Streickeisen, A., and Zanettin, B. (1986). A chemical classification of volcanic rocks based on the total alkali–silica diagram. *J. Petrol.*, 27, 745–750.

Leat, P. T., Macdonald, R., and Smith, R. L. (1984). Geochemical evolution of the trachytic caldera volcano Menengai, Kenya. *J. Geophys. Res.*, 89, 8571–8592.

Lees, J. M. (2007). Seismic tomography of magmatic systems. *J. Volcanol. Geotherm. Res.*, 167, 37–56.

LeMasurier, W. E. (2019). Rhyolites from the mantle, Marie Byrd Land, west Antarctica. In *American Geophysical Union Fall Meeting*. Abstract No. 548106.

LeMasurier, W. E., Choi, S. H., Kawachi, Y., Mukasa, S. B., and Rogers, N. W. (2011). Evolution of

pantellerite-trachyte-phonolite volcanoes by fractional crystallization of basanite magma in a continental rift setting, Marie Byrd Land, Antarctica. *Contrib. Mineral. Petrol.*, 162, 1175–1199.

LeMasurier, W. E., Choi, S. H., Kawachi, Y., Mukasa, S. B., and Rogers, N. W. (2018). Dual origins for pantellerites, and other puzzles, at Mount Takahe volcano, Marie Byrd Land, West Antarctica. *Lithos*, 296–299, 142–162.

Lightfoot, P. C., Hawkesworth, C. J., and Sethna, S. F. (1987). Petrogenesis of rhyolites and trachytes from the Deccan trap: Sr, Nd and Pb isotope and trace element evidence. *Contrib. Mineral. Petrol.*, 85, 44–54.

Liszewska, K. M., White, J. C., Macdonald, R., and Bagiński, B. (2018). Compositional and thermodynamic variability in a stratified magma chamber: Evidence from the Green Tuff Ignimbrite (Pantelleria, Italy). *J. Petrol.*, 59, 2245–2272.

Lowenstern, J. B. (1994). Chlorine, fluid immiscibility, and degassing in peralkaline magmas from Pantelleria, Italy. *Am. Mineral.*, 79, 353–369.

Lowenstern, J. B., Charlier, B. L. A., Clynne, M. A., and Wooden, J. L. (2006). Extreme U–Th disequilibrium in rift-related basalts, rhyolites and granophyric granite and the timescale of rhyolite generation, intrusion and crystallization at Alid volcanic center, Eritrea. *J. Petrol.*, 47, 2105–2122.

Lowenstern, J. B. and Mahood, G. A. (1991). New data on magmatic H$_2$O contents with implications for petrogenesis and eruptive dynamics at Pantelleria. *Bull. Volcanol.*, 54, 78–83.

Luhr, J. F., Nelson, S. A., Allan, J. F., and Carmichael, I. S. E. (1985). Active rifting in southwestern Mexico: Manifestations of an incipient eastward spreading ridge jump. *Geology*, 13, 54–57.

Lustrino, M., Fedele, L., Melluso, L., Morra, V., Ronga, F., Geldmacher, J., Duggen, S., Agostini, S., Cucciniello, C., Franciosi, L., and Meisel, T. (2013). Origin and evolution of Cenozoic magmatism of Sardinia (Italy). A combined isotopic (Sr–Nd–Pb–O–Hf–Os) and petrological view. *Lithos*, 180–181, 138–158.

Macdonald, R. (1974). Nomenclature and petrochemistry of the peralkaline oversaturated extrusive rocks. *Bull. Volcanol.*, 38, 498–516.

Macdonald, R. (1994). Petrological evidence regarding the evolution of the Kenya Rift Valley. *Tectonophysics*, 236, 373–390.

Macdonald, R. (2012). Evolution of peralkaline silicic complexes: Lessons from the extrusive rocks. *Lithos*, 152, 11–22.

Macdonald, R., Bagiński, B., Belkin, H. E., White, J. C., and Noble, D. C. (2019). The Gold Flat Tuff, Nevada: insights into the evolution of peralkaline silicic magmas. *Lithos*, 328–329, 1–13.

Macdonald, R., Bagiński, B., Leat, P. T., White, J. C., and Dzierżanowski, P. (2011). Mineral stability in peralkaline silicic rocks: Information from trachytes of the Menengai volcano, Kenya. *Lithos*, 125, 553–568.

Macdonald, R., Bagiński, B., Ronga, F., Dzierżanowski, P., Lustrino, M., Marzoli, A., and Melluso, L. (2012). Evidence for extreme fractionation of peralkaline silicic magmas, the Boseti volcanic complex, Main Ethiopian Rift. *Mineral. Petrol.*, 104, 163–175.

Macdonald, R., Bagiński, B., and Upton, B. G. J. (2014). The volcano-pluton interface: The Longonot (Kenya) and Kûngnât (Greenland) peralkaline complexes. *Lithos*, 196–197, 232–241.

Macdonald, R. and Bailey, D. K. (1973). *The Chemistry of the Peralkaline Oversaturated Obsidians*. US Geol. Surv. Prof. Paper 440-N-1.

Macdonald, R., Belkin, H. E., Fitton, J. G., Rogers, N. W., Nejbert, K., Tindle, A. G., and Marshall, A. S. (2008). The roles of fractional crystallization, magma mixing, crystal mush remobilization and volatile-melt interactions in the genesis of a young basalt-peralkaline rhyolite suite, the Greater Olkaria Volcanic Complex, Kenya Rift Valley. *J. Petrol.*, 49, 1515–1547.

Macdonald, R., Davies, G. R., Bliss, C. M., Leat, P. T., Bailey, D. K., and Smith, R. L. (1987). Geochemistry of high-silica peralkaline rhyolites, Naivasha, Kenya Rift Valley. *J. Petrol.*, 28, 979–1008.

Macdonald, R., Davies, G. R., Upton, B. G. J., Dunkley, P. N., Smith, M., and Leat, P. T. (1995). Petrogenesis of Silali volcano, Gregory Rift, Kenya. *J. Geol. Soc., Lond.*, 152, 703–720.

Macdonald, R., Navarro, J. M., Upton, B. G. J., and Davies, G. R. (1994). Strong compositional zonation in peralkaline magma, Menengai, Kenya Rift Valley. *J. Volcanol. Geotherm. Res.*, 60, 301–325.

Macdonald, R., Rogers, N. W., Fitton, J. G., Black, S., and Smith, M. (2001). Plume-lithosphere interactions in the generation of the basalts of the Kenya Rift, East Africa. *J. Petrol.*, 42, 877–900.

Macdonald, R., Smith, R. L., and Thomas, J. E. (1992). *Chemistry of the Subalkalic Silicic Obsidians*. US Geol. Surv. Prof. Paper 1523.

Macdonald, R., Sumita, M., Schmincke, H.-U., Bagiński, B., White, J. C., and Ilnicki, S. (2015). Peralkaline felsic magmatism at the Nemrut volcano, Turkey: impact of volcanism on the evolution of Lake Van (Anatolia) IV. *Contrib. Mineral. Petrol.*, 169, article no. 34.

Magee, C., Stevenson, C. T. E., Ebmeier, S. K., Keir, D., Hammond, J. O. S., Gottsman, J. H., Whaler, K. A., Schofield, N., Jackson, C. A.-L., Petronis, M. S., O'Driscoll, B. O., Morgan, J., Cruden, A., Vollgger, S. A., Dering, G., Micklethwaite, S., and Jackson, M. D. (2018). Magma plumbing systems: a geophysical perspective. *J. Petrol.*, 59, 1217–1251.

Mahatsente, R., Jentzsch, G., and Jahr, T. (1999). Crustal structure of the Main Ethiopian Rift from gravity data: 3-dimensional modeling. *Tectonophysics*, 31, 363–382.

Mahood, G. and Hildreth, W. (1986). Geology of the peralkaline volcano at Pantelleria, Strait of Sicily. *Bull. Volcanol.*, 48, 143–172.

Mahood, G. A. (1980). Geological evolution of a Pleistocene rhyolitic center—Sierra La Primavera, Jalisco, Mexico. *J. Volcanol. Geotherm. Res.*, 8, 199–230.

Mahood, G. A. (1981a). A summary of the geology and petrology of the Sierra La Primavera, Jalisco, Mexico. *J. Geophys. Res.*, 86, 10137–10152.

Mahood, G. A. (1981b). Chemical evolution of a Pleistocene rhyolitic center—Sierra La Primavera, Jalisco, Mexico. *Contrib. Mineral. Petrol.*, 77, 129–149.

Mahood, G. A. (1984). Pyroclastic rocks and calderas associated with strongly peralkaline magmatism. *J. Geophys. Res.*, 89, 8540–8552.

Mahood, G. A. and Baker, D. R. (1986). Experimental constraints on depths of fractionation of mildly alkali basalts and associated felsic rocks: Pantelleria, Strait of Sicily. *Contrib. Mineral. Petrol.*, 93, 251–264.

Mahood, G. A., Gilbert, C. M., and Carmichael, I. S. E. (1985). Peralkaline and metaluminous mixed-liquid ignimbrites of the Guadalajara region, Mexico. *J. Volcanol. Geotherm. Res.*, 25, 259–271.

Mahood, G. A. and Stimac, J. A. (1990). Trace-element partitioning in pantellerites and trachytes. *Geochim. Cosmochim. Acta*, 54(8), 2257–2276.

Margari, V., Pyle, D. M., Bryant, C., and Gibbard, P. L. (2007). Mediterranean tephra stratigraphy revisited: results from a long terrestrial sequence on Lesvos Island, Greece. *J. Volcanol. Geotherm. Res.*, 163, 34–54.

Markl, G., Marks, M. A. W., and Frost, B. R. (2010). On the controls of oxygen fugacity in the generation and crystallization of peralkaline melts. *J. Petrol.*, 51, 1831–1847.

Marshall, A. S., Macdonald, R., Rogers, N. W., Fitton, J. G., Tindle, A. G., Nejbert, K., and Hinton, R. W. (2009). Fractionation of peralkaline silicic magmas: the Greater Olkaria Volcanic Complex, Kenya Rift Valley. *J. Petrol.*, 50, 323–359.

Martel, C., Champallier, R., Prouteau, G., Pichavant, M., Arbaret, L., Balcone-Boissard, H., Boudon, G., Boivin, P., Bourdier, J.-L., and Scaillet, B. (2013). Trachyte phase relations and implication for magma storage conditions in the Chaîne des Puys (French Massif Central). *J. Petrol.*, 54, 1071–1107.

Martz, A. M. and Brown, F. H. (1981). Chemistry and mineralogy of some Plio-Pleistocene tuffs from from the Shungura Formation, southwest Ethiopia. *Quat. Res.*, 16, 240–257.

Masotta, M., Mollo, S., Freda, C., Gaeta, M., and Moore, G. (2013). Clinopyroxene-liquid thermometer and barometers specific to alkaline differentiated magmas. *Contrib. Mineral. Petrol.*, 166, 1545–1561.

Masturyono, M. R., Wark, D. A., Roecker, S. W., Fauzi, I., and Sukhyar, G. (2001). Distribution of magma beneath the Toba caldera complex, north Sumatra, Indonesia, constrained by three-dimensional P wave velocities, seismicity, and gravity data. *Geochem. Geophys. Geosyst.*, 2, article no. 2000GC00096.

Mattia, M., Bonaccorso, A., and Guglielmino, F. (2007). Ground deformations in the Island of Pantelleria (Italy): Insights into the dynamic of the current intereruptive period. *J. Geophys. Res.*, 112, article no. B11406.

Mbowou, G. I. B., Lagmet, C., Nomade, S., Ngounouno, I., Déruelle, B., and Ohnenstetter, D. (2012). Petrology of the Late Cretaceous peralkaline rhyolites (pantellerite and comendite) from Lake Chad, Central Africa. *J. Geosci.*, 57, 127–141.

McCurry, M. (1988). Geology and petrology of the Woods Mountain Volcanic Center, southeastern

California: implications for the genesis of peralkaline rhyolite ash flow tuffs. *J. Geophys. Res.*, 93, 14835–14855.

McGarvie, D. W., Burgess, R., Tindle, A. G., Tuffen, H., and Stevenson, J. A. (2006). Pleistocene rhyolitic volcanism at the Torfajökull central volcano, Iceland: eruption ages, glaciovolcanism, and geochemical evolution. *Jokull*, 56, 57–75.

McNamara, K., Cashman, K. V., Rust, A. C., Fontijn, K., Chalié, F., Tomlinson, E. L., and Yirgu, G. (2018). Using lake sediment cores to improve records of volcanism at Aluto volcano in the Main Ethiopian Rift. *Geochem. Geophys. Geosyst.*, 19, 3164–3188.

Metrich, N. and Rutherford, M. J. (1992). Experimental study of chlorine in hydrous silicic melts. *Geochim. Cosmochim. Acta*, 56, 607–616.

Miranda, J. M., MendesVictor, L. A., Simões, J. Z., Luis, J. F., Matias, L., Shimamura, H., Shiobara, H., Nemoto, H., Mochizuki, H., Hirn, A., and Lépine, J. C. (1998). Tectonic setting of the Azores Plateau deduced from a OBS survey. *Mar. Geophys. Res.*, 20, 171–182.

Mondal, S., Upadhyay, D., and Banerjee, A. (2021). REE mineralization in Siwana peralkaline granite, western India—role of fractional crystallization, hydrothermal remobilization, and feldspar–fluid interaction. *Lithos*, 396–397, article no. 106240.

Morra, V., Secchi, F. A., and Assorgia, A. (1994). Petrogenetic significance of peralkaline rocks from Cenozoic calc-alkaline volcanism from SW Sardinia, Italy. *Chem. Geol.*, 118, 109–142.

Mungall, J. E. and Martin, R. F. (1995). Petrogenesis of basalt-comendite and basalt-pantellerite suites, Terceira, Azores, and implications for the origin of ocean-island rhyolites. *Contrib. Mineral. Petrol.*, 119, 43–55.

Mungall, J. E. and Martin, R. F. (1996). Extreme differentiation of peralkaline rhyolite, Terceira, Azores: a modern analogue of Strange Lake, Labrador? *Can. Mineral.*, 34, 769–777.

Mushkin, A., Stein, M., Halicz, I., and Navon, O. (2002). The Daly gap: low-pressure fractionation and heat-loss from a cooling magma chamber. *Geochim. Cosmochim. Acta*, 66(Supplement 1), article no. A539.

Neave, D. A. (2020). Chemical variability in peralkaline magmas and magma reservoirs: insights from the Khaggiar lava flow, Pantelleria, Italy. *Contrib. Mineral. Petrol.*, 175, article no. 39.

Neave, D. A., Fabbro, G., Herd, R. A., Petrone, C. M., and Edmonds, M. (2012). Melting, differentiation and degassing at the Pantelleria volcano, Italy. *J. Petrol.*, 53, 637–663.

Nekvasil, H., Dondolini, A., Horn, J., Filiberto, J., Long, H., and Lindsley, D. H. (2004). The origin and evolution of silica-saturated alkalic suites: an experimental study. *J. Petrol.*, 45, 693–721.

Nelson, S. A. and Hegre, J. (1990). Volcán Las Navajas, a Pliocene-Pleistocene trachyte/peralkaline rhyolite volcano in the northwestern Mexican volcanic belt. *Bull. Volcanol.*, 52, 186–204.

Nicholls, J. and Carmichael, I. S. E. (1969). Peralkaline acid liquids: a petrological study. *Contrib. Mineral. Petrol.*, 20, 268–294.

Nivin, V. A., Treloar, P. J., Konopleva, N. G., and Ikorsky, S. V. (2005). A review of the occurrence, form and origin of C-bearing species in the Khibiny Alkaline Igneous Complex, Kola Peninsula, *Lithos*, 85, 93–112.

Novak, S. W. and Mahood, G. A. (1986). Rise and fall of a basalt-trachyte-rhyolite magma system at the Kane Springs Wash Caldera, Nevada. *Contrib. Mineral. Petrol.*, 94, 352–373.

O'Neil, H. S. C. and Pownceby, M. I. (1993). Thermodynamic data from redox reactions at high temperatures. I. an experimental and theoretical assessment of the electrochemical method using stabilized zirconia electrolytes, with revised values for the Fe-"FeO", Co–CoO, Ni–NiO, and Cu–Cu$_2$O oxygen buffers, and new data for the W–WO$_2$ buffer. *Contrib. Mineral. Petrol.*, 114, 296–314.

Pan, B., de Silva, S. I., Xu, J., Chen, Z., Miggins, D. P., and Wei, W. (2017). The VEI-7 Millennium eruption, Changbaishan-Tianchi volcano, China/DPRK: New field, petrological, and chemical constraints on stratigraphy, volcanology, and magma dynamics. *J. Volcanol. Geotherm. Res.*, 343, 45–59.

Pan, B., de Silva, S. I., Xu, J., Liu, S., and Xu, D. (2020). Late Pleistocene to present day eruptive history of the Changbaishan-Tianchi volcano, China/DPRK: New field, geochronological and chemical constraints. *J. Volcanol. Geotherm. Res.*, 399, article no. 106870.

Papale, P., Moretti, R., and Barbaro, D. (2006). The compositional dependence of the saturation surface of H$_2$O + CO$_2$ fluids in silicate melts. *Chem. Geol.*, 229, 78–95.

Parker, D. F. (2019). Generation of alkali flood rhyolite: Insights from evolution of the Paisano volcano, Davis mountains, Trans-Pecos Texas, USA. *J. Volcanol. Geotherm. Res.*, 374, 120–130.

Parker, D. F. and Henderson, G. D. (2021). Geochemical evolution of the Paradise Mountain caldera complex, Davis Mountains: Implications for the tectonic and magmatic evolution of Trans-Pecos Texas and adjacent Mexico. *Lithos*, 404–405, article no. 106453.

Parker, D. F. and White, J. C. (2008). Large-scale silicic alkali magmatism associated with the Buckhorn Caldera, Trans-Pecos Texas, USA: comparison with Pantelleria, Italy. *Bull. Volcanol.*, 70, 403–415.

Parker, D. F., White, J. C., Ren, M., and Barnes, M. (2017). Basement control of alkalic flood rhyolite magmatism of the Davis Mountains volcanic field, Trans-Pecos Texas, USA. *Lithos*, 292–293, 234–249.

Peccerillo, A., Barberio, M. R., Yirgu, G., Ayalew, D., Barbieri, M., and Wu, T. W. (2003). Relationships between mafic and peralkaline silicic magmatism in continental rift settings: a petrological, geochemical, and isotopic study of the Gedemsa volcano, central Ethiopian rift. *J. Petrol.*, 44, 2002–2032.

Peretyazhko, I. S., Savina, E. A., and Karmanov, N. S. (2015). Comendites and pantellerites of Nemrut Volcano, Easter Turkey: genesis and relations between the trachyte-comenditic, comenditic and pantelleritic melts. *Petrology*, 23, 576–622.

Pimentel, A., Self, S., Pacheco, J. M., Jeffery, A. J., and Gertisser, R. (2021). Eruption style, emplacement dynamics and geometry of peralkaline ignimbrites: Insights from the Lajes-Angra ignimbrite formation, Terceira Island, Azores. *Front. Earth Sci.*, 9, article no. 673686.

Pimentel, A., Zanon, V., de Groot, L. V., Hipólito, A., Di Chiara, A., and Self, S. (2016). Stress-induced comenditic trachyte effusion triggered by trachybasalt intrusion: multidisciplinary study of the AD 1761 eruption at Terceira Island (Azores). *Bull. Volcanol.*, 78, article no. 22.

Pownceby, M. I. and O'Neil, H. S. C. (1994). Thermodynamic data from redox reactions at high temperatures III. Activity-composition relations in Ni–Pd alloys from EMF measurements at 850–1250 K, and calibration of the NiO + Ni–Pd assemblage as a redox sensor. *Contrib. Mineral. Petrol.*, 116, 327–339.

Prestvik, T., Goldberg, S., and Goles, G. (1999). Petrogenesis of the volcanic suite of Bouvetøya (Bouvet Island), South Atlantic. *Norsk Geol. Tidsskr.*, 79, 205–218.

Prestvik, T., Goldberg, S., Karlsson, H., and Grönvold, K. (2001). Anomalous strontium and lead isotope signatures in the off-rift Öræfajökull central volcano in south-east Iceland. Evidence for enriched endmember(s) of the Iceland mantle plume? *Earth Planet. Sci. Lett.*, 190, 211–220.

Putirka, K. (2008). Thermobarometers and barometers for volcanic systems. In Putirka, K. and Tepley, F., editors, *Minerals, Inclusions and Volcanic Processes*, volume 69, pages 61–120. PERALK Workshop on Peralkaline Rocks, Tuebingen, Germany.

Rapprich, V., Źáček, V., Verner, K., Erban, V., Goslar, T., Bekele, Y., Legesa, F., Hroch, T., and Hejtmánková, P. (2016). Wendo Koshe Pumice: The latest Holocene silicic explosive eruption product of the Corbetti Volcanic System (Southern Ethiopia). *J. Volcanol. Geotherm. Res.*, 310, 159–171.

Ren, M., Omenda, P. A., Anthony, E. Y., White, J. C., Macdonald, R., and Bailey, D. K. (2006). Application of the QUILF thermobarometer to the peralkaline trachytes and rhyolites of the Eburru volcanic complex, East African Rift, Kenya. *Lithos*, 91, 109–124.

Renna, M. R., Tribuzio, R., and Braga, R. (2013). Petrogenetic relationships between peralkaline rhyolite dykes and mafic rocks in the post-Variscan gabbroic complex from Bocca di Tenda (northern Corsica, France). *Contrib. Mineral. Petrol.*, 165, 1073–1085.

Rogers, N. W., Evans, P. J., Blake, S., Scott, S. C., and Hawkesworth, C. J. (2004). Rates and time-scales of fractional crystallization from ^{238}U–^{230}Th–^{226}Ra disequilibrium in trachyte lavas from Longonot volcano, Kenya. *J. Petrol.*, 45, 1747–1776.

Rogers, N. W., Macdonald, R., Fitton, J. G., George, R., Smith, M., and Barreiro, B. (2000). Two mantle plumes beneath the East African rift system: Sr, Nd and Pb isotope evidence from Kenya Rift basalts. *Earth Planet. Sci. Lett.*, 176, 387–400.

Romano, P., Andújar, J., Scaillet, B., Romengo, N., di Carlo, I., and Rotolo, S. G. (2018). Phase equilibria of Pantelleria trachytes (Italy): constraints on pre-eruptive conditions and on the metaluminous to peralkaline transition in silicic magmas. *J. Petrol.*, 59, 559–588.

Romano, P, Di Carlo, I., Andújar, J., and Rotolo, S. G.

(2021). Water solubility in trachytic and pantelleritic melts: an experimental study. *C. R. Géosci.*, 353, 1–17.

Romano, P., Scaillet, B., White, J. C., Andújar, J., Di Carlo, I., and Rotolo, S. G. (2020). Experimental and thermodynamic constraints on mineral equilibrium in pantelleritic magmas. *Lithos*, 376–377, article no. 105793.

Romano, P., White, J. C., Ciulla, A., Di Carlo, I., D'Oriano, C., Landi, P., and Rotolo, S. G. (2019). Volatiles and trace element contents in melt inclusions from the zoned Green Tuff ignimbrite (Pantelleria, Sicily): petrological inferences. *Ann. Geophys.*, 61, article no. VO09.

Romengo, N., Landi, P., and Rotolo, S. G. (2012). Evidence of basaltic magma intrusions in a trachytic magma chamber at Pantelleria (Italy). *Period. Mineral.*, 81, 163–178.

Rondet, M., Martel, C., and Bourdier, J.-L. (2019). The intermediate step in fractionation trends of mildly alkaline volcanic suites: An experimental insight from the Pavin trachyandesite (Massif Central, France). *C. R. Géosci.*, 351, 525–539.

Ronga, F., Lustrino, M., Marzoli, A., and Melluso, L. (2010). Petrogenesis of a basalt-comendite-pantellerite rock suite: the Boseti volcanic complex (Main Ethiopian Rift). *Mineral. Petrol.*, 98, 227–243.

Rooney, T. O., Hart, W. K., Hall, C. M., Ayalew, D., Ghiorso, M. S., Hidalgo, P., and Yirgu, G. (2012). Peralkaline magma evolution and the tephra record in the Ethiopian Rift. *Contrib. Mineral. Petrol.*, 164, 407–426.

Rotolo, S. G., Scaillet, S., Speranza, F., White, J. C., Williams, R., and Jordan, N. J. (2021). Volcanological evolution of Pantelleria Island (Strait of Sicily) peralkaline volcano: a review. *C. R. Géosci.*, 353, 1–22.

Rutherford, N. F. (1978). A comment on the source of Mayor Island pantellerite magma. *N. Z. J. Geol. Geophys.*, 21, 449–453.

Salvi, S. and Williams-Jones, A. E. (2006). Alteration, HFSE mineralisation and hydrocarbon formation in peralkaline igneous systems: Insights from the Strange Lake Pluton, Canada. *Lithos*, 91, 19–34.

Samrock, F., Grayver, A. V., Bachmann, O., Karakas, O., and Saar, M. O. (2021). Integrated magnetotelluric and petrological analysis of felsic magma reservoirs: Insights from Ethiopian rift volcanoes. *Earth Planet. Sci. Lett.*, 559, article no. 116765.

Sauerzapf, U., Lattard, D., Burchard, M., and Engelmann, R. (2008). The titanomagnetite-ilmenite equilibrium: new experimental data and thermo-oxybarometric application to the crystallization of basic to intermediate rocks. *J. Petrol.*, 49, 1161–1185.

Sawyer, D. A., Fleck, R. J., Lanphere, M. A., Warren, R. G., Broxton, D. E., and Hudson, M. R. (1994). Episodic caldera volcanism in the Miocene southwestern Nevada volcanic field: Revised stratigraphic framework, ^{40}Ar/^{39}Ar geochronology, and implications for magmatism and extension. *Geol. Soc. Am. Bull.*, 106, 1304–1318.

Scaillet, B. and Macdonald, R. (2001). Phase relations of peralkaline silicic magmas and petrogenetic implications. *J. Petrol.*, 42, 825–845.

Scaillet, B. and Macdonald, R. (2003). Experimental constraints on the relationships between peralkaline rhyolites of the Kenya Rift Valley. *J. Petrol.*, 44, 1867–1894.

Scaillet, B. and Macdonald, R. (2006a). Experimental and thermodynamic constraints on the sulphur yield of peralkaline and metaluminous silicic flood eruptions. *J. Petrol.*, 47, 1413–1437.

Scaillet, B. and Macdonald, R. (2006b). Experimental constraints on pre-eruption conditions of conditions of pantelleritic magmas: evidence from the Eburru complex, Kenya Rift. *Lithos*, 91, 95–108.

Scaillet, S., Rotolo, S. G., La Felice, S., and Vita-Scaillet, G. (2011). High-resolution ^{40}Ar/^{39}Ar chronostratigraphy of the post-caldera (<20 ka) volcanic activity at Pantelleria, Sicily Strait. *Earth Planet. Sci. Lett.*, 309, 280–290.

Scaillet, S., Vita-Scaillet, G., and Rotolo, S. G. (2013). Millenial-scale phase relationships between ice-core and Mediterranean marine records: insights from high-precision ^{40}Ar/^{39}Ar dating of the Green Tuff of Pantelleria, Sicily Strait. *Quat. Sci. Rev.*, 78, 141–154.

Schmincke, H.-U. (1974). Volcanological aspects of peralkaline silicic welded ash flow tuffs. *Bull. Volcanol.*, 39, 594–636.

Schmincke, H.-U. and Sumita, M. (2010). *Geological Evolution of the Canary Islands*. Gorres-Verlag, GMBH, Koblenz.

Schulz, K. J., DeYoung Jr., J. H., Seal II, R. R., and Bradley, D. C. (2017). *Critical mineral resources of the United States—an introduction (No. 1802-A)*. U.S. Geological Survey.

Self, S. and Gunn, B. M. (1976). Petrology, volume and age relations of alkaline and saturated peralkaline volcanics from Terceira, Azores. *Contrib. Mineral. Petrol.*, 54, 293–313.

Siegburg, M., Gernon, T. M., Bull, J. M., Keir, D., Barfod, D. N., Taylor, R. N., Abebe, B., and Ayele, A. (2018). Geological evolution of the Boset-Bericha Volcanic Complex, Main Ethiopian Rift: ^{40}Ar/^{39}Ar evidence for episodic Pleistocene to Holocene volcanism. *J. Volcanol. Geotherm. Res.*, 351, 115–133.

Smith, I. E. M. (1976). Peralkaline rhyolites from the D'Entrecasteaux Islands, Papua New Guinea. In Johnson, R. W., editor, *Volcanism in Australasia*, pages 275–285. Elsevier, Amsterdam.

Smith, I. E. M., Chappell, B. W., Ward, G. K., and Freeman, R. S. (1977). Peralkaline rhyolites associated with andesitic arcs of the southwest Pacific. *Earth Planet. Sci. Lett.*, 37, 230–236.

Snyder, D. C., Widom, E., Pietruszka, A. G., and Carlson, R. W. (2004). The role of open-system processes in the development of silicic magma chambers: a chemical and isotopic investigation of the Fogo A trachyte deposit, São Miguel, Azores. *J. Petrol.*, 45, 723–738.

Sosa-Ceballos, G., Macías, J. L., Avellán, D. R., Salazar-Hermenegildo, N., Boijseauneau-López, M. E., and Pérez-Orozco, J. D. (2018). The Acoculco Caldera Complex magmas: Genesis, evolution and relation with the Acoculco geothermal system. *J. Volcanol. Geotherm. Res.*, 358, 288–306.

Souther, J. G., Armstrong, R. L., and Harakal, J. (1984). Chronology of the peralkaline, late Cenozoic Mount Edziza Volcanic Complex, northern British Columbia, Canada. *Geol. Soc. Am. Bull.*, 95, 337–349.

Souther, J. G. and Hicks, C. S. (1984). Crystal fractionation of the basalt—comendite series of the Mt. Edziza Complex, British Columbia: major and trace elements. *J. Volcanol. Geotherm. Res*, 21, 79–106.

Spampinato, S., Ursino, A., Barbano, M. S., Pirrotta, C., Rapisarda, S., Larocca, G., and Platania, P. R. (2017). A reappraisal of seismicity and eruptions of Pantelleria Island and the Sicily Channel (Italy). *Pure Appl. Geophys.*, 174, 2475–2493.

Sparks, R. S. J. and Cashman, K. V. (2017). Dynamic magma systems: implications for forecasting volcanic activity. *Elements*, 13, 35–40.

Stabile, P., Arzilli, F., and Carroll, M. R. (2021). Crystallization of peralkaline rhyolitic magmas: pre- and syn-eruptive conditions of the Pantelleria system. *C. R. Géosci.*, 353, 1–20. (in this issue).

Stabile, P., Webb, S., Knipping, J. L., Behrens, H., Paris, E., and Giuli, G. (2016). Viscosity of pantelleritic and alkali-silicate melts: Effect of Fe redox state and Na/(Na+K) ratio. *Chem. Geol.*, 442, 73–82.

Stevenson, R. J., Bagdassarov, N. S., Dingwell, D. B., and Romano, C. (1998). The influence of trace amounts of water on the viscosity of rhyolites. *Bull. Volcanol.*, 60, 89–97.

Stevenson, R. J. and Wilson, L. (1997). Physical volcanology and eruption dynamics of peralkaline agglutinates from Pantelleria. *J. Volcanol. Geotherm. Res.*, 79, 97–122.

Stolz, A. J. (1985). The role of fractional crystallization in the evolution of the Nandewar volcano, northeastern New South Wales, Australia. *J. Petrol.*, 26, 1002–1026.

Sumita, M. and Schmincke, H.-U. (2013a). Impact of volcanism on the evolution of Lake Van (Turkey). II. Temporal evolution of Nemrut Volcano (eastern Anatolia) during the past ca. 0.4 Ma. *J. Volcanol. Geotherm. Res.*, 253, 15–34.

Sumita, M. and Schmincke, H.-U. (2013b). Impact of volcanism on the evolution of Lake Van. I: evolution of explosive volcanism of Nemrut Volcano (eastern Anatolia) during the past >400,000 years. *Bull. Volcanol.*, 75, 1–32.

Sumner, J. M. and Wolff, J. (2003). Petrogenesis of mixed-magma, high-grade, peralkaline ignimbrite "TL" (Gran Canaria): diverse styles of mixing in a replenished, zoned magma chamber. *J. Volcanol. Geotherm. Res.*, 126, 109–126.

Thompson, R. N. and MacKenzie, W. S. (1967). Feldspar-liquid equilibria in peralkaline acid liquids: an experimental study. *Am. J. Sci.*, 265, 714–734.

Troll, V. R. and Schmincke, H.-U. (2002). Magma mixing and crustal recycling recorded in ternary feldspar from compositionally zoned peralkaline ignimbrite A, Gran Canaria, Canary Islands. *J. Petrol.*, 43, 243–270.

Trua, T., Deniel, C., and Mazzuoli, R. (1999). Crustal control in the genesis of Plio-Quaternary bimodal magmatism of the Main Ethiopian Rift (MER): geochemical and isotopic (Sr, Nd, Pb) evidence. *Chem. Geol.*, 155, 201–231.

van den Bogaard, P. (2013). The origin of the Canary Island Seamount Province—New ages of old

seamounts. *Nat. Sci. Rep.*, 3, article no. 2107.

Vezzoli, L. and Acocella, V. (2009). Easter Island, SE Pacific: An end-member type of hotspot volcanism. *Geol. Soc. Am. Bull.*, 121, 869–886.

Vogel, T. A., Ryerson, F. J., Noble, D. C., and Younker, L. W. (1987). Limits to magma mixing based on chemistry and mineralogy of pumice fragments erupted from a chemically zoned magma body. *J. Geol.*, 95, 659–670.

Watson, E. B., Wark, D. A., and Thomas, J. B. (2006). Crystallization thermometers for zircon and rutile. *Contrib. Mineral. Petrol.*, 151, 413–433.

Weaver, B., Kar, A., Davidson, J., and Colucci, M. (1996). Geochemical characteristics of volcanic rocks from Ascension Island, South Atlantic Ocean. *Geothermics*, 25, 449–470.

Weaver, S. D. (1977). The Quaternary caldera volcano Emuruangogolak, Kenya Rift, and the petrology of a bimodal ferrobasalt-pantelleritic trachyte association. *Bull. Volcanol.*, 40, 209–230.

Webster, J. D., Taylor, R. P., and Bean, C. (1993). Pre-eruptive melt composition and constraints on degassing of a water-rich pantellerite magma, Fantale volcano, Ethiopia. *Contrib. Mineral. Petrol.*, 114, 53–62.

Wei, H., Liu, G., and Gill, J. (2013). Review of eruptive activity at Tianchi volcano, Changbaishan, northeast China: Implications for possible future eruptions. *Bull. Volcanol.*, 75, article no. 708.

Whaler, K. A. and Hautot, S. (2006). The electrical resistivity of the crust beneath the northern Main Ethiopian Rift. In Yirgu, G., Ebinger, C. J., and Maguire, P. K. H., editors, *The Afar Volcanic Province Within the East African Rift System*, volume 259, pages 293–305. Geological Society, Special Publications, London.

White, J. C., Benker, S. C., Ren, M., Urbanczyk, K. M., and Corrick, D. W. (2006). Petrogenesis and tectonic setting of the peralkaline Pine Canyon caldera, Trans-Pecos Texas, USA. *Lithos*, 91, 74–94.

White, J. C., Neave, D. A., Rotolo, S. G., and Parker, D. F. (2020). Geochemical constraints on basalt petrogenesis in the Strait of Sicily Rift Zone (Italy): Insights into the importance of short lengthscale mantle heterogeneity. *Chem. Geol.*, 545, article no. 119650.

White, J. C., Parker, D. F., and Ren, M. (2009). The origin of trachyte and pantellerite from Pantelleria, Italy: Insights from major element, trace ele-

ment, and thermodynamic modelling. *J. Volcanol. Geotherm. Res.*, 179, 33–55.

White, J. C., Ren, M., and Parker, D. F. (2005). Variation in mineralogy, temperature, and oxygen fugacity in a suite of strongly peralkaline lavas and tuffs, Pantelleria, Italy. *Can. Mineral.*, 43, 1331–1347.

White, J. C., Rotolo, S. G., and Parker, D. (2013). *Petrologic Constraints on Melting Conditions in the Strait of Sicily Rift Zone. Basalt 2013: Cenozoic Magmatism in Central Europe. April 2013, Görlitz, Germany*. 19–20.

White, J. C. and Urbanczyk, K. M. (2001). Origin of a silica-oversaturated quartz trachyte ± rhyolite suite through combined crustal melting, magma mixing, and fractional crystallization: the Leyva Canyon volcano, Trans-Pecos Magmatic Province, Texas. *J. Volcanol. Geotherm. Res.*, 111, 155–182.

Wilding, M. C., Macdonald, R., Davies, J. R., and Fallick, A. E. (1993). Volatile characteristics of peralkaline rhyolites from Kenya: an ion microprobe, infrared spectroscopic and hydrogen isotope study. *Contrib. Mineral. Petrol.*, 44, 681–690.

Wilks, M., Rawlinson, N., Kendall, J.-M., Nowacki, A., Biggs, J., Ayele, A., and Wookey, J. (2020). The coupled magmatic and hydrothermal systems of the restless Aluto caldera, Ethiopia. *Front. Earth Sci.*, 8, article no. 579699.

Wolff, J. A., Ellis, B. S., Ramos, F. C., Starkel, W. A., Boroughs, S., Oiln, P. H., and Bachmann, O. (2015). Remelting of cumulates as a process for producing chemical zoning in silicic tuffs: A comparison of cool, wet and hot, dry rhyolitic magma systems. *Lithos*, 336–337, 275–286.

Wolff, J. A., Forni, F., Ellis, B. S., and Szymanowski, D. (2020). Europium and barium enrichments in compositionally zoned felsic tuffs: A smoking gun for the origin of chemical and physical gradients by cumulate melting. *Earth Planet. Sci. Lett.*, 340, article no. 116251.

Xu, J., Pan, B., Liu, T., Hajdas, I., Zhao, B., Yu, H., Liu, R., and Zhao, P. (2013). Climatic impact of the Millenium eruption of Changbaishan volcano in China: New insights from high-precision radiocarbon wiggle-match dating. *Geophys. Res. Lett.*, 40, 54–59.

Yan, L., He, Z., Beier, C., and Klemd, R. (2018). Geochemical constraints on the link between volcanism and plutonism at the Yunshan caldera complex, SE China. *Contrib. Mineral. Petrol.*, 173, ar-

ticle no. 4.

Yang, B., Lin, W., Hu, X., Fang, H., Qiu, G., and Wang, G. (2021). The magma system beneath Changbaishan-Tianchi volcano, China/North Korea: constraints from three-dimensional magnetotelluric imaging. *J. Volcanol. Geotherm. Res.*, 419, article no. 107385.

Zou, H., Fan, Q., and Zhang, H. (2010). Rapid development of the great Millennium eruption of Changbaishan (Tianchi) Volcano, China/North Korea: Evidence from U–Th zircon dating. *Lithos*, 119, 289–296.